FINAL REPORT

For

THE DESIGN AND DEVELOPMENT OF A SILICON ULTRA-HIGH FREQUENCY POWER TRANSISTOR CAPABLE OF DELIVERING 20 WATTS OF OUTPUT POWER AT 430 Mc WITH A MINIMUM EFFICIENCY OF 50 PERCENT AND A POWER GAIN OF 6 dB

(29 June 1964 – 1 December 1965)

Contract No. NAS5-3705

Prepared By
RADIO CORPORATION OF AMERICA
Electronic Components and Devices
Somerville, New Jersey

For
GODDARD SPACE FLIGHT CENTER
Greenbelt Maryland

FINAL REPORT

For

THE DESIGN AND DEVELOPMENT OF A SILICON ULTRA-HIGH FREQUENCY POWER TRANSISTOR CAPABLE OF DELIVERING 20 WATTS OF OUTPUT POWER AT 430 Mc WITH A MINIMUM EFFICIENCY OF 50 PERCENT AND A POWER GAIN OF 6 dB

(29 June 1964 - 1 December 1965)

Contract No. NAS5-3705

Prepared By

RADIO CORPORATION OF AMERICA
Electronic Components and Devices
Somerville, New Jersey

For

GODDARD SPACE FLIGHT CENTER
Greenbelt Maryland

ABSTRACT

This report describes the technical efforts made and the achievements accomplished in the design and development of a silicon ultra-high frequency power transistor capabable of delivering 20 watts of output power at 430 megacycles with a minimum efficiency of 50 percent and a power gain of 6 dB. The work was performed under a program sponsored by National Aeronautics and Space Administration Contract No. NAS5-3705.

The program called for the delivery of 300 silicon power transistors capable of meeting the following requirements.

Maximum Ratings at 25°C

BV_{CEO}	BV_{CEX}	BV_{EBO}	I_C	P_C	T_J	T_{STG}
65 Vdc	75 Vdc V_{EB}=-1.5Vdc	5 Vdc	2 Adc	35 watts @T_C=25°C	200°C	-65°C to +200°C

Device Specifications

Parameter	Conditions	Sym.	Min.	Max.	Units
Power out	V_{CE}=28 Vdc RF P_{in}=5W f=430 Mc/s T_C=25°C	P.O.	20	-	watts
Power gain	V_{CE}=28 Vdc RF P_o=20W f=430 Mc/s T_C=25°C	P.G.	6	-	dB
Efficiency (DC to RF)	V_{CE}=28 Vdc f=430Mc/s RF P_o=20W RF $P_{in} \leq$5W DC $P_{in} \leq$40W	Eff.	50	-	percent

Device Specifications (cont.)

Parameter	Conditions	Sym.	Min.	Max.	Units
Static forward current transfer ratio	V_{CE}=4 Vdc I_C=1.0 Adc	h_{FE}	15	-	-
Saturation voltage	I_C=750 mAdc I_B=150 mAdc	$V_{CE(SAT)}$	-	1.0	volts
Collector cutoff current	V_{CE}=75 Vdc I_B=0	I_{CEO}	-	100	µA
Collector cutoff current	V_{CE}=28 Vdc V_{EB}=0	I_{CES}	-	1	µA
Collector cutoff current	V_{CE}=75 Vdc V_{EB}=0	I_{CES}	-	100	µA
Emitter cutoff current	V_{EB}=5 Vdc I_C=0	I_{EBO}	-	100	µA
Breakdown voltage	V_{EB}=-1.5 Vdc	BV_{CEX}	75	-	volts
Thermal Resistance		θ_{J-C}	-	5	°C/W

Environmental Tests and End Point Specifications

Environmental tests

TEST	CONDITIONS	SYM.	MIN.	MAX.	UNITS
Lead fatigue	according to MIl Spec MIL-STD-750				
Soldering	according to MIL Spec MIL-S-19,500				
Temperature	-65 to + 200°C 5 cycles				
Shock	non-operating 1500 g for 0.2 msec.				
Hermetic Seal	according to MIL Spec. MIL-STD-202B Notice 2, Method 112, either Test Condition A or B (10^{-5} atm cc/sec leak rate and test condition C (10^{-8} atm cc/sec leak rate)				

TEST	CONDITIONS	SYM.	MIN.	MAX.	UNITS
Power out	V_{CE}=28 Vdc RF P_{in}= 5W f=430 Mc/s TC=25°C	P.O.	15	-	watts
Collector cut-off current	V_{CE}=75 Vdc I_B=0	I_{CEO}	-	200	μA
Collector cut-off current	V_{CE}=28 Vdc V_{EB}=0	I_{CES}	-	2	μA
Emitter cut-off current	V_{EB}=5 Vdc I_C=0	I_{EBO}	-	200	μA

To meet the goals of the contract an improved overlay structure was developed which results in higher emitter periphery to emitter area and emitter periphery to base area ratios than werepreviously obtainable with silicon power transistors. The emitter structure was changed from the 0.5 mil squares used on the RCA 2N3375 device, to 0.1 by 1.4 mil lines.

A unit cell approach was used to develop the necessary technology and determine the gain and power capabilities of the structure. The unit cell was capable of one watt of output power at 430 megacycles with a power gain in excess of 10 dB.

The unit cell was scaled up 26 times for the initial design of the 20-watt unit. A power output of 21 1/2 watts was obtained with 7 watts of input power with an efficiency of 53 percent. However, a special package was required for this performance. The unit was redesigned for higher power gain and efficiency. The emitter cell size was reduced from 0.15 by 2.0 mils to 0.1 by 1.4 mils.

Three hundred and five final transistor samples mounted in the standard TO-60 case were submitted to the contracting agency. Power gain measurements made on these devices, using a 430-megacycle Class C amplifier that employed tuned lines, revealed power outputs of as much as 21.3 watts with a 5-watt drive. The median device had a power output of 17.7 watts with a power gain of 5.5 dB and an efficiency of 60 percent.

TABLE OF CONTENTS

TABLE OF CONTENTS (CONT.)

LIST OF ILLUSTRATIONS

LIST OF ILLUSTRATIONS (CONT.)

LIST OF TABLES

I. INTRODUCTION

The design and fabrication of a transistor capable of delivering 20 watts of output power at 430 megacycles requires tight control of starting material, diffusion depths, base width, and surface geometry. Alignment tolerances of one micron must be maintained, and variations in base width must be controlled to within $\pm$0.05 micron.

Parasitic capacitances and inductances associated with the pellet and the package become increasingly important to device performance in high power, high frequency applications in that they have a degenerate effect on power gain. To minimize parasitic capacitance, the emitter periphery dictated by the output power requirements of the device must be contained within the smallest possible base area. An improved overlay structure was developed, under this contract, to achieve this aim. The structure incorporated a smaller emitter and a tighter packing density than those of previous overlay devices, such as the 2N3375.

Several pellet and package configurations of improved overlay structure were investigated for the purpose of reducing emitter lead inductances. The results of these investigations led to a final design which incorporated a long pellet with a base aspect ratio of 10 to 1 for low emitter lead inductance.

The 6dB power gain at 20 watts output and over 50 percent efficiency at 430 megacycles achieved by the device developed under this contract enphasizes the advantages afforded by the overlay structure. Significant advances in the state-of-the-art in the areas of diffusion and photoresist technology were required to meet the device goals.

II. DISCUSSION

A. Device Design Considerations

1. Introduction

The frequency response of a device is related to the finite time required for the effect of a change of potential at the emitter to be felt at the collector terminal of the device. This time is required due to the mobility and velocity of carriers and results in a phase lag between input and output signal. As the frequency increases, a point is reached where the device does not respond to input signal variations, thereby resulting in a decrease in the power gain of the device.

The total time delay, τ_{ec}, of a device is comprised of four terms: the emitter junction capacitance charging time, τ_e, the base transit time, τ_b, the depletion region transit time, τ_x, and the collector junction capacitance charging time, τ_c as shown below in equation (1).

$$\tau_{ec} = \tau_e + \tau_b + \tau_x + \tau_c \qquad (1)$$

where: τ_{ec} = emitter to collector delay time,

τ_e = emitter junction charging time,

τ_b = base transit time,

τ_x = depletion region transit time, and

τ_c = collector junction charging time.

Since a major problem area is the high operation frequency of 430 megacycles, this section covers in detail the many factors affecting frequency response. Only through a thorough analysis of these factors can a successful pellet design be accomplished.

The manner in which transistor performance varies with frequency is determained by various transit times and R-C charging times, both internal and external, to the semiconductor pellet. An analysis of the transistor behavior at high frequencies can be treated in two sections: device

cross sectional and surface geometry limitations and package degeneration effects. The high frequency performance of the transistor can be characterized by the superposition of these two effects.

2. Emitter Charging Time

As can be seen from the plot of the proposed impurity profile shown in Figure 1, the emitter-base junction is very nearly an n-p step junction. It is well known that in a semiconductor junction an equilibrium contact potential is established due to the diffusion of free carriers across the junction, which results in ionized impurity atoms on either side of the junction. This diffusion process and subsequent equilibrium contact potential results in a depletion region in the vicinity of the junction which is devoid of free carriers. In order that the electric field be confined to the junction area, a condition of charge neutrality must exist; that is, the total number of ionized donor atoms on the n side of the junction must equal the total number of ionized acceptor atoms on the p side of the junction. By integrating the areas under the emitter and base diffusion profiles, it can be determined that a small depletion region on the emitter side of the junction requires a much larger depletion region on the base side due to the large concentration difference between the emitter and base sides. The difference in depletion layer length is great enough so that the entire depletion region can be closely approximated by considering only that portion in the high resistivity (base) side of the junction.

The effect of applying a forward or reverse bias to the emitter base junction is the contraction or expansion of the depletion region widths respectively. Integration of Poisson's equation and the application of electric field boundary conditions, together with the approximation that practically all the depletion region spreading takes place on the high resistivity side of the junction, results in the following relationship

$$x_m = \sqrt{\frac{2\varepsilon\varepsilon_o V_T}{q N_A}} \qquad (2)$$

where: x_m = depletion layer width,

ε = dielectric constant of the material,

ε_o = permittivity of free space,

V_T = total potential across the junction (external bias, V, plus equilibrum contact potential, V_i),

q = electron charge , and

N_A = impurity concentration in the base (high resistivity side of the junction).

The step junction capacitance can be obtained by treating the depletion layer as a parallel-plate capacitor with the charges separated by a distance x_m in a dielectric. Therefore, the depletion region capacitance C_T is

$$C_T = \frac{\varepsilon \varepsilon_o}{x_m} \quad \text{farads/cm}^2 \tag{3}$$

Substituting the expression for the depletion region width and multiplying by the total emitter area results in the emitter-base junction capacitance expression shown as

$$C_{Te} = A_e \sqrt{\frac{q \varepsilon \varepsilon_o N_A}{2 (V + V_i)}} \quad \text{farads} \tag{4}$$

where: C_{Te} = emitter base junction capacitance and

A_e = emitter base junction area.

The forward current characteristic of an n-p junction can be predicted from the following equation

$$I_F = C_1 e^{qV/kT} \tag{5}$$

If this expression is differentiated with respect to V and inverted, the following expression is obtained,

$$r_e = \frac{dv}{dI_F} = \frac{kT}{q} \left[\frac{1}{C_1 e^{qv/KT}} \right] = \frac{kT}{qI_F} \tag{6}$$

where: r_e = emitter junction resistance,

ε = Boltzmann's constant

T = junction temperature (^{o}K),

q = electron charge, and

I_F = injected current.

The emitter capacitance shunts the input resistance of the transistor and establishes the emitter charging time, $\tau_e = r_e C_{Tc}$. This charging time can be related to the device geometry as follows

$$\tau_e = r_e C_{Te} = \frac{kT}{qI_e} A_e \sqrt{\frac{q \varepsilon \varepsilon_o N_A}{2(V+V_i)}} \qquad (7)$$

3. Base Transit Time

The base transit time is the time required for the minority carriers injected at the emitter to traverse the base of the transistor. This transit time is a function of the mobility of the carriers which in turn is influenced by the effective masses of the carriers, the impurity type,and impurity concentration. It can be shown that the impurity mobility decreases with increasing impurity concentration.(1) In a diffused base device, the minority carriers pass through material of continually decreasing impurity concentration while traversing the base width, and consequently these carriers have a mobility which increases as the carriers drift across the base. Because of this, an average drift velocity can be assumed which results in an average diffusion constant for the minority carriers in the base region.

The values for the diffusion constants are related to the mobiliyy by the Einstein relationship which states that

$$D = \mu \frac{kT}{q} \qquad (8)$$

where: D = minority carrier diffusion constant,

μ = minority carrier mobility,

k = Boltzmann's constant,

T = temperature ^{o}K, and

q = electron charge.

The base transit time is calculated from the expression

$$\tau_b = \frac{W_b^2}{2\,D} \qquad (9)$$

where: τ_b = base transit time,

W_b = base width, and

D = average electron diffusion constant in the base.

4. Collector Depletion Region Transit Time

The collector-base junction of a transistor has an associated depletion region spread similar to that discussed for the emitter base junction. As can be seen from the impurity distribution plot shown in Figure 1, the p-n junction formed by the base diffusion into the epitaxial collector region will result in an equilibrium contact potential and subsequent depletion region larger than that of the emitter base junction due to the higher resistivity epitaxial layer. Furthermore, since the collector-base junction is operated with a large reverse-bias, the depletion region spread is further enhanced to the point that the time required for a current carrier to traverse this region becomes significant.

As with the emitter-base junction, the depletion region occurs on both sides of the collector-base junction. Since in a UHF transistor the base width is extremely narrow, that portion of the depletion region on the base side of the junctions results in a reduction in the base width with increasing collector bias and, therefore, a reduction in base transit time. The net effect of increasing collector bias is a simultaneous reduction in the base transit time and an increase in the collector depletion region transit time such that the sum of these delay times becomes a minimum at some low collector potential.

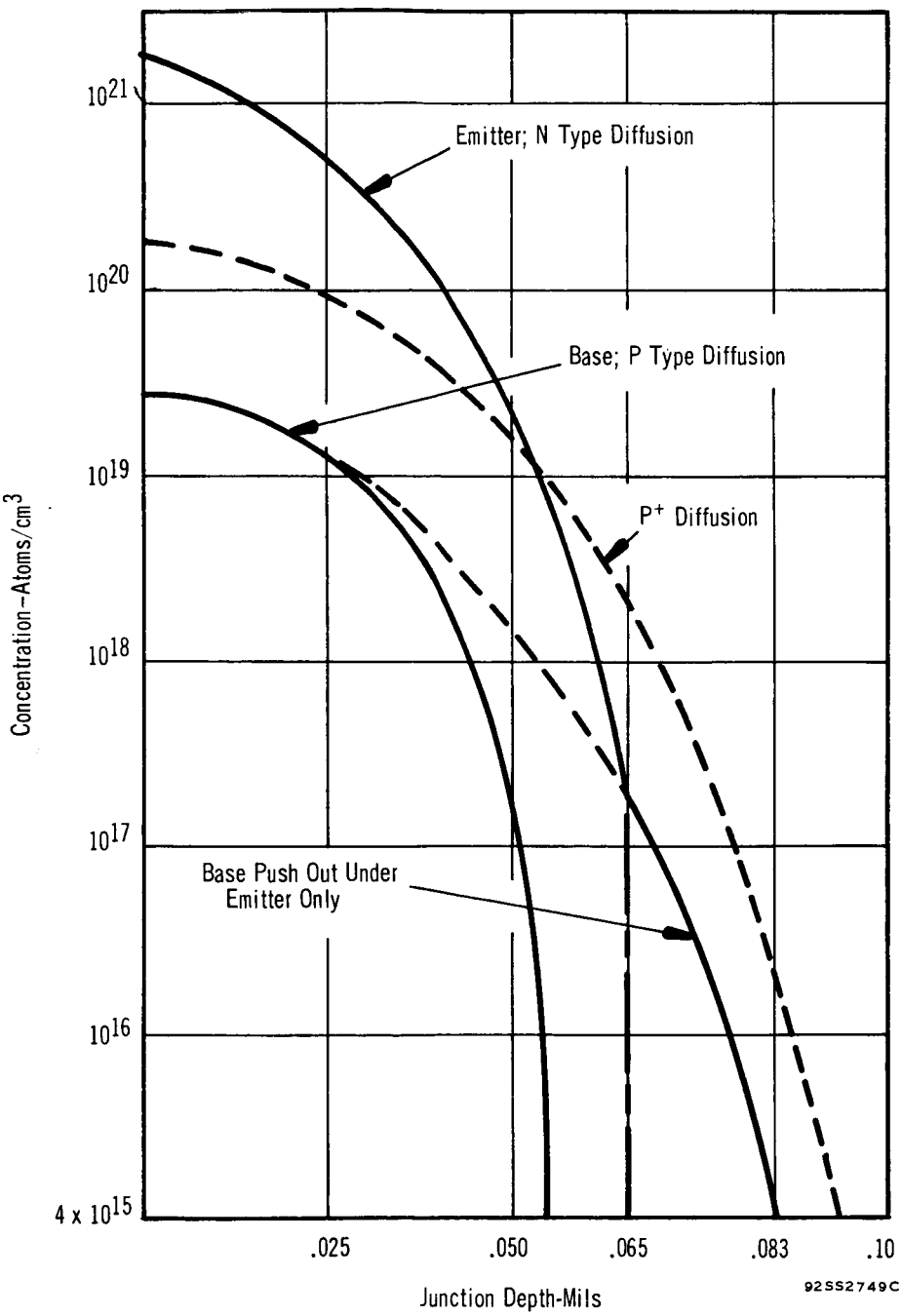

FIGURE 1 IMPURITY PROFILE

The collector depletion region transit time can be calculated from the expression

$$\tau_x = x_m / 2V_L \qquad (10)$$

where: τ_x = collector depletion region transit time,

x_m = total depletion region width, and

V_L = scattering limiting velocity.

The lattice scattering limiting velocity V_L is reached at electric field strengths of approximately 1.5×10^4 volts/cm[2]. Since this field strength is reached at very low values of collector bias, the above equation is applicable down to collector potentials of approximately two volts. At voltage levels below this value, which are obtained during output voltageswings in the collector potential, the field strength must be calculated and the drift velocity, V_D, as determined from Ryder's data must be substituted in the above equation in place of the lattice scattering limiting velocity.

5. Collector Junction Capacitance Charging Time

The collector junction capacitance, C_c, which appears across the output of the transistor must be charged up through any series resistance in the collector of the transistor.

This collector series resistance junction capacitance charging time can be calculated from the expression

$$\tau_c = R_c C_c \qquad (11)$$

where: τ_c = collector series resistance, collector capacitance charging time,

R_c = collector series resistance, and

C_c = collector base junction capacitance.

As in the case of the emitter-base junction, the collector-base

capacitance can be calculated as

$$C_c = \frac{A_c \varepsilon \varepsilon_o}{x_m} \tag{12}$$

where: C_c = collector base junction capacitance,

A_c = collector base junction area,

ε = dielectric constant of semiconductor material,

ε_o = permittivity of free space, and

x_m = total collector depletion region length.

The collector series resistance can be calculated using the equation

$$R_c = \frac{\rho}{W} \frac{d}{l} \tag{13}$$

where: R_c = collector series resistance,

ρ = resistivity of the epitaxial layer,

W = emitter finger width,

l = emitter periphery, and

d = epitaxial layer thickness.

The above equation is for the resistance of a rectangular cross section semiconductor geometry and is a worst case condition, since the effect of current divergence, while traversing the epitaxial layer, and the subsequent increase in effective current carrying cross sectional area is neglected. A second consideration which is neglected using the above equation is the reduction in epitaxial layer length through which current must flow, due to the depletion spread with collector bias. Because of this the calculated value of collector series resistance is extremely pessimistic and the actual value will be considerably less.

6. High Frequency Relationships

The manner in which various device parameters vary with frequency is

related to the emitter-to-collector delay times as shown below

$$f_T = \frac{1}{2\pi \tau_{ec}} \tag{14}$$

where: f_T = current gain bandwidth, the frequency at which current gain is equal to 1, and

τ_{ec} = total emitter-to-collector delay time

Although the current gain is equal to unity at f_t, there is still power gain available because of the impedance ratios of the device. Thus,

$$PG = 10 \log \frac{P_o}{P_{in}} = 20 \log \frac{I_o}{I_{in}} + 10 \log \frac{R_o}{R_{in}} \tag{15}$$

The frequency limitation of a device is actually the maximum frequency of oscillation, f_{max}, which is defined as the frequency at which the power gain is 1.

The maximum frequency of oscillation and therefore the power gain is inversely proportional to an additional time constant, $r_{bb'} C_c$, which is associated with the resistance of the base region. This time constant results from the flow of the base current through the finite resistance associated with the base region, from the emitter edge to the ohmic base contact. If the relationship between f_T and f_{max} is expressed as

$$f_{max} = \sqrt{f_T / 25\ r_{bb'} C_c} \tag{16}$$

where: f_{max} = maximum frequency of oscillation, and

f_T = gain bandwidth

C_c = collector capacitance

Taking into account the degenerative effect of emitter lead inductance, power gain is given by the following equations

$$PG = \frac{1}{2}\left(\frac{f_T}{f}\right)^2 \left(\frac{1}{r_{bb'} + 2\pi f_T L_e}\right)\left(1 + \frac{R_L}{\frac{R_L}{R_o}}\right) \tag{17}$$

$$R_o = \frac{1}{2\pi f_T C_c} \tag{18}$$

$$R_L = V_{cc}^2/2P_o \tag{19}$$

where: f = frequency of operation,
R_o = output impedance of transistor,
C_c = total collector to base capacitance,
R_L = load resistance,
V_{cc} = supply voltage,
P_o = power out,
$r_{bb'}$ = base spreading resistance, and
L_e = emitter lead inductance.

From past experience on devices of this sort we know that $r_{bb'}$ will be a fraction of an ohm and will be a fraction of $2\pi f_T L_e$. To determine first order effects we, therefore, can simplify equation (17) to

$$PG = \frac{1}{2}\left(\frac{f_T}{f}\right)^2\left(\frac{1}{W_T L_e}\right)\left(\frac{R_L}{1+\frac{R_L}{R_o}}\right) \tag{20}$$

The load resistance (R_L) and the frequency of operation are specified, leaving f_T L_e and R_o as the important device parameters. f_T must be specified at the operating current of the device. The device must be designed to provide for a sufficient current handling capability so that f_T will be high at the operating current. Because of edge injection effects, this translates into sufficient emitter periphery to maintain a high f_T. The collector capacitance determines the output impedance and the collector efficiency. The collector efficiency will be higher and the collector current will be lower as the collector capacitance decreases. Less emitter periphery will be needed as the collector capacitance is lowered. To obtain long emitter periphery (high current handling capacity) and minimum base area (high efficiency), the surface geometry of the device must be designed to place the greatest amount of emitter periphery within the smallest possible base area.

The emitter lead inductance (L_e) is determined both by the case

design and the pellet geometry. The pellet geometry will determine the number of emitter bond wires, the configuration, spacing and, hence, mutual inductance effects. This immediately suggests that the pellet should be made as long as possible. Multiple base areas with many bond wires or ribbons could also be used to minimize mutual inductance effects.

7. Degradation of f_T at High Current Levels

The equations presented in the previous section on collector depletion region transit time and base width transit time assume that only the charge due to ionized donors and acceptors exists in the collector depletion region. At high injected carrier levels, however, the density of carriers present in this region may result in a significant contribution to the overall space charge. Under these conditions, the depletion region can no longer be treated as if it were devoid of carriers.

It can be shown that the observed high current falloff in the f_T of a transistor is a direct result of a spreading of the neutral base layer into the collector region of the device [3]. This effect begins when the mobile carrier space charge density in the collector transition region becomes approximately equal to the fixed impurity charge density on the high resistivity side of the collector junction. This can be expressed mathematically as

$$I_{max} = q A_e N_D V_L \tag{21}$$

where: I_{max} = current at which base widening or base spreading begins to occur,

q = electron charge,

A_e = effective emitter area,

N_D = impurity concentration in the collector region, and

V_L = scattering limited velocity.

For collector currents in excess of this value, the neutral base layer widens by spreading into the collector region resulting in a decrease in f_T.

8. High Frequency Output Power

The high frequency output power of a transistor is a function of the collector current flowing in the device. For the proposed transistor to deliver 20 watts of output power at 430 megacycles at 50 percent collector efficiency, an average collector current of 1430 milliamperes at 28 volts is required. This current handling capability imposes an emitter periphery requirement on the device to prevent base widening effects due to current crowding.

In transistor operation, at low current levels, the device injects over the entire emitter area. As the injected current level is increased, lateral voltage drops under the emitter due to base current flow biases the emitter-base junction such that the emitter edges are most forward biased. This results in these edges accounting for the majority of injected current at high current levels. The disadvantage associated with this effect is that the current is injected from only a small portion of the total emitter area and results in base widening due to current crowding at lower levels than predicted utilizing small signal theory. Base widening increases the base transit time of the device and decreases f_T.

To minimize the effect, a large emitter periphery is required; however, an increase in periphery requires an increase in emitter area and results in a decrease in f_T due to the larger emitter transit time associated with an emitter area increase, as well as a decrease in collector efficiency due to the larger base area.

This effect is observable in all transistor designs and particularly in VHF and UHF devices. The saturated output power is a function of the operating frequency of the device. A somparison of the saturated output power of various RCA 2N3375 devices at 100 and 400 megacycles reveals that about 11 watts are obtained at 100 megacycles and below,

but only 6 watts are possible at 400 megacycles.

This saturated output power falloff with frequency is also influenced by base impedance changes with frequency and output impedance changes with frequency.

The base impedance change with frequency can be seen by treating the emitter-base junction as a series of distributed resistances shunted by the junction capacitance between the emitter and base. As the operating frequency is increased, the shunting effect of the capacitance dominates and the sections of the emitter closest to the base terminal injects most of the ac current. This results in ac current crowding of the device. This effect results in a modification of the input impedance of the device with increasing frequency and base widening effects due to the ac component of collector current.

The saturated output power of a transistor is also influenced by the effects of the device output capacitance on output impedance. As the operating frequency is increased, the output resistance due to this capacitance decreases and shunts the load resistance. This results in a decrease of collector efficiency of the device. Since the emitter periphery and collector doping concentration limit the currents which can be drawn in the device, further increases in input drive power result in very small increases in output power level.

The transistor power output can be improved by the use of emitter geometries which have high emitter periphery to emitter area and base area ratios and by using improved techniques in the growth of collector substrate material. Both of these techniques will result in minimizing current crowding effects. Furthermore, improved emitter designs require less collector-base junction area and result in a lower value of output capacitance. The device geometry and cross sectional structure is discussed in Section II-B-2.

9. Thermal Resistance

Thermal resistance is a function of the aspect ratio of the base. Figure 2 shows an emperical plot of thermal resistance as a function of base periphery. The plot is valid only for packages with a beryllium oxide insulator brazed to a copper stud. To get maximum base periphery, the base area or base areas should be made as long and thin as possible. As discussed previously, the long base areas will also help minimize emitter lead inductance.

B. Device Design Calculations

1. Emitter Periphery

The program required that the device deliver 20 watts with 50 percent collector efficiency and a supply voltage of 28 volts. The average collector current was to be 1430 milliamperes or less. Past experience has shown that approximately one mil of emitter periphery is required per milliampere of average collector current.

Twenty percent extra periphery was added to allow for loss in power-out, caused by paralleling a large number of emitters, resulting in a total emitter periphery of 1700 mils.

2. Device Structure

The surface geometry must be designed to obtain the maximum emitter periphery to emitter area, and emitter periphery to base area. The EP/BA ratio is important in that it will determine the collector efficiency. The overlay structure used on the 2N3375 had the highest EP/EA and EP/BA ratios obtainable at that time. However, further refinements in the overlay structure were needed to meet the requirements of the program. Both ratios can be improved by going from a square emitter electrode structure, used on the 2N3375, to a line emitter structure. Figure 3 shows a comparison of the two cell structures. The dimensions indicated on the line structure are what was considered to be minimum practical emitter widths and emitter to P^+ spacings at the

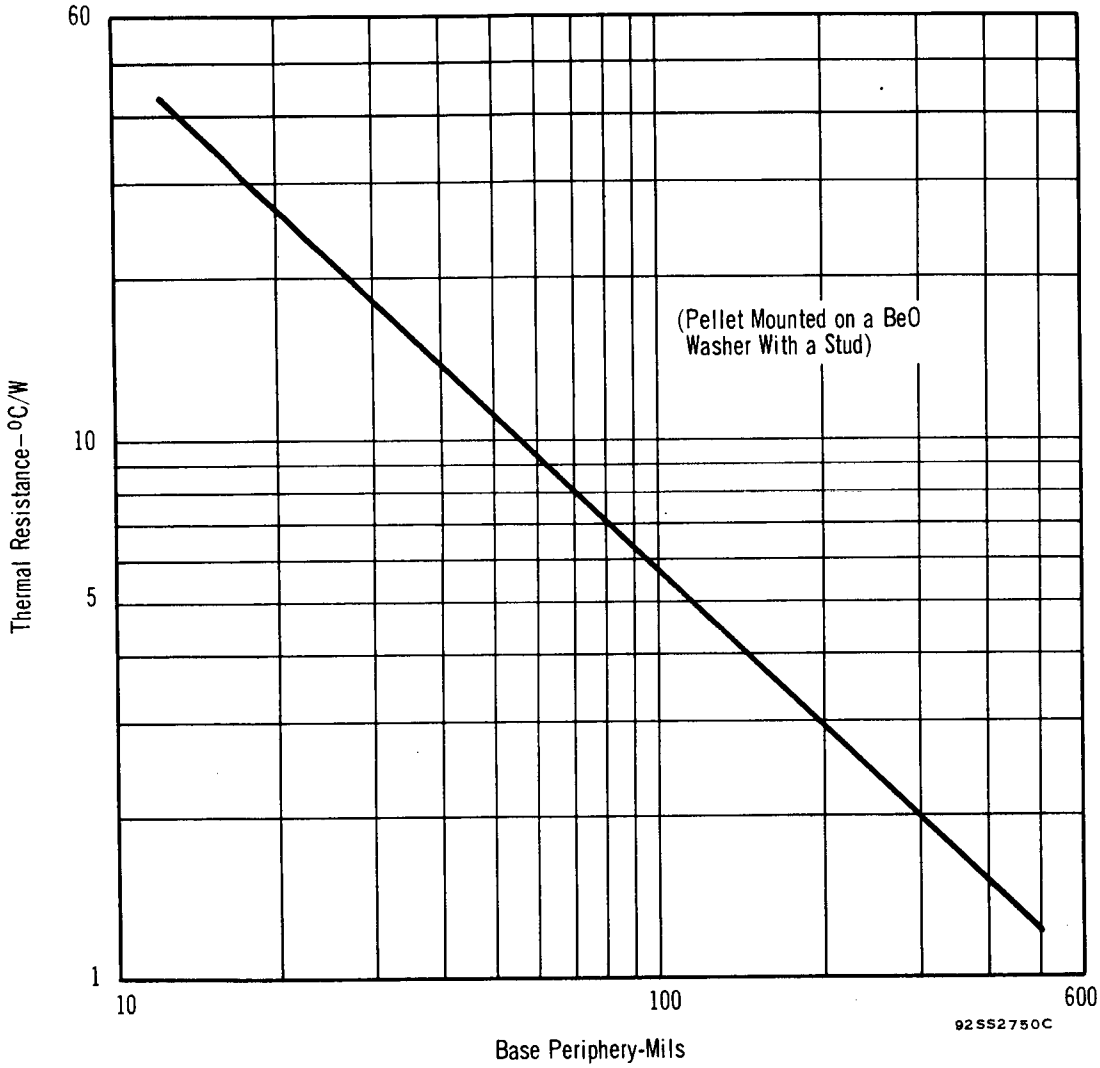

FIGURE 2 BASE PERIPHERY AS A FUNCTION OF THERMAL RESISTANCE

start of the contract.

The cell structure shown in Figure 3 was paralleled as shown in Figure 4. Two seperate base areas were used to give minimum emitter lead inductance and thermal resistance. A 12 by 17 array of emitters was used in each base area. The complete device is shown in Figure 5. A comparison of the new structure which is called the TA2675, and the 2N3375 is shown in Table I.

3. Emitter Charging Time - τ_e

The emitter charging time equation can be expressed as

$$\tau_e = \frac{kT}{qI_e} C_{T_e} \qquad (22)$$

and can be determined as follows

$$= \frac{(.026)\ (2.66 \times 10^{-10})}{2.3} = 3 \times 10^{-12} \text{sec.}$$

where: I_e = 2.31 amperes (f_t assumed 700 megacycles),

$\frac{kT}{q}$ = 0.026 volt, and

the emitter base junction transition capacitance in picofarads (C_{Te}) from Eq. (4).

$$C_{T_e} = A_e \left[\frac{q\varepsilon\varepsilon_o N_a}{2(V+V_i)}\right]^{1/2}$$

$$= (7.9\text{x}10^{-4}) \left[\frac{(1.6\text{x}10^{-19})(12)\ (8.85\text{x}10^{-14})(8\text{x}10^{17})}{2\ (0.6)}\right]^{1/2} = 266\text{Pf}$$

where: $A_e = 7.90\text{x}10^{-4}$ cm^2,
$N_A = 8\text{x}10^{17}$,
$(V+V_i) = 0.6$ volts,
$\varepsilon = 12$, and
$\varepsilon_o = 8.85\text{x}10^{-14}$ f/cm.

a. 2N3375

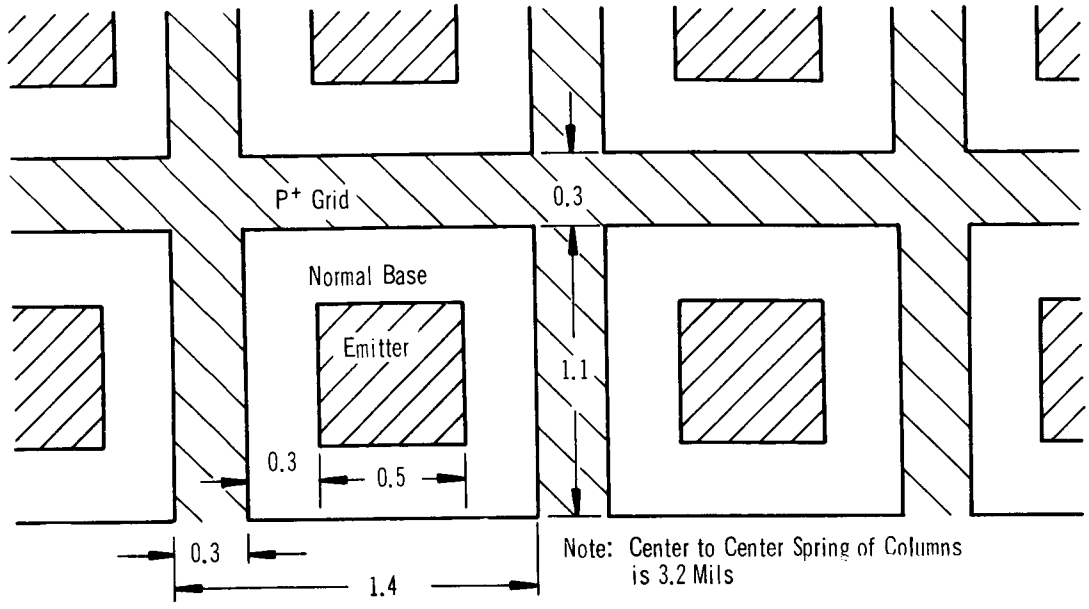

b. TA2675

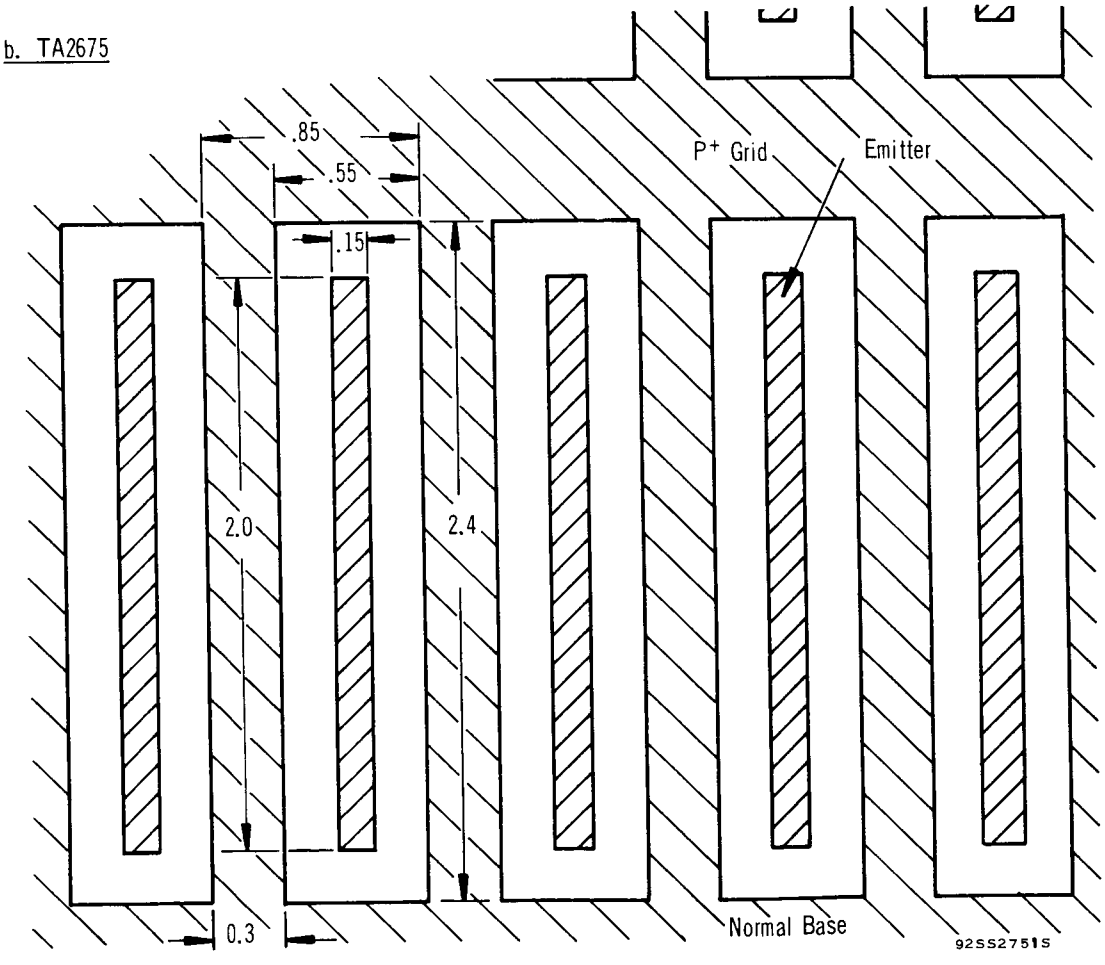

All Dimensions in Mils

FIGURE 3 TA2675 AND 2N3375 CELL STRUCTURES

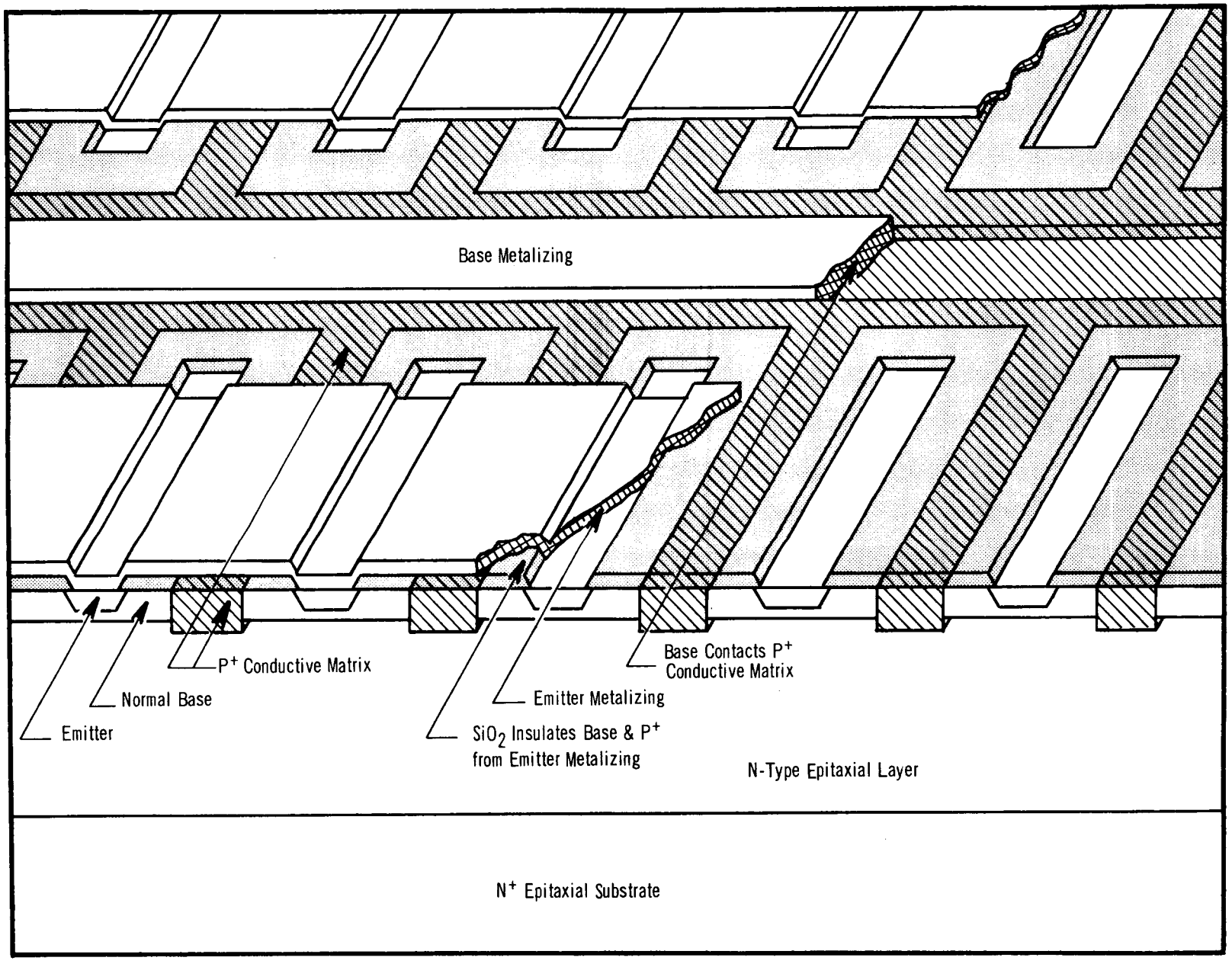

FIGURE 4 CROSS SECTIONAL VIEW OF RCA TA2675

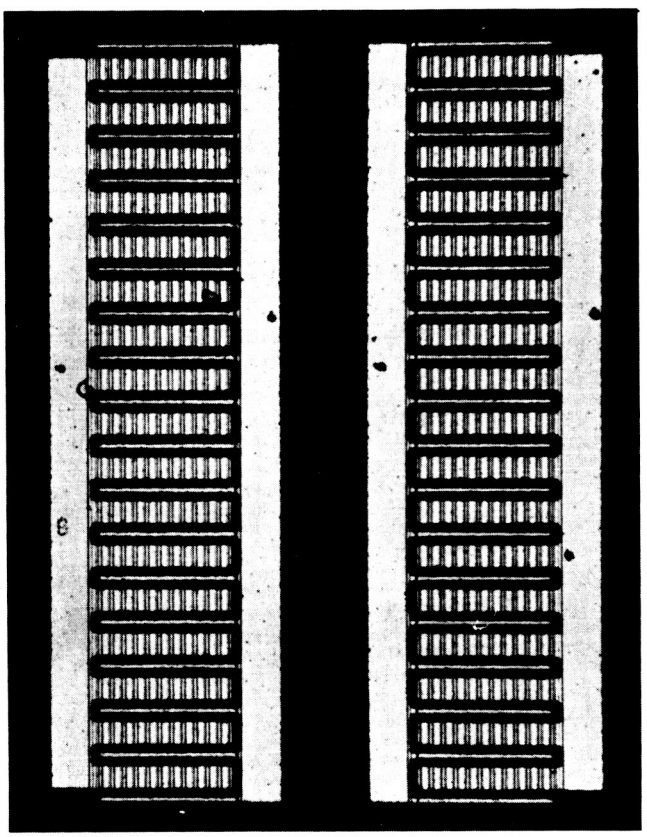

92SS2761P

FIGURE 5 MICROPHOTOGRAPH OF TA2675

TABLE I

Comparison Of The TA2675 And The 2N3375

Characteristics	20W(TA2675)	2N3375
No. of Emitter Sites	408	156
Emitter Periphery (mils)	1754	312
Emitter Area ($mils^2$)	122	39
Base Area ($mils^2$)	1160	380
$\frac{\text{Emitter Peripheries (mils/mils}^2\text{)}}{\text{Emitter Area}}$	14.3	8
$\frac{\text{Emitter Peripheries (mils/mils}^2\text{)}}{\text{Base Area}}$	1.51	0.82
Base Metallizing over Collector Oxide ($mils^2$)	325	0
Emitter Metallizing over Collector Oxide ($mils^2$)	318	0
Pellet Size (mils)	70 x 60	30 x 30
Base Periphery (mils)	345	76

4. Base Transit Time, τ_b

The base transit time can be determined from:

$$\tau_b = \frac{W^2}{2D} = 1.54\text{x}10^{-10}$$

where: $W_b = 0.017$ mil $= 4.3\text{x}10^{-5}$cm, and
$D = 6\text{cm}^2/\text{sec}$

The diffusion constant listed in the literature for the base doping being used is $12\text{cm}^2/\text{sec}$. Measurements of f_T and base width on transistors with the proposed diffusion have indicated an effective D of $6\ \text{cm}^2/\text{sec}$. The effective diffusion constant in the base is lower than previously thought, by a factor of two. This is probably caused by strains in the lattice, due to the high surface concentration emitter and base diffusions.

5. Collector Depletion Layer Transit Time, τ_x

The collector depletion region transit time can be determined from:

$$\tau_x = \frac{x_m}{2V_L} = \frac{3.6\text{x}10^{-4}}{2\text{x}8\text{x}10^{6}} = 0.23\text{x}10^{-10}\ \text{sec}$$

where: $V_L = 8\text{x}10^{6}$ cm/sec, and

the depletion layer spread (x_m) can be determined from:

$$x_m = \left(\frac{2\varepsilon\varepsilon_o V}{q\ N_D}\right)^{1/2}$$

$$= 3.6\text{x}10^{-4}\text{cm} = \left(\frac{2\text{x}12\text{x}8.85\text{x}10^{-14}\text{x}28.6}{1.6\text{x}10^{-19}\text{x}3\text{x}10^{15}}\right)^{1/2}$$

where: $V = 28.6$v,

$\varepsilon_o = 8.85\text{x}10^{-14}$f/cm,

$\varepsilon = 12$, and

$N_D = 3 \times 10^{15}/cm^3$

6. Collector Junction Capacitance Charging Time, τ_c

The collector junction capacitance charging time (τ_c) is given by

$$\tau_c = R_c C_{bc}, \text{ and}$$

$$= (1.68)\ (2.2)\ (10^{-11}) = 3.7 \times 10^{-11} \text{sec}$$

where: $C_{bc} = 22$ picofarads,

$R_c = 1.68$ ohms,

$C_{bc} = \dfrac{k\varepsilon_o A_c}{x_m} = 22$ picofarads,

$A_c = 7.5 \times 10^{-3} cm^2$,

$R_c = \dfrac{\rho_d}{Wl} = 1.68$ ohms,

$\rho = 2\ \Omega$-cm,

$d = 1.52 \times 10^{-4}$cm,

$W = 4 \times 10^{-4}$cm, and

$l = 4.45$cm

To determine C_{ob} the capacitance of both the emitter base metalizing over collector oxide must be added to C_{bc}. The total metalizing over collector oxide is 643 mil^2. The oxide thickness is 12,000Å and has a 0.0183 picofarad/mil^2 capacitance, which adds a total of 12 picofarads to C_{bc}. Therefore, the C_{ob} of the device will be 34 picofarads.

7. Emitter to Collector Transit Time, τ_{ec}

The emitter to collector transit time (τ_{ec}) is given by

$$\tau_{ec} = \tau_e + \tau_b + \tau_x + \tau_c$$

$$= 2.17 \times 10^{-10} \text{ sec} = (0.03 + 1.54 + 0.23 + 0.37) \times 10^{-10} \text{ sec}$$

8. Base Spreading Resistance, $r_{bb'}$

The base spreading resistance is determined by the sheet resistance between the emitter and base contacts and by the resistance under the injecting emitter edge.

The portion under the emitter can be calculated on the basis of the 430-megacycle current gain requirement of the device. At 430 megacycles (f_T=700 megacycles), I_B = 890 milliamperes. Since more than 60 percent of the injected current occurs within the length required to produce a 26-millivolt drop under the emitter, that portion of $r_{bb'}$ contributed by this region is

$$r_{bb_1'} = \frac{26\text{mV}}{880\text{ mA}} = 0.03 \text{ ohm} \qquad (23)$$

That portion of $r_{bb_2'}$ contributed between the normal base and the P^+ contact is determined by the sheet resistance of that region.

$$r_{bb_2'} = \frac{\rho_s \ell}{d} = \frac{(100)\ (0.2)}{1754} = .01 \text{ ohms} \qquad (24)$$

where: ρ_s = sheet resistance in the base between the emitter and P^+ = 100 ohm/square

ℓ = spacing between the emitter and P^+ grid = 0.2 mil, and

d = emitter periphery = 1754 mils.

The total base spreading resistance ($r_{bb'}$) is the sum of $r_{bb_1'}$ and $r_{bb_2'}$, or 0.04 ohm, plus some contact resistance.

9. High Frequency Relationship

The current gain bandwidth of the device is determined by the expression

$$f_T = \frac{1}{2\pi\tau_{ec}} = \frac{1}{6.28(2.17 \times 10^{-10})} = 730 \text{ megacycles}$$

The maximum frequency of oscillation, f_{max}, neglecting emitter lead inductance, can be calculated from the relation:

$$f_{max} = \sqrt{\frac{f_T}{25\, r_{bb'}\, C_{ob}}}$$

$$\sqrt{\frac{7.3 \times 10^8}{25(.04)(34)(10^{-12})}}$$

$$f_{max} = 4.65 \text{ gigacycles}$$

This illustrates how optimistic the calculation can be by neglecting emitter lead inductance. The f_{max} is more accurately calculated from equation 17 and is about 800 megacycles.

$$P\,G = 1/2 \left(\frac{f_T}{f}\right) \left[\frac{1}{r_{bb'} + 2\pi f_T L_e}\right] \left[\frac{R_L}{1 + \frac{R_L}{R_O}}\right]$$

$$= 1/2 \left(\frac{730}{430}\right)^2 \left[\frac{1}{.04 + 2.28}\right]\left[\frac{19}{1 + \frac{19}{6.45}}\right]$$

$$= 3.1$$

where: $f_T = 730$ megacycles,

$f = 430$ megacycles,

$R_L = \frac{V_{CC}^2}{2P_o} = 19$ ohms

$R_o = \frac{1}{2\pi f_T C_c} = 6.45$ ohms

$V_{cc} = 28$ volts,

$P_o = 20$ watts,

$r_{bb'} = 0.04$ ohms, and

$L_e = 0.50$ nanohenry (obtained on the grounded emitter TO-60).

The predicted gain is only 3.1 times as compared to the contract goal of 4 times. However, power gain could not be accurately predicted during the early stages of development, otherwise this design would have been changed during the design phase. In addition emitter lead inductance could not be calculated or measured accurately during the early stages of the program.

10. Device Current Handling Capability

The maximum current that this transistor can carry before base widening begins is given by

$$I = q\, A_e\, N_D\, V_L$$

It has been shown in Section 8 that 63 percent of the total emitter current is injected within that length under the emitter which results in a 26 millivolt drop. This length can be computed from the relationship

$$r = \rho_s \frac{\ell}{L} = \frac{26\ mV}{I_B} \qquad (25)$$

where: ρ_s = sheet resistivity under the emitter = 5000 Ω/sq.,
ℓ = current path length - injecting region of emitter,
L = total emitter periphery = 4.45 cm,
I_b = total base current at 430 mc = 880 milliamperes,

$$r = \frac{26\ mV}{880mA} = 0.03 \text{ ohm, and}$$

$$\ell = \frac{r\, L}{\rho_s} \qquad \frac{0.03\ (4.45)}{5000} = 2.7 \times 10^{-5} \text{ cm}$$

It can be shown that as the collector current traverses the base width in the presence of a field, a lateral diffusion of these minority carriers occurs. Experimental data of various high frequency devices indicates that the spreading angle is approximately 30 degrees. Since this device has a base width of 0.017 mil and injects from a region under the emitter of 2.7×10^{-5} cm, the width of the collector area inter-

cepted by these minority carriers is 5.20×10^{-5} cm. This area results in a maximum current density of:

$$I_{max} = q\, A_e\, N_D\, V_L$$

$$= (5.2 \times 10^{-5})(4.45)(1.6 \times 10^{-19})(4 \times 10^{15})(8 \times 10^{6})$$

$$= 1{,}200 \text{ milliamperes}$$

where: $N_D = 4 \times 10^{15}/cm^3$

The above calculations are pessimistic for two reasons. First, the injecting emitter length was computed on the basis of a 26 millivolt drop (25°C) rather than a 37 millivolt drop (150°C junction temperature). This larger voltage drop indicates the emitter will actually be injecting over approximately a 50 percent larger region. Secondly, only 63 percent of the total collector current is injected over the above calculations. Taking into account the second effect only indicates that the emitter periphery of this device is large enough to handle the required current of 1,430 milliamperes.

11. Thermal Resistance

The base periphery of the proposed device is 345 mils. From Figure 2 the thermal resistance is predicted to be 1.8°C/W.

C. Unit Cell Experimental Vehicle

A much smaller unit was designed to develop the necessary technology and determine the power gain and output power of the new overlay structure. The same cell structure was used for the full unit shown in Figure 5. Figure 6 shows a picture of the completed unit. Two rows of eight emitters each were used. The emitter periphery is 68 mils with a base area of 48 $mils^2$. The device is presently known as the TA2658 or the 2N3866.

D. Device and Package Evaluation

1. Unit Cell

Figure 7 shows a plot of power output versus power input and frequency with a 28-volt supply for the unit cell. For 1 watt of output power,

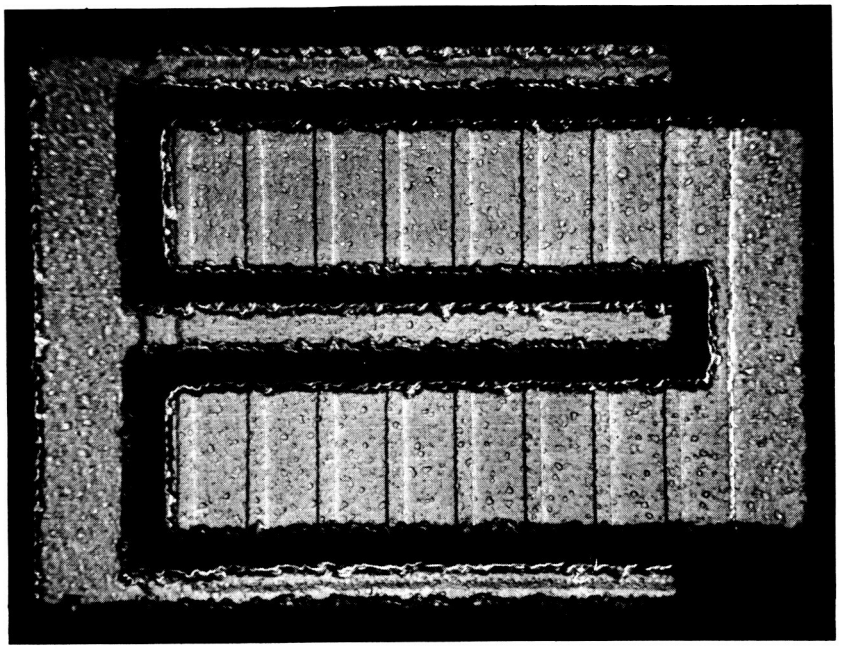

92SS2762P

FIGURE 6 MICROPHOTOGRAPH OF TA2658

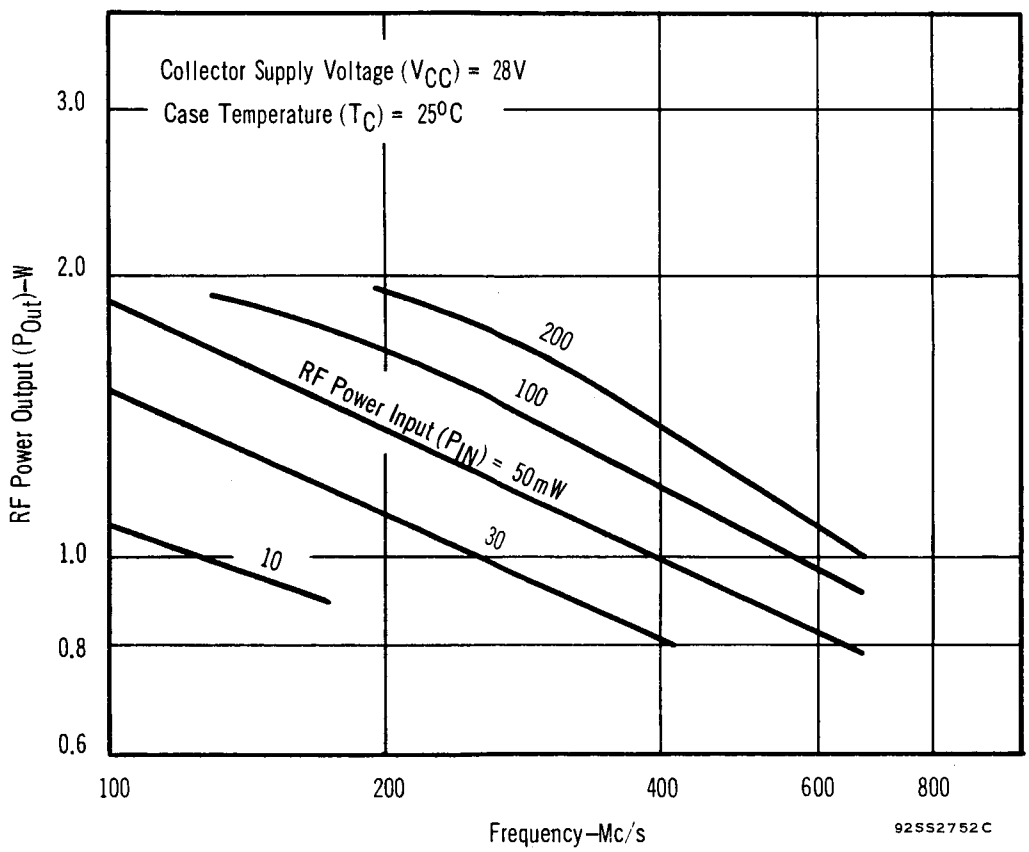

FIGURE 7 POWER OUTPUT AS A FUNCTION OF POWER INPUT AND FREQUENCY FOR THE TA2658

the device is capable of 11 dB power gain and 50 percent efficiency. The lumped constant circuit used for the measurements is shown in Figure 8.

With the proposed emitter periphery of 1754 mils, the TA2658 has been scaled up a factor of 26 times. A power out of 26 watts can be expected at 430 megacycles, with reasonable gain providing the emitter lead inductance can be kept low.

2. Full Unit

a. Stripline Package

The full unit was first mounted in the stripline package shown in Figures 9and 10. Gain could not be obtained at 430 megacycles. An investigation of inductive voltage drops down the base metalizing showed the cause of the problem. The base was bonded at one end of each bonding stripe. The inductance down the base bonding stripe is 1 nanohenry and the average base current is 404 milliamperes for each base bonding stripe. The inductive voltage drop is 2.7 volts. Even a 0.1 volt drop in V_{be} would be enough to decrease the emitter injection on the side of the unit furthest from the bond by 90 percent. The pellet and package must be designed so that equal emitter and bond lead lengths can be maintained. This was accomplished by scribing the pellet in two so that each base area is on a seperate pellet. The pellets were then mounted side by side in a grounded emitter TO-60, as shown in Figure 11. Figure 12 shows a complete TO-60.

b. Grounded Emitter TO-60

Good results still could not be obtained for the full unit in the grounded emitter TO-60. One of the two pellets would burn out before power out measurements could be obtained. The problem appeared to be caused by the length of the collector lead from one end of the pellet to the other. The collector current must flow this whole length to reach different parts of the collector. There is 3.3 ohms of inductive reactance from one end of the pellet to the other. For

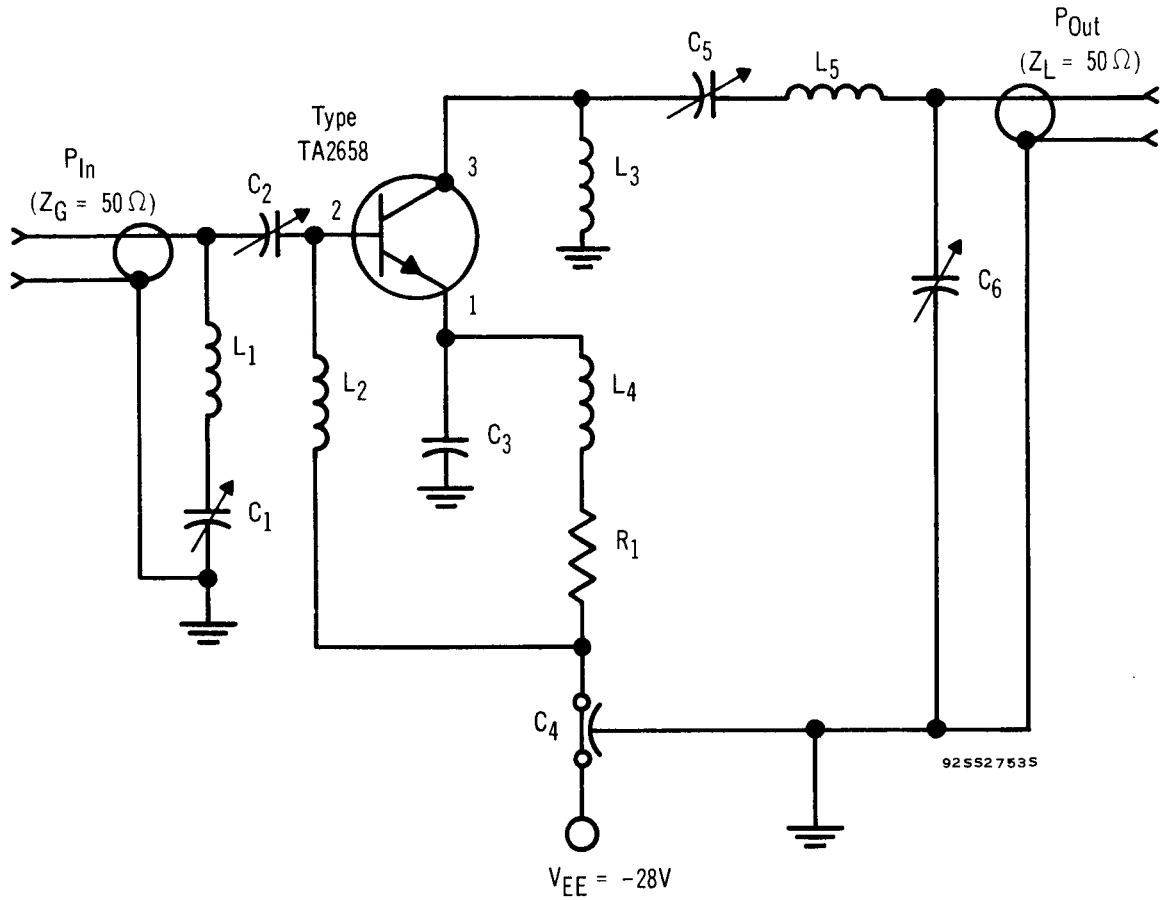

C_1: 3-35pF

C_2, C_5: 8-60pF

C_3: 12pF

C_4: 1,000pF

C_6: 0.9-7pF

L_1: 2 Turns No. 18 Wire, 1/4" ID, 1/8" Long

L_2: Ferrite rf Choke, 1 turn, Z = 450 Ω

L_3, L_4: RF Choke, 0.1 μH

L_5: 2-1/2 Turns, No. 18 Wire, 1/4" ID, 3/16" Long

R_1: 5.6 Ω, 1W

FIGURE 8 RF AMPLIFIER CIRCUIT FOR TA2658 POWER OUTPUT TEST (430Mc/s OPERATION)

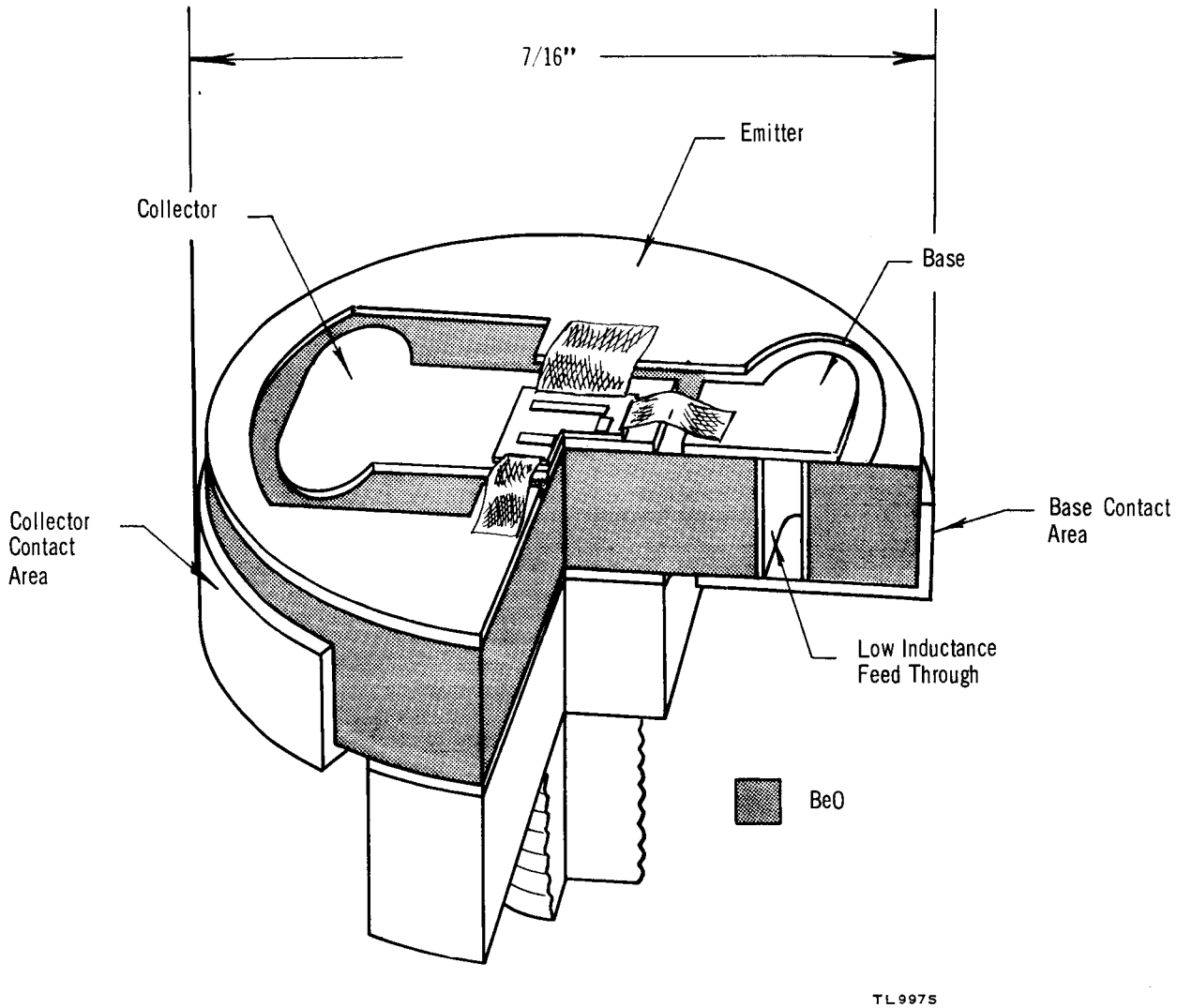

FIGURE 9 STRIPLINE PACKAGE

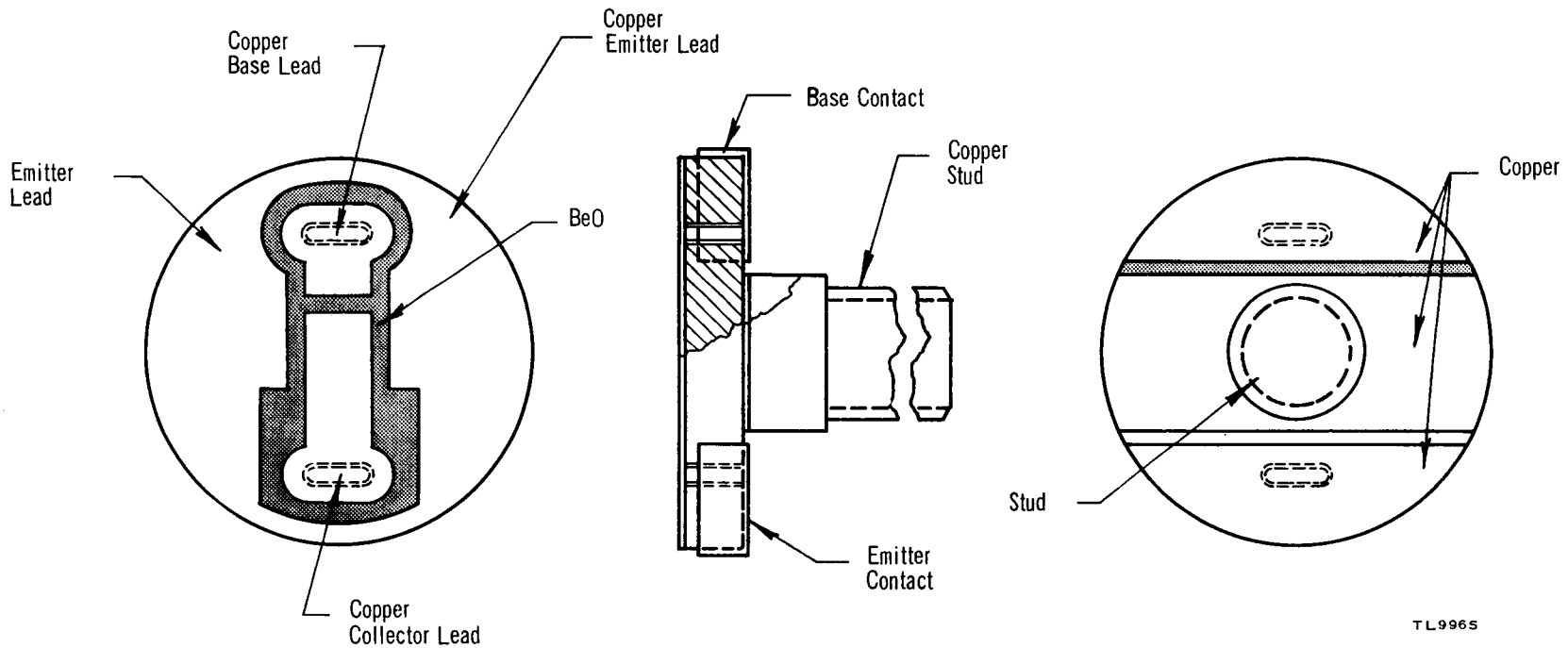

FIGURE 10 DETAILED DRAWING OF STRIPLINE PACKAGE

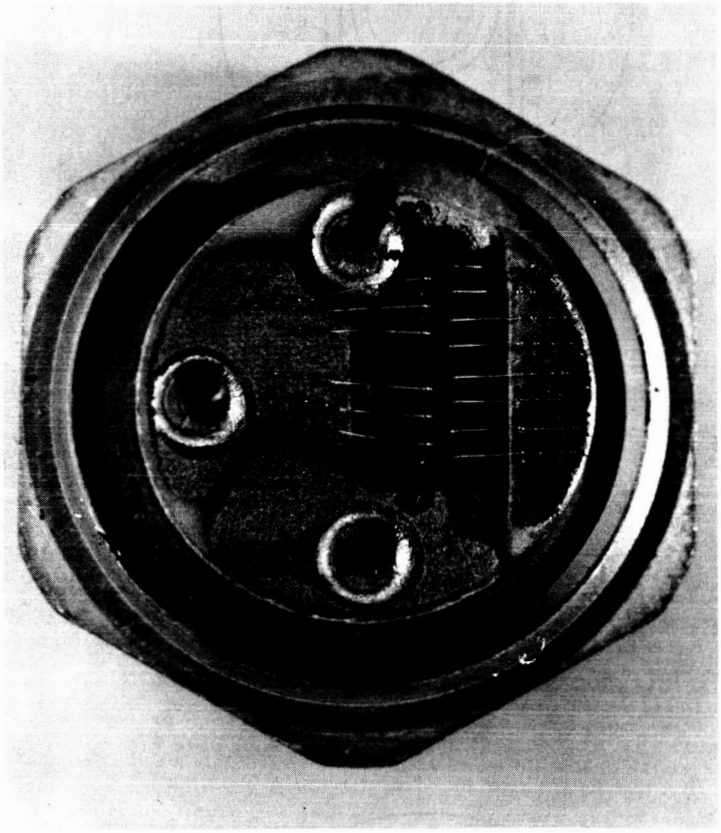

92SS2763P

FIGURE 11 TWO HALF PELLETS IN A GROUNDED EMITTER TO-60

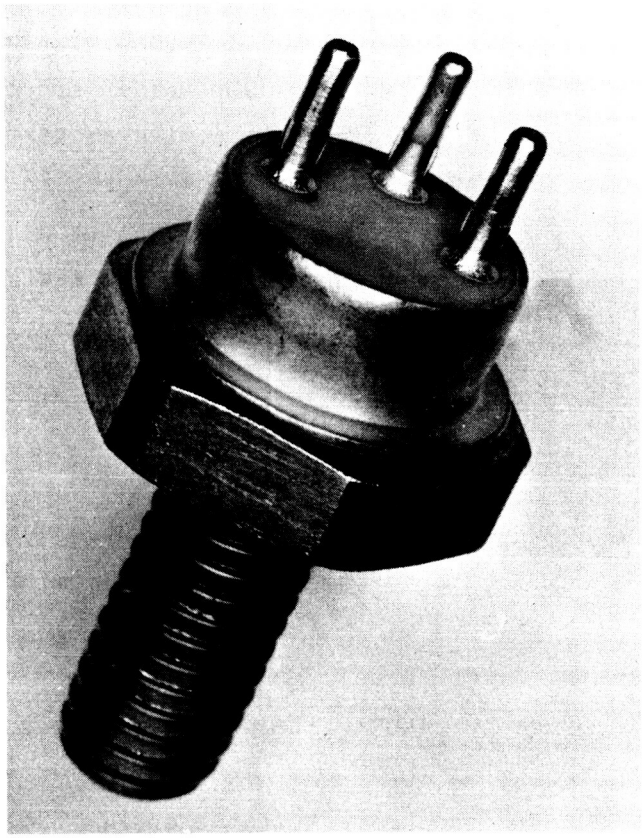

92SS2764P

FIGURE 12 SEALED TO-60

20 watts power out with 50 percent efficiency, the peak collector current is approximately 5.6 amperes. The peak voltage drop down the collector is 9.3 volts, assuming that one-half the collector current flows down the entire length of the collector contact. The voltage drop down the collector lead can result in a missmatch of the load and the output impedance for different parts of the device.

Half pellets were evaluated in the grounded emitter TO-60. Figure 13 shows a plot of power out versus power in and collector efficiency at 430 megacycles. Figure 14 shows a diagram of the tuned line circuit used. Figure 15 shows the socket used in the tuned line circuit. With 2.5 watts drive the half pellet delivers 10.4 watts with 59 percent efficiency. The half pellet meets the required gain and efficiency and delivers half of the required power out. The next step consists of getting the entire unit working.

c. Experimental Stripline Package

To solve the burnout problem for the full unit, an experimental stripline package was developed which gives equal emitter and base bond lead lengths as well as minimum distributed collector lead inductance. Figure 16 is the experimental package, showing the full unit (two half units mounted side by side). The pellets are mounted on a BeO insulator in the center of the slot. The emitter wires are bonded to the top of the stud on the left of the slot. The base wires are bonded over the emitter bond wires to the base ribbon on the left. The collector bond wires are bonded from the top of the BeO in the slot to the collector ribbon on the right. The base and collector ribbons are isolated from the stud by BeO insulators.

Figure 17 shows a plot of power out versus power in and efficiency for the full unit in the experimental package. Measurements were made in the tuned line circuit shown in Figure 14. For 7 watts drive, the unit delivers 21.5 watts at 52 percent efficiency. Higher power gain is needed to meet the contract objectives. This can be accomplished by either lowering the emitter lead inductance or redesigning

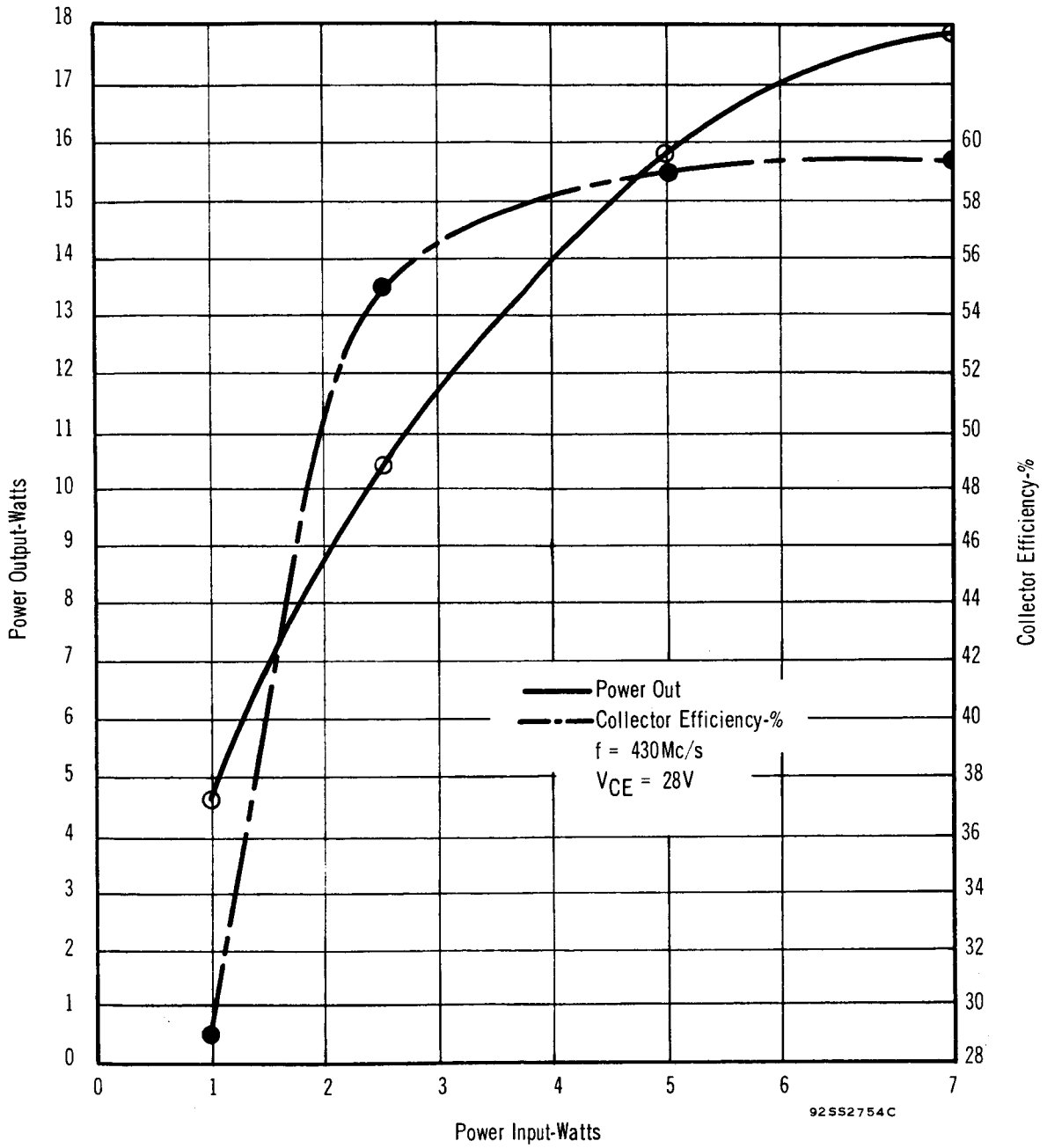

FIGURE 13 POWER OUT AND EFFICIENCY AS A FUNCTION OF POWER INPUT-½ TA2675

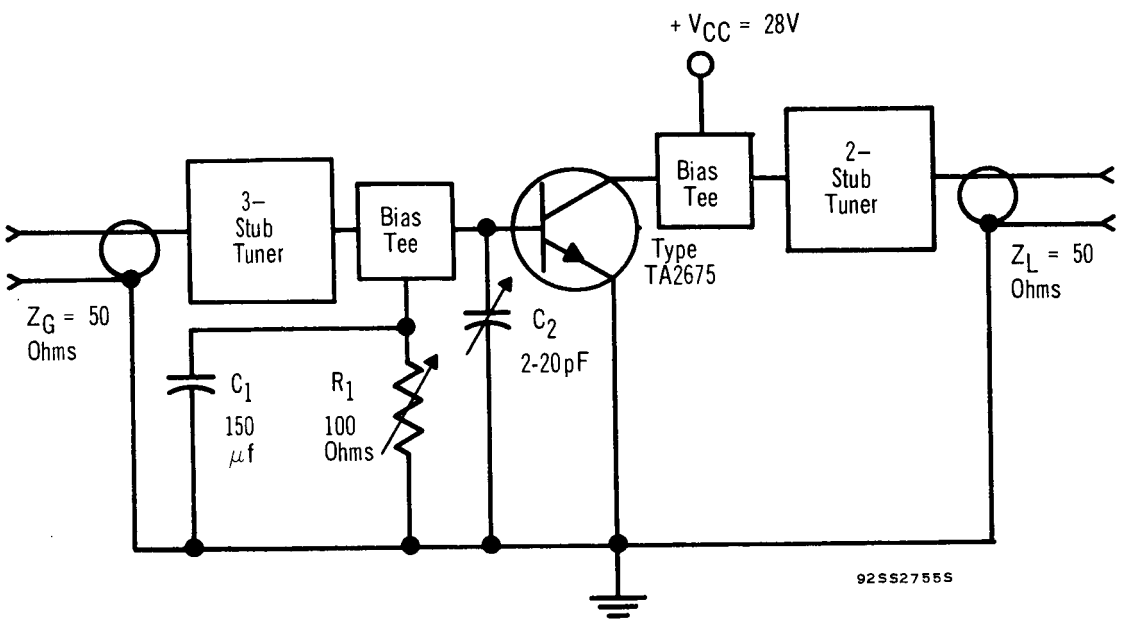

FIGURE 14 TUNED LINE CIRCUIT

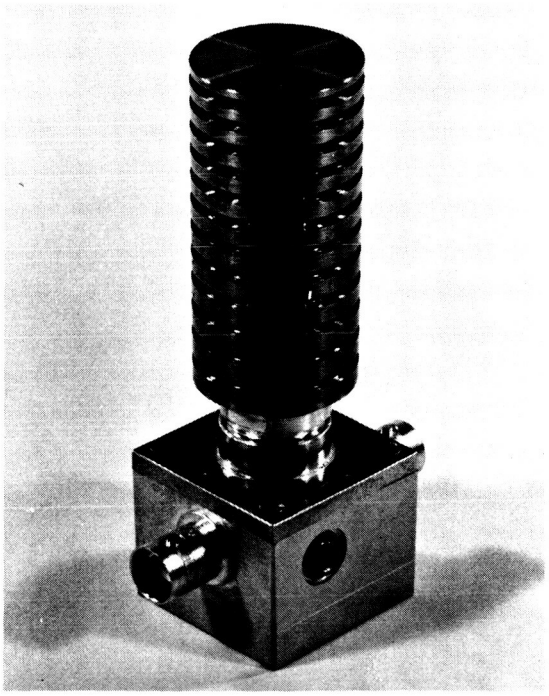

92SS2765P

a. Completely Assembled Socket

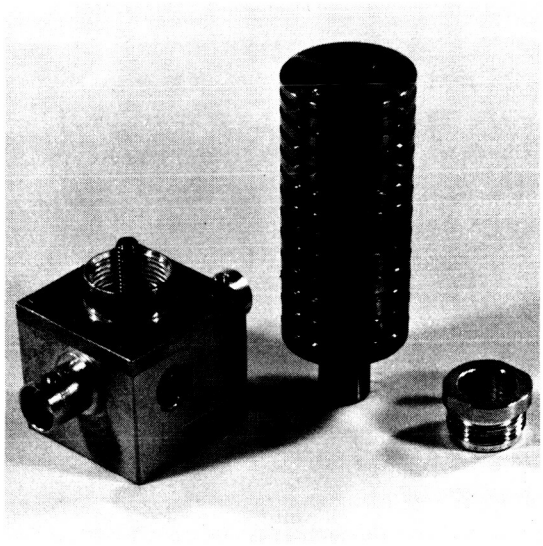

92SS2765P

b. Socket with Heat Sink Removed

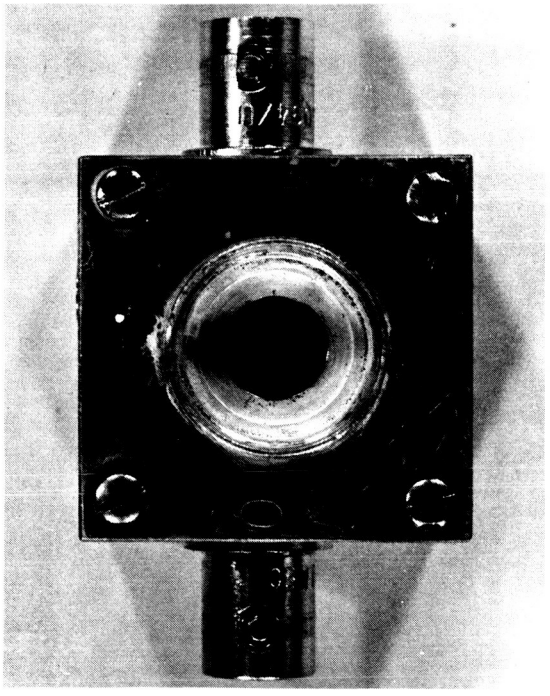

92SS2765P

c. Test Socket with Transistor Removed (Top View)

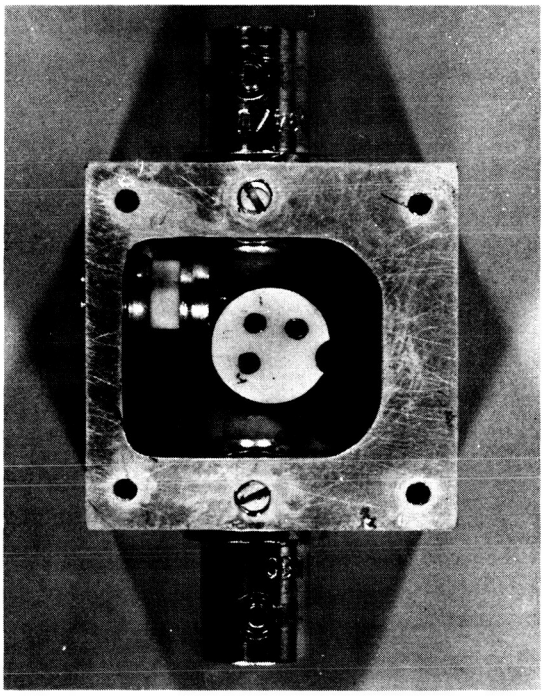

92SS2765P

d. Test Socket with Cover Removed (Top View)

FIGURE 15 TEST SOCKET FOR TUNED LINE CIRCUIT

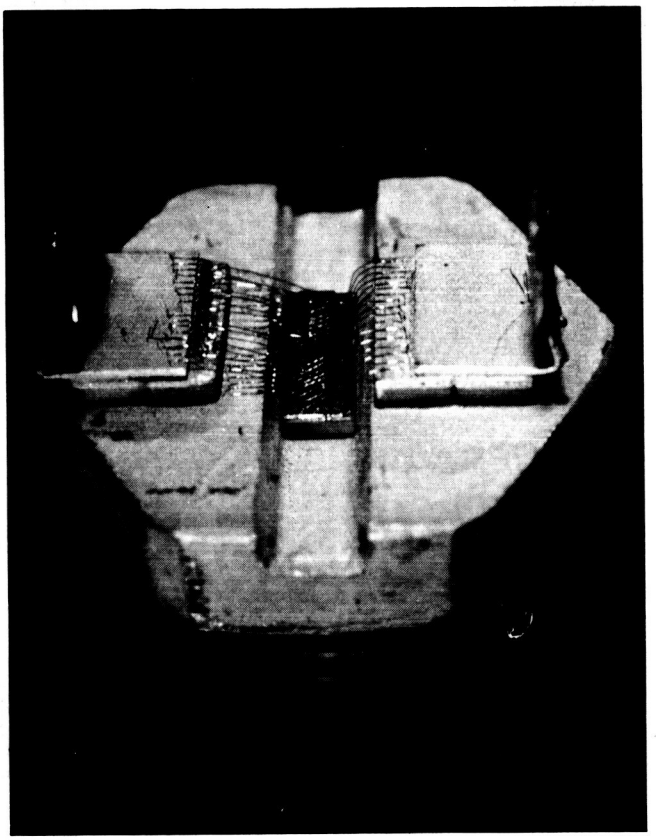

92SS2770P

FIGURE 16 EXPERIMENTAL STRIPLINE PACKAGE

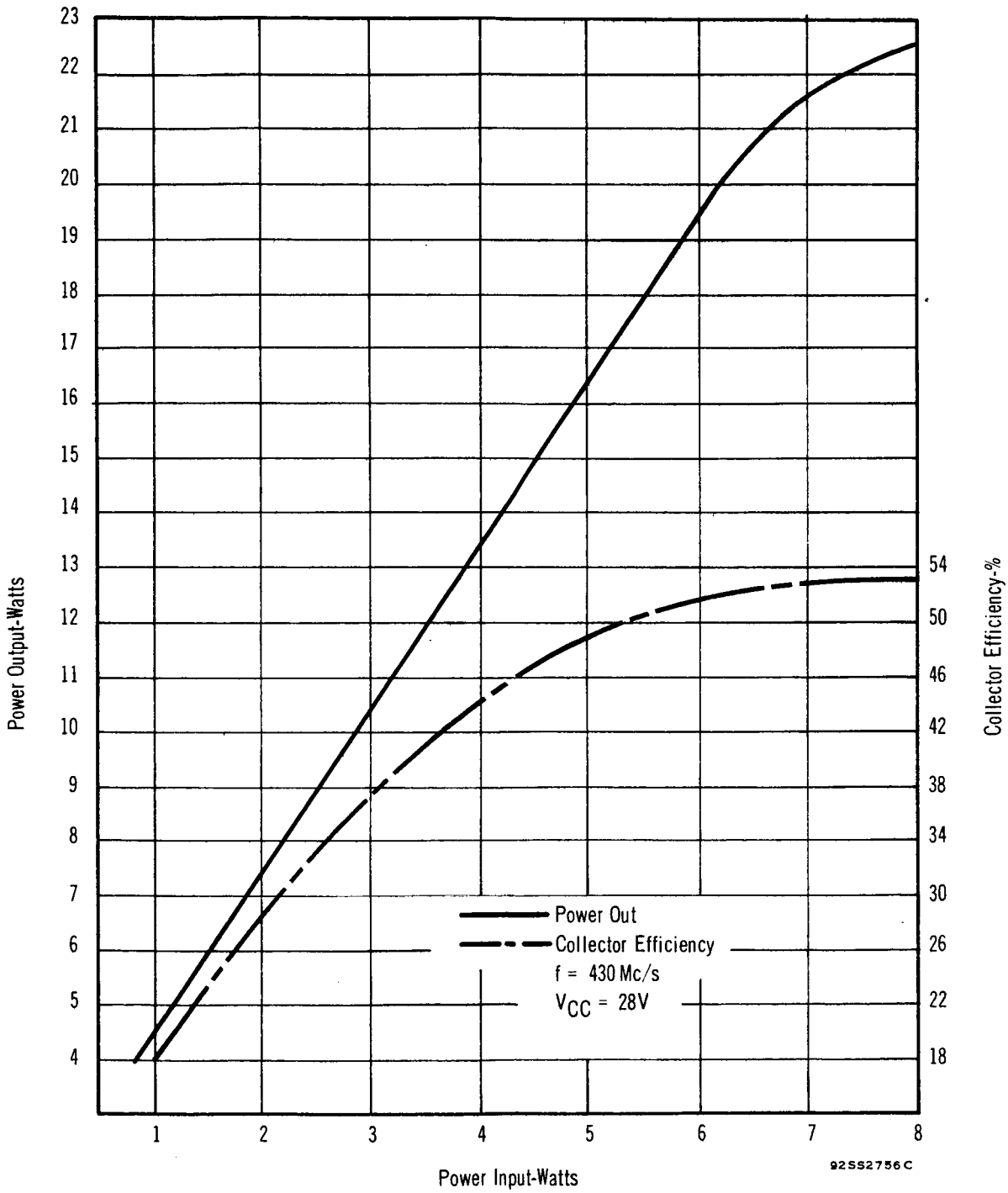

FIGURE 17 POWER OUTPUT AND EFFICIENCY AS A FUNCTION OF POWER INPUT
(FULL TA2675 IN EXPERIMENTAL STRIPLINE PACKAGE)

the pellet. RCA chose to redesign the pellet so it could be used in the grounded emitter TO-60 rather then requiring special undeveloped packaging techniques.

d. Pellet Redesign

To increase power gain and increase efficiency, the critical dimensions of the surface gwometry were reduced. Figure 18 shows the reduced cell dimensions of the redesigned unit. A total of 408 emitters is included in a 34 by 12 matrix. Figure 19 shows the completed unit. Table II shows a comparison of the surface geometry of the two units. The base area was reduced by a factor of two to increase collector efficiency. The emitter periphery was decreased from 1754 mils to 1,222 mils. Less emitter periphery is needed because of the higher collector efficiency that will result. Table III shows a comparison of the predicted high frequency characteristics of the first and second designs. A narrower base width of 0.015 mil, as compared to 0.017 mil, was used for the redesigned unit. Narrower base widths are possible because of the smaller emitter area and the lower probability of localized punch-through due to imperfections and other faults.

The results from the first group of units were disappointing. Only 15 watts could be obtained for 5 watts of drive. A plot of direct current beta versus collector current, shown in Figure 20, indicates that the cause of the low power out is poor current handling capability. Beta should peak over one ampere. The problem was thought to be caused by missalignment of the emitter in the P^+ grid. On some units the registration was so bad that the emitter opening in the oxide coincided with the P^+ grid opening in the oxide. The result is that the emitter has diffused into the P^+ grid. Poor emitter injection efficiency and a wider base width is found where the emitter diffuses into the heavier base doping in the P^+ region.

To determine quantatively the effect of emitter to P^+ spacing on power out, an experiment was made using the unit cell. A small

TABLE II

COMPARISON OF SURFACE GEOMETRY FOR THE FIRST AND SECOND DESIGN OF THE TA2675

	First Design	Second Design
No of Emitter Sites	408	408
Emitter Periphery (mils)	1754	1222
Emitter Area ($mils^2$)	122	57
Base Area ($mils^2$)	1160	575
$\frac{\text{Emitter Periphery}}{\text{Emitter Area}}\left(\frac{\text{mils}}{\text{mil}^2}\right)$	14.3	21.4
$\frac{\text{Emitter Periphery}}{\text{Base Area}}\left(\frac{\text{mils}}{\text{mil}^2}\right)$	1.51	2.13
Base Metalizing over (mil^2) Over Collector Oxide	325	150
Emitter Metalizing (mil^2) Over Collector Oxide	318	150
Pellet Size ($mils^2$)	70 x 60	30 x 85
Base Periphery (mils)	345	166

TABLE III

COMPARISON OF PREDICTED HIGH FREQUENCY
CHARACTERISTICS OF THE FIRST AND SECOND DESIGNS

	First Design	Second Design
Emitter Charging Time-τ_e(sec)	$.03 \times 10^{-10}$	0.015×10^{-10}
Base Transit Time-τ_b(sec)	1.54×10^{-10}	1.2×10^{-10}
Collector Depletion Layer Transit Time-τ_x(sec)	0.23×10^{-10}	0.23×10^{-10}
Collector Junction-Capacitance Charging Time-τ_c(sec)	0.37×10^{-10}	0.37×10^{-10}
Collector To Emitter Transit Time-τ_{ec}(sec)	2.17×10^{-10}	1.81×10^{-10}
Collector Capacitance (Pf)	34	18
Base Spreading Resistance (ohms)	.04	.04
Emitter Lead Inductance-Grounded Emitter TO-60(nH)	0.5	0.62
Current Gain Bandwidth Product-f_T(megacycles)	730	880
Power Gain at 430 Mc For 20 Watts	3.1	4.1

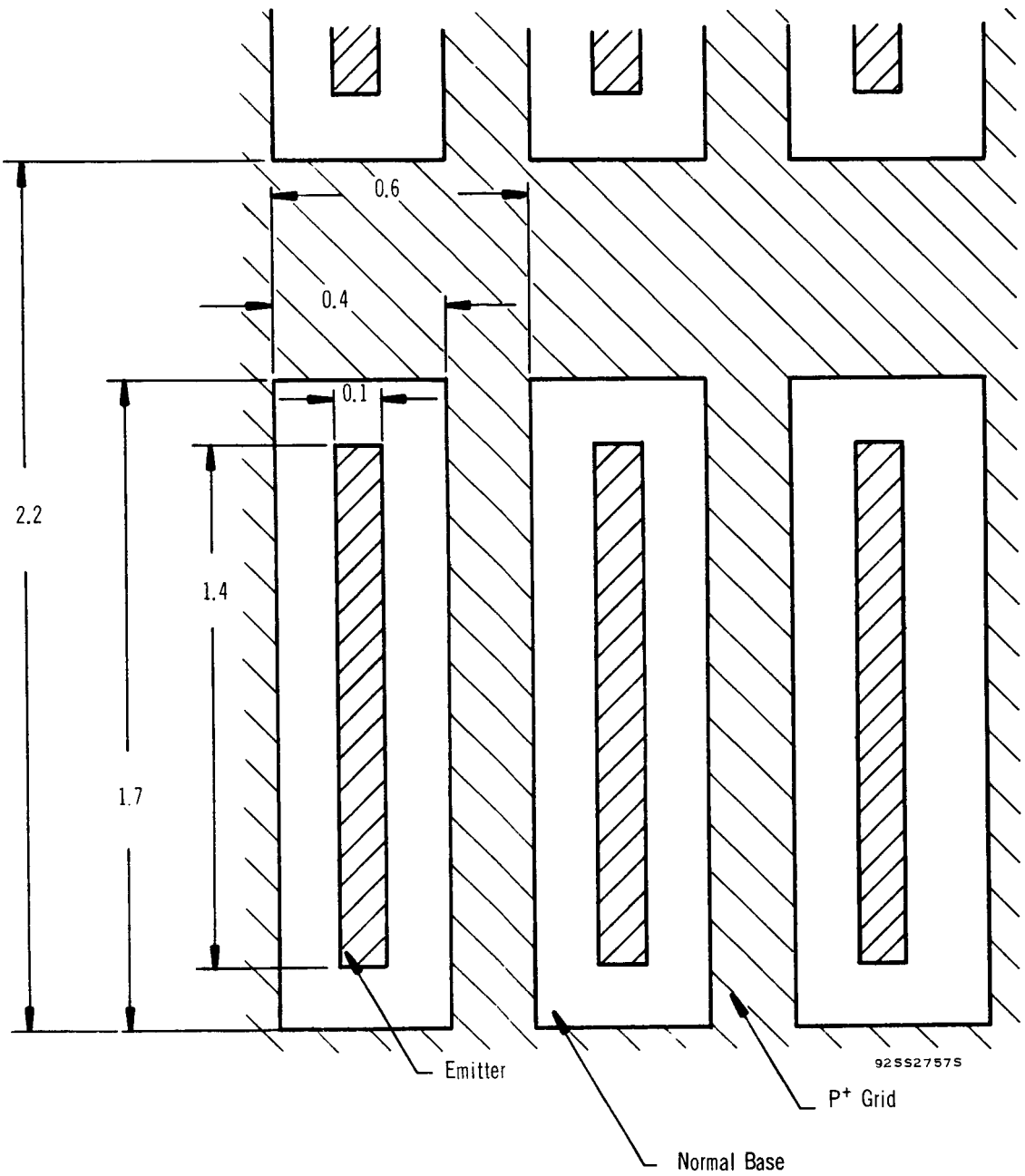

All Dimensions in Mils

FIGURE 18 CELL STRUCTURE OF REDESIGNED TA2675

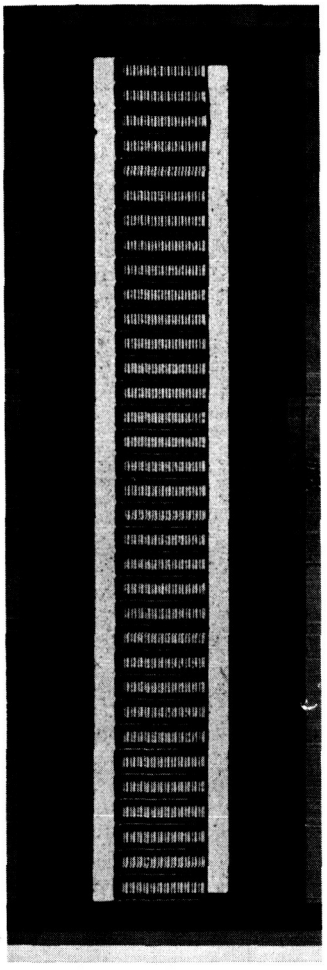

92SS2771P

FIGURE 19 MICROPHOTOGRAPH OF REDESIGNED TA2675

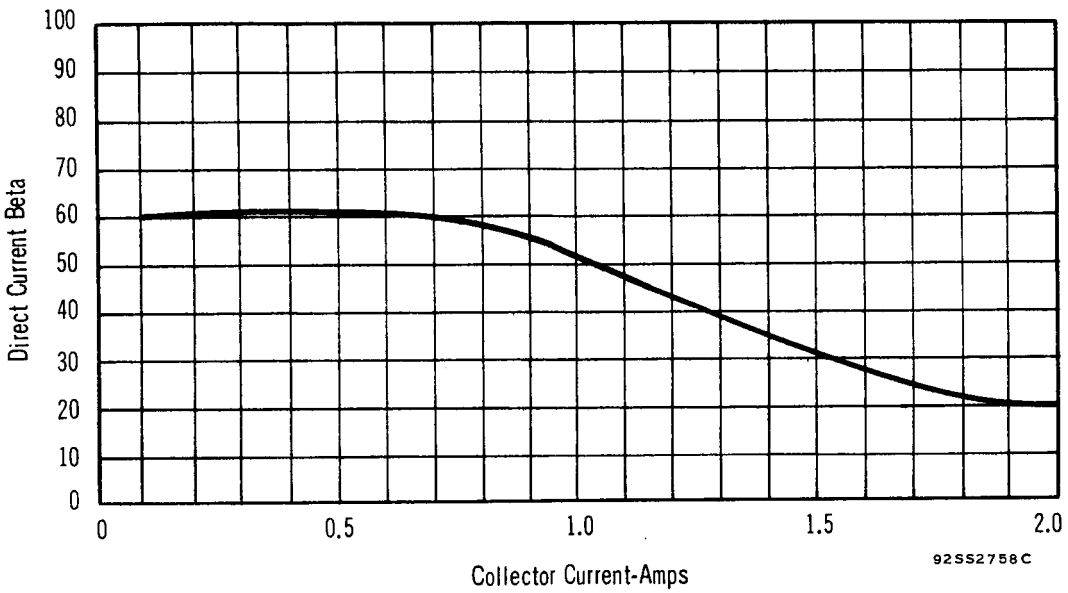

FIGURE 20 DIRECT CURRENT BETA AS A FUNCTION OF COLLECTOR CURRENT OF LOW POWER OUTPUT TA2675 UNIT

portion of a wafer was purposely misaligned rotationaly, so that perfectly aligned units and badly misaligned units could be obtained on the same region of the wafer. Figure 21 shows a plot of f_T versus P^+ to emitter spacing and Figure 22 shows a plot of 400 megacycles power out versus P+ to emitter spacing for the purposely misaligned units. Figure 22 indicates that if the spacing is decreased below 0.1 mil, power out is drastically reduced. Zero spacing means that the edge of the emitter and P^+ openings in the oxide conincide. Minus values indicate that they overlap. Perfect alignment on these graphs would be + 0.2 mil. The experiment indicates that P^+ to emitter spacing must be at least 0.1 mil for optimum performance. New sets of masks for the TA2675 were obtained to maintain a minimum P^+ to emitter spacing of 0.1 mil. Since the maximum P^+ to emitter spacing is 0.15 mil, the maximum allowable mask misregistration and misalignment is only 0.05 mil.

Figure 23 shows a plot of power out versus power in and collector efficiency obtained with the improved mask, for one of the better units. For 5 watts drive,20.5 watts power out was obtained with 70 percent collector efficiency. Measurements were made in the tuned line circuit. Figure 24 shows the redesigned unit in the grounded emitter TO-60 package that was used for the measurement.

Table IV shows a comparison of the contract goals, predicted results and the results achieved.

e. Radial Lead Package.

Work was done on a hermetric radial lead package to isolate all leads from the stud. Figure 25 shows a picture of the package developed. The pellet is mounted on a metalized BeO insulator which has a window frame sealed to it with a glass frit. The package is sealed by brazing the ceramic lid to the window frame with gold germanium. The emitter lead is the wide lead and the collector the narrowest.

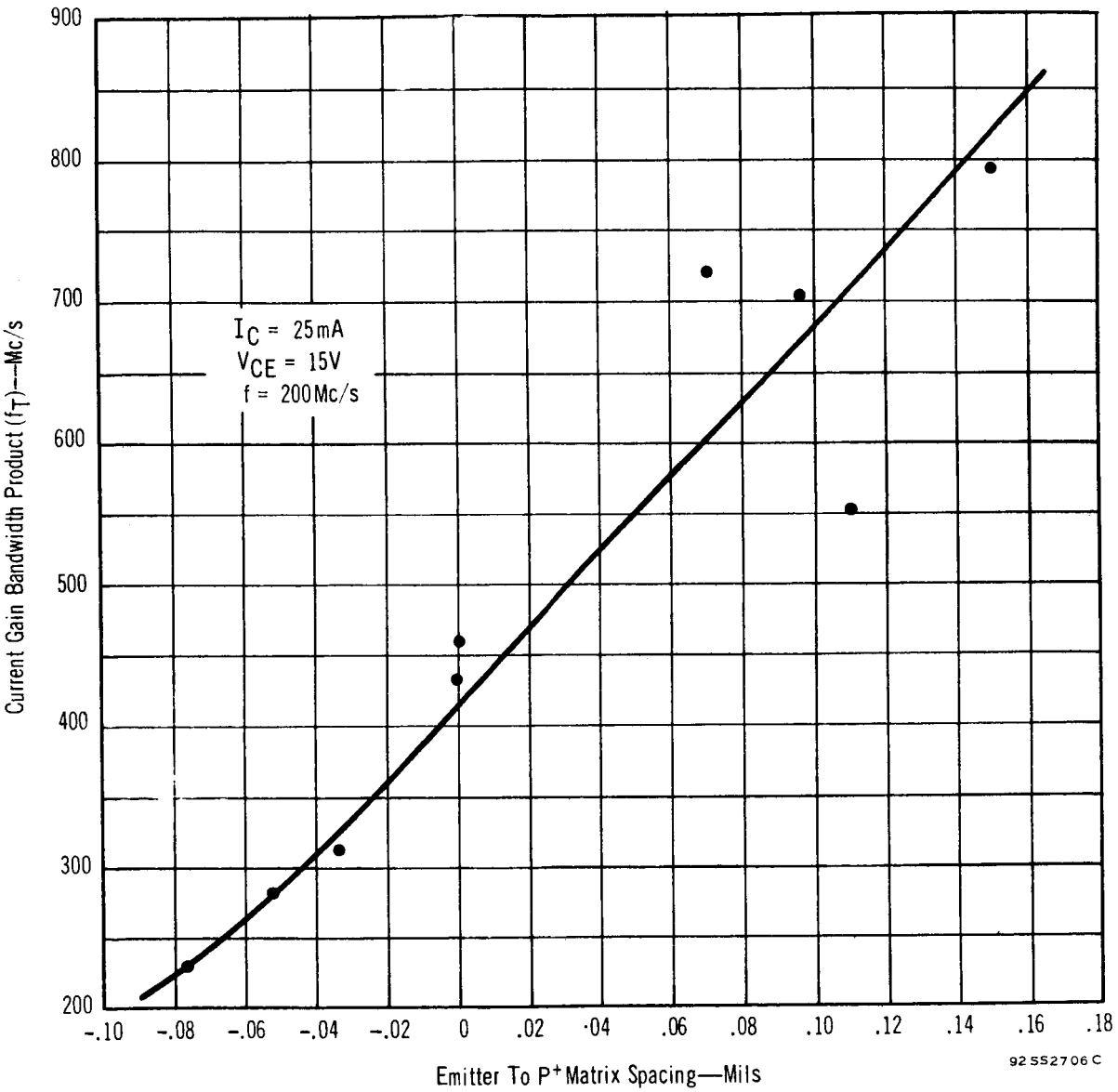

FIGURE 21 CURRENT GAIN BANDWIDTH(f_T) VS. EMITTER TO P+ MATRIX SPACING

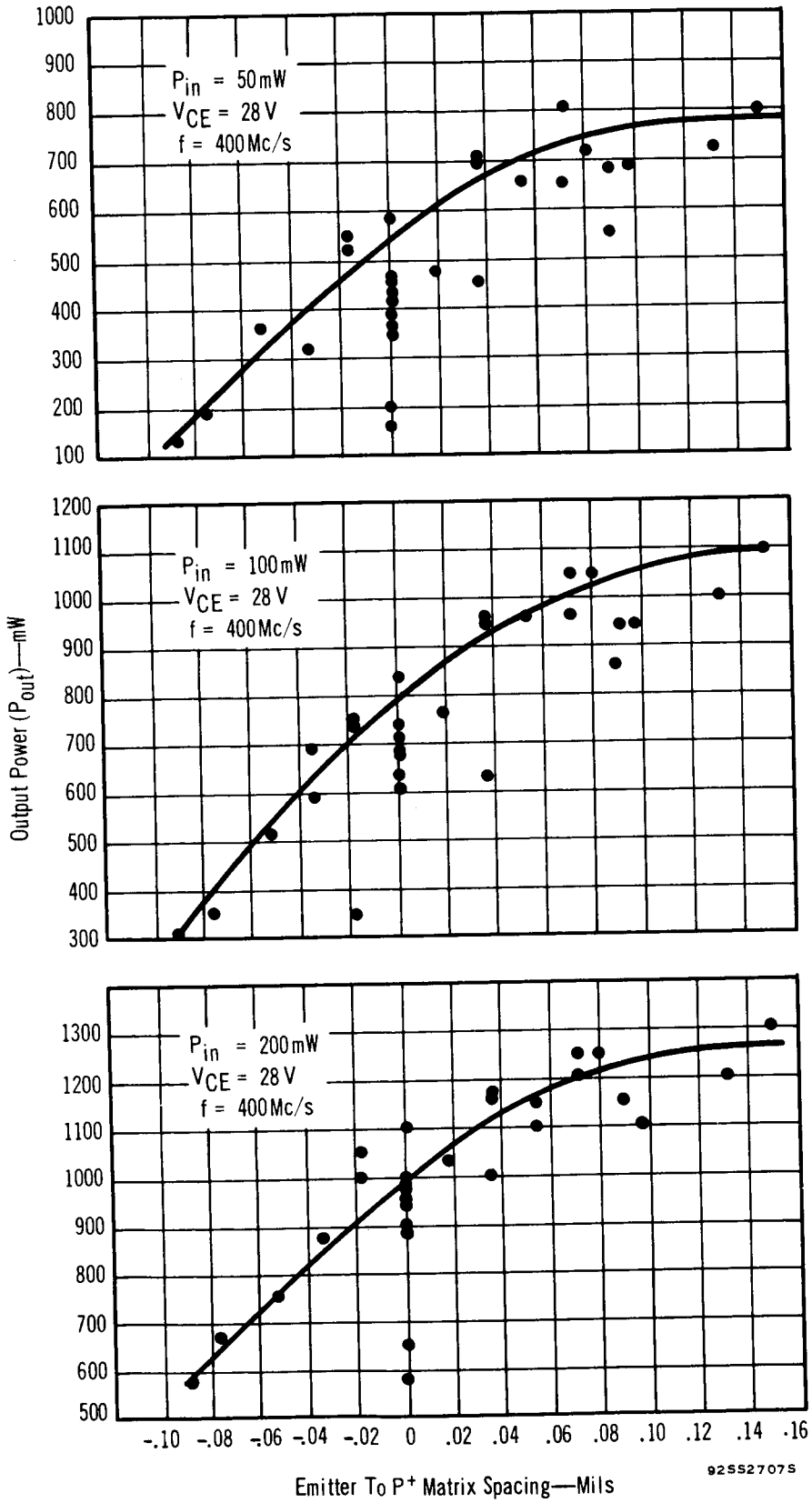

FIGURE 22 400 MEGACYCLE OUTPUT POWER VS. EMITTER TO P+ MATRIX SPACING

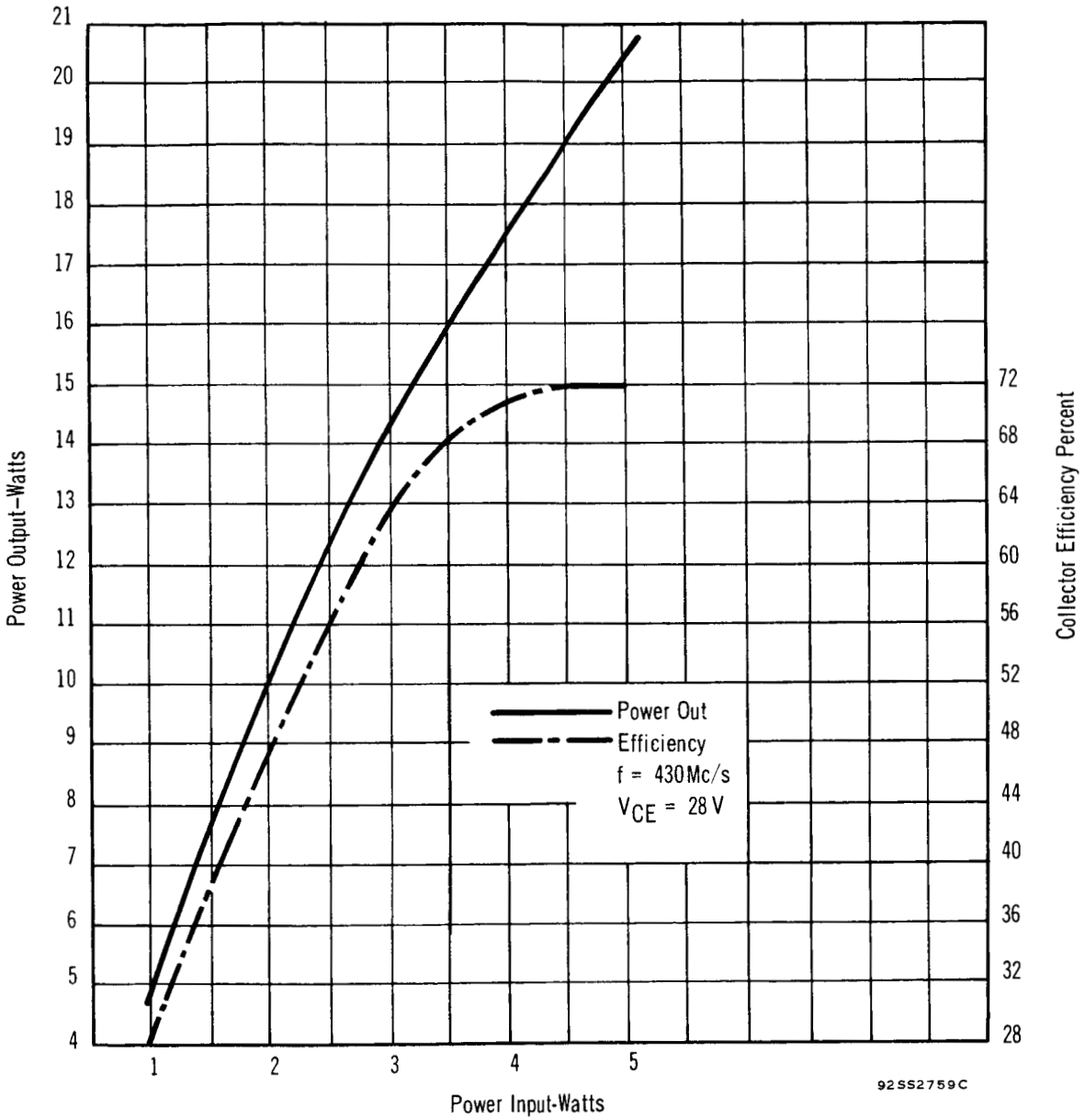

FIGURE 23 POWER OUTPUT AND EFFICIENCY AS A FUNCTION OF POWER INPUT–REDESIGNED TA2675

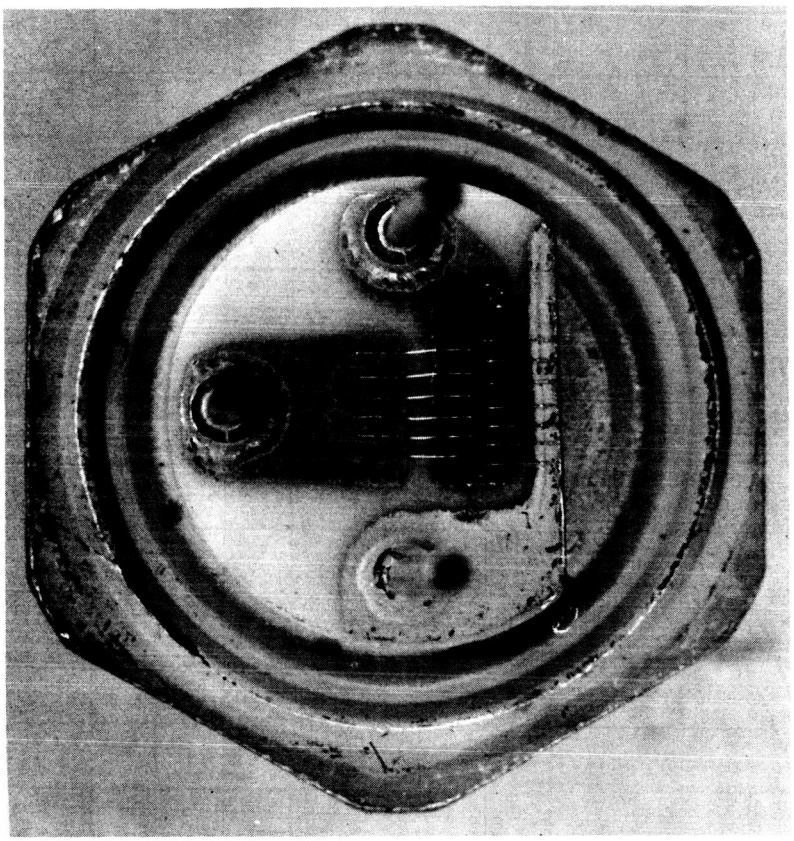

92SS2772P

FIGURE 24 REDESIGNED TA2675 IN A GROUNDED EMITTER TO-60

TABLE IV

COMPARISON OF CONTRACT GOALS, CALCULATED PERFORMANCE, AND PERFORMANCE ACHIEVED

Parameter	Contract Goals	Calculated Performance	Performance achieved with Best Units
Power Out V_{CE} =28 V, f=430 Mc P_{in} = 5 W	20 Watts	20 Watts	21.3 Watts
Power Gain V_{CE} =28 V, f=430 Mc P_{out}=20 W	6 dB	6.1	6.3
Collector Efficiency V_{CE} =28 V, f=430 Mc P_{out}=20 W, P_{in} =5 W	50%	-	70%
Thermal Resistance (θ_{j-c})	5°C/W	3.5°C/W	2.2 to 3.45°C/W

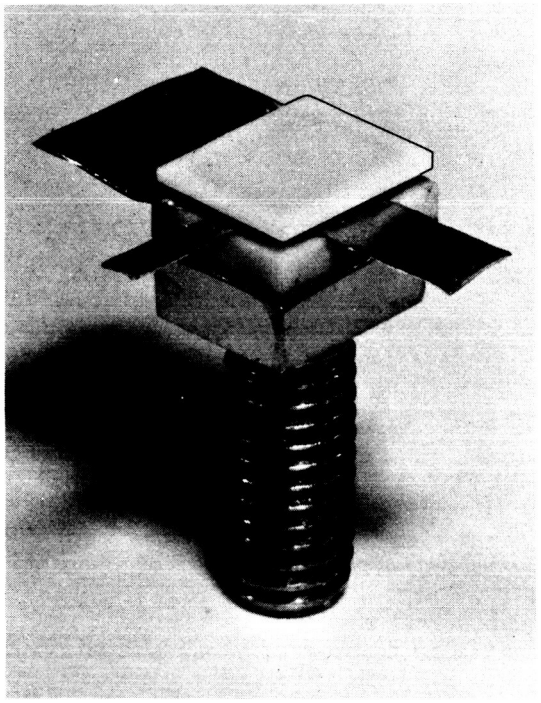

92SS2774P

a. Plan View

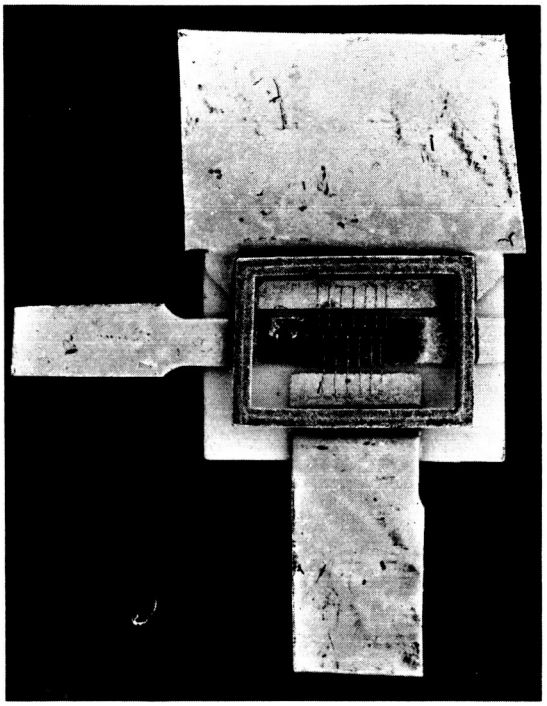

92SS2773P

b. Top View

FIGURE 25 RADIAL LEAD PACKAGE

Measurements made in the tuned line circuit showed 17.6 watts out and 58 percent efficiency with 5 watts drive. The lower power out is explained by the slightly higher emitter lead inductance, as compared to the grounded emitter TO-60.

f. Equivalent Circuit of Packages

In general parasitic inductance and capacitance within a transistor package adversely effect RF performance and, thus, should be minimal (consistent with the frequency range of operation). The package should show no spurious resonances within the frequency range of interest and residual losses at these frequencies should be as low as practical. In addition, while the package design should be consistent with the above and other system requirements (e.g., plug-in, coaxial, microstrip), the design should also meet the normal requirements of low cost, reproducibility, desired power dissipation capability, as well as other required environmental characteristics.

The packages developed for the TA2675 which operate in the UHF range, were of the plug-in type, (e.g., TO-60 case), and radial-lead types, (e.g., the microstrip versions). Typical measured values for the parasitic elements in these packages are shown in Figure 26. Element values were determined by direct measurements on dummy package units. The inductance elements were measured on a General Radio Company Type 1607-A Immitance Bridge. Mutual inductance effects were considered negligible. Confirming measurements of the important common emitter lead inductance were made using an insertion loss method.[4] Capacitance elements were measured directly, at a frequency of 1 megacycle, using the Boonton Electronic Corporation Model 75A-58 Capacitance Bridge.

Typical parasitic element values for the standard TA2675 unit, packaged in the plug-in type TO-60 case with emitter grounded, are given in Figure 26a. The emitter leads are bonded directly to a

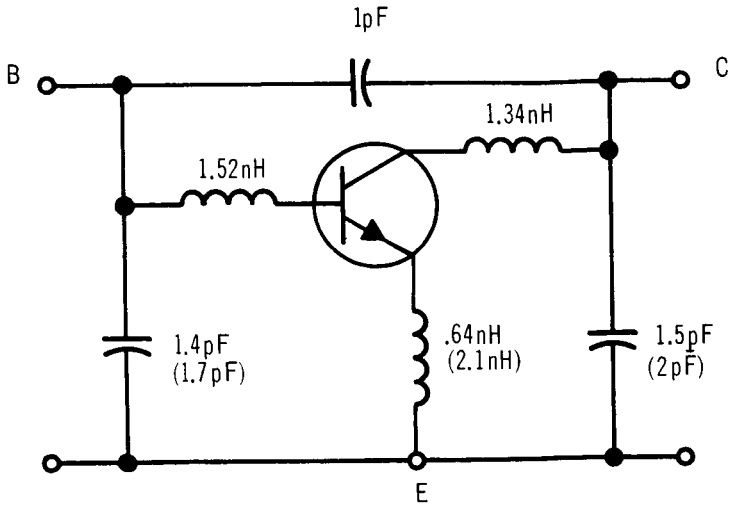

Values in Parenthesis Were Measured Using The Emitter Pin as The Emitter Connection. Others Were Made Using The Stud as The Emitter Connection.

a. Standard TO-60 Package

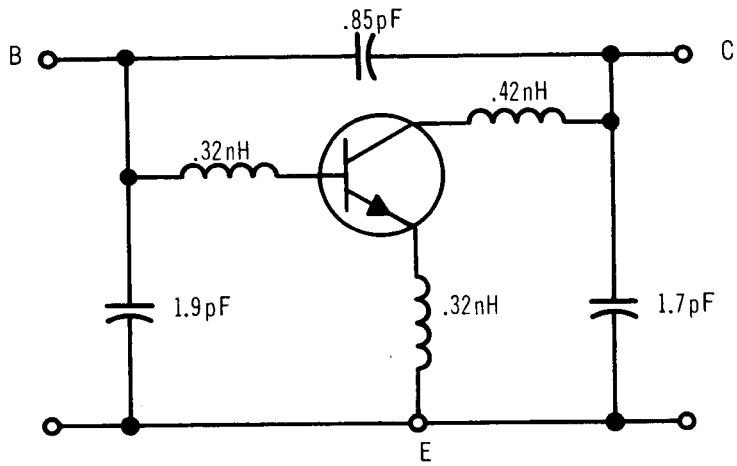

b. Experimental Stripline Package

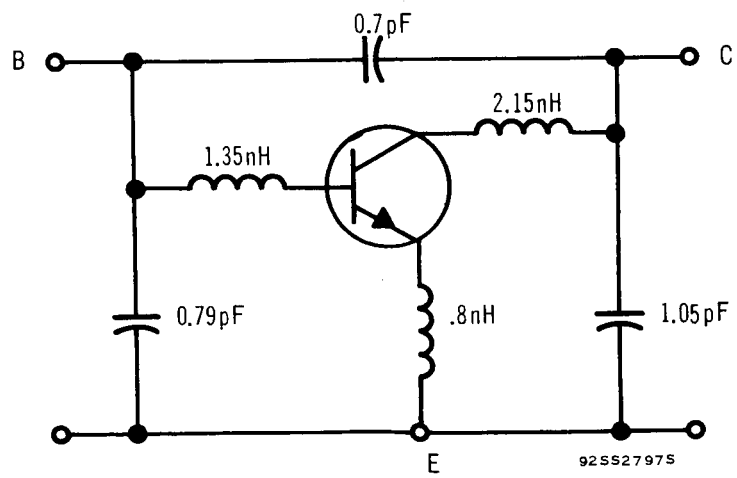

c. Radial Lead Package

FIGURE 26 CASE PARASITIC ELEMENTS

metallizing pad which leads directly to the stud to reduce the emitter lead inductance as much as possible. Note that the emitter lead inductance, as measured at the top edge of the TO-60 cap, is less than one-third the inductance which is measured at the emitter pin directly. (Parenthetical values in Figure 26a are those measured with reference to the emitter pin).

This is an important consideration in high frequency design work since common emitter lead inductance acts as a feed-back element, reducing stability, and also causes an additional resistive component to appear in the transistor input impedance. In general all common emitter Y-parameters are adversely modified by the common emitter impedance [4] and thus UHF transistor designs generally place great emphasis on the reduction of this parameter.

Base and collector lead inductances are relatively low for the plug-in TO-60 case and should present no difficulties in the present frequencies of interest (e.g., 200 to 500 megacycles).

Shunt capacitances, to the case, in the plug-in TO-60 unit are sufficiently low so as to cause no serious degrading effects up to about 700 megacycles. However, the interelectrode capacitance between base and collector, about 1 picofarad, is somewhat higher than desirable and may have contributed to the tendency for this package to develop low frequency oscillations under certain conditions of mismatch.

An experimental stripline package, shown in Figure 16 mounted on a 7/16-inch stud, had the parasitic elements shown in Figure 26b. This package configuration which is readily adaptable to stripline circuitry, showed extremely low parasitic inductance values for all transistor leads. The emitter lead inductance was approximately one-half of that measured in the plug-in TO-60 case under grounded emitter conditions. Shunt capacitances, to stud, were somewhat higher than the plug-in unit, but the important base-to-collector interelectrode capacitance was substantially lower. Improved RF performance could be expected in this package and has actually been

verified in experimental tests. However, the standard plug-in TO-60 case was found capable of good performance in conventional lumped-constant circuits and was selected for general program evaluation purposes because of highly developed production facilities for this type.

A smaller-version radial-lead package, shown in Figure 25, in which the pellet was isolated from the stud, was also evaluated. Parasitic elements measured for this unit, which is also adaptable to strip-line techniques, are given in Figure 26(c). The emitter lead inductance for this particular devi e measured somewhat higher than the other two versions evaluated. However, the basic design concepts used in this version can lead to much lower values.

As mentioned previously, the plug-in TO-60 case package was selected for the sample units which were delivered on this program. Extensive data for performance in this package has been collected during the course of this program.

g. Measurement of f_T

The gain-bandwidth products shown in Figure 27 were determined from small signal parameters as measured on the General Radio Company Type 1607-A Transfer-Function Bridge. Small-signal β measurements were made on a number of early samples incorporating the second design. These units are from the group that gave low power output because of the small emitter to P^+ spacing previously described. Later units with the correct emitter to P^+ spacing, oscillated during measurements, so that results could not be obtained. However, f_T values of the later units should be higher than the following measurements indicate. Figure 21 indicates the effect of emitter to P^+ spacing on f_T.

Sample TA2675 units and the averaged values were used to determine f_T from the relation:

$$f_T = \beta f \qquad (26)$$

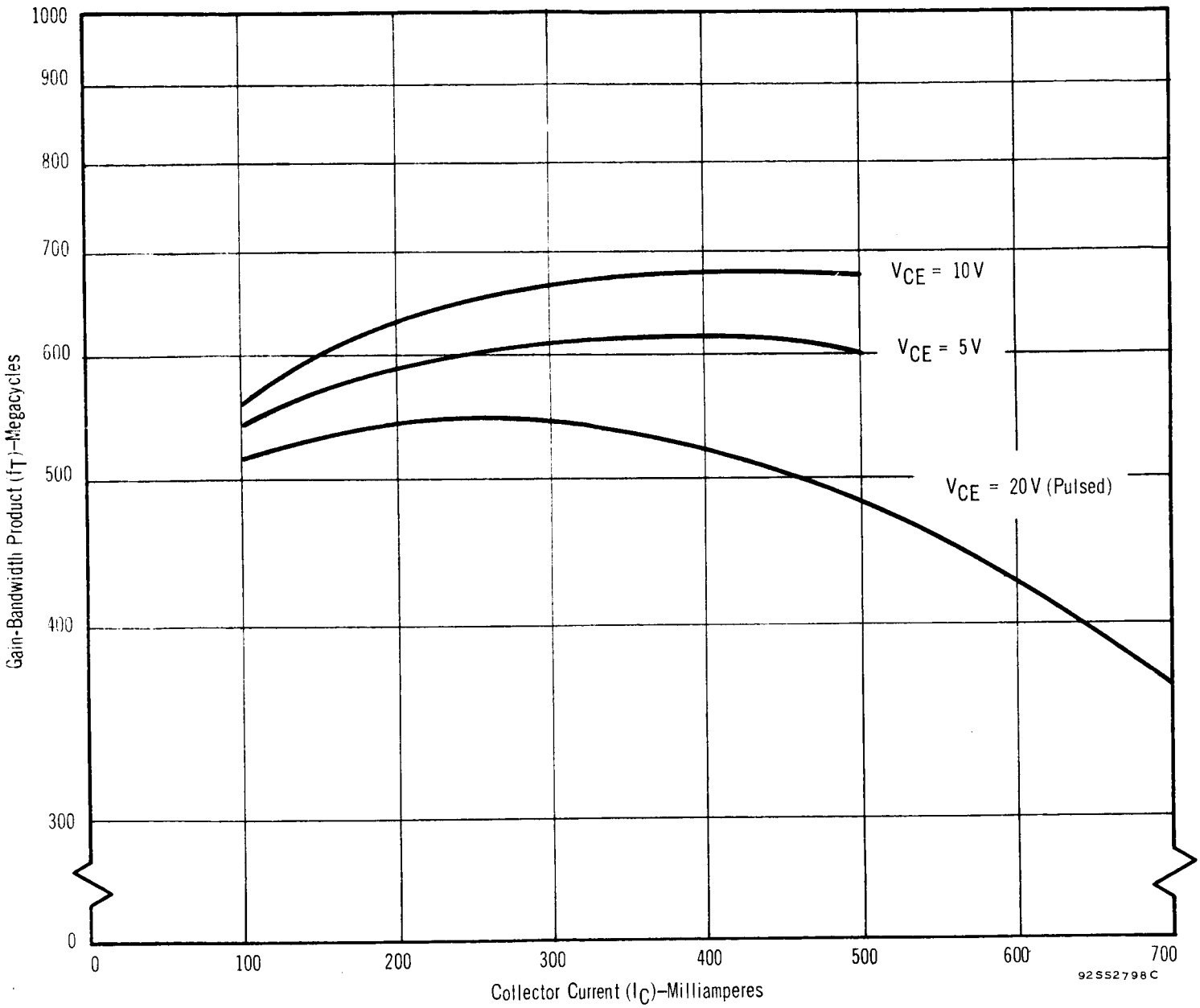

FIGURE 27 GAIN-BANDWIDTH PRODUCT VERSUS COLLECTOR CURRENT TYPE TA2657

The measurements were made at 300, 400, and 500 megacycles. Measurements were made at bias levels of 5 and 10 volts and with collector currents up to 500 milliamperes to avoid spurious results due to the appearance of second breakdown effects. Operation at these levels also avoided degradations due to general thermal effects, since heat sinking possibilities for the bridge test fixture were limited.

An attempt at higher-level operation was made through the use of simple pulse techniques. The data shown in Figure 27 was obtained at the 20-volt bias level, with the transistor pulsed on for about 50 milliseconds at a 5 percent duty cycle. The collector current, under these conditions, could be increased to about the 900 milliampere level before second breakdown (S_b) effects again appeared. An oscilloscope was used to sample the collector current, and second breakdown effects could be determined from the decay in the pulse current level. Use of a limiting resistance in the emitter generally prevented run away damage. The pulsed data shown in Figure 27 was obtained just below this observed level. The value of f_T at (V_{CE} = 20 volts), as measured by the pulse technique, is somewhat lower than the low level dc measurements. This appears to be due to general thermal effects since pulse measurements at the 5 and 10 volt level generally agreed with the dc measurements at these voltages.

Bridge measurements, thus, indicate that f_T is in the order of 600 to 700 megacycles at the 400 to 500 milliampere collector current level. The f_T values is higher than 700 megacycles on later units that incorporated the correct P^+ to emitter spacing.

h. Determination of $r_{bb'}$

The base spreading resistance is, at best, a very difficult parameter to determine with accuracy. The effect of parasitic elements tends to mask these determinations, especially at medium frequencies. However, at very high frequencies, i.e., where $f >> f_{BCO}$, the impedance of $C_{b'e}$ and $C_{b'c}$ is very much smaller than $r_{bb'}$, so that the base

resistance becomes the significant part of the series input resistance. At these same very high frequencies; however, emitter lead inductance increases the effective input resistance so that:

$$R_{in} = r_{bb'} + \omega_T L_e \qquad (27)$$

where L_e is the emitter lead inductance.

Thus, $r_{bb'}$ can be approximately determined by measuring the real part of h_{ie} at some appropriate high frequency. Emitter inductance is best determined from direct experimental measurements.

For the TA2675 at 400 megacycles, with I_C= 500 milliamperes @ V_{CC}=10 volts, $Re\left|h_{ie}\right|$ was found to be approximately 2.7 ohms (as determined from transfer-function bridge measurements). The emitter lead inductance (L_e) under grounded emitter conditions in the plug-in TO-60 case was determined to be in the order of 0.62 nanohenry. The value of f_T was previously found to be in the order of 680 megacycles.

Thus, from experimentally determined values, $r_{bb'}$ can be determined as follows:

$$\begin{aligned} r_{bb'} &= R_e \left|h_{ie}\right| - \omega_T L_e \\ &= 2.7 - 2.6 \text{ ohms} \\ &= 0.1 \text{ ohms} \end{aligned}$$

Three measurements were required to arrive at this value of $r_{bb'}$. Slight errors in making any one of the three measurements would cause the measured $r_{bb'}$ to vary considerably. The results agree closely with the $r_{bb'}$ value of 0.04 ohm predicted in Section II-B8. Therefore, $r_{bb'}$ is very small in comparison to $W_T L_e$ and can be neglected.

i. Measurement of Small Signal Input and Output Parameters

Small-signal parameters were measured at 300, 400, and 500 megacycles using the General Radio Company Type 1607-A Immittance Bridge. Measurements were generally limited to a maximum V_{CE} of 10 volts and a maximum I_C of 500 milliamperes, in the dc tests, to avoid

second breakdown effects which appear at higher power operating levels. Some data was obtainable at V_{CE} = 20 volts and V_{CE} = 28 volts, but at I_C levels below 200 milliamperes.

The data for h parameter measurements, which are plotted in Figures 28, 29 and 30 illustrate the very low input and output impedances for the type TA2675 transistor. It is seen that the real part of the series input impedance, at 430 megacycles, is about 2.5 ohms when V_{CE} is about 10 volts. It must be remembered that a substantial component in this real part is due to the effect of the common emitter inductance. The base resistance, at this frequency and current level, is much less than one ohm, thus, emitter inductance contributes the major portion of the input resistance. The data shown is for the grounded-emitter configuration which has the least amount of emitter inductance. The real part of the input impedance would have increased substantially if the emitter connection had been made through the emitter pin alone. The imaginary part of the input impedance indicates a slight inductive component, which, at these frequencies, is probably composed largely of package parasitic inductance elements seen by the input circuit.

The output impedance is highly capacitive, at typical operating conditions, with the real part of the impedance (at 430 megacycles and V_{CE} = 10 volts) in the order of seven ohms. At V_{CE} = 20 volts and I_C = 200 milliamperes, the real part of the output impedance is in the order of ten ohms. At the typical operating level of V_{CE} = 28 volts and $I_C \cong$ 600 milliamperes the output impedance appears to be in the order of 15 ohms and has been largely verified in the design of matching networks used at this level.

Prelininary determinations for high level parameters, e.g., V_{CE}= 28 volts, I_C = 1.0 ampere, were made using the General Radio Company Type 1607-A Bridge under pulse conditions. Pulse lengths of about 50 milliseconds and 5 percent duty cycle were obtainable from a simplified pulsing unit, but the measurements which were made still gave indications of excessive power dissipation in the device. Further work in this area was necessary and , therefore, systematic pulse data was secured for this program.

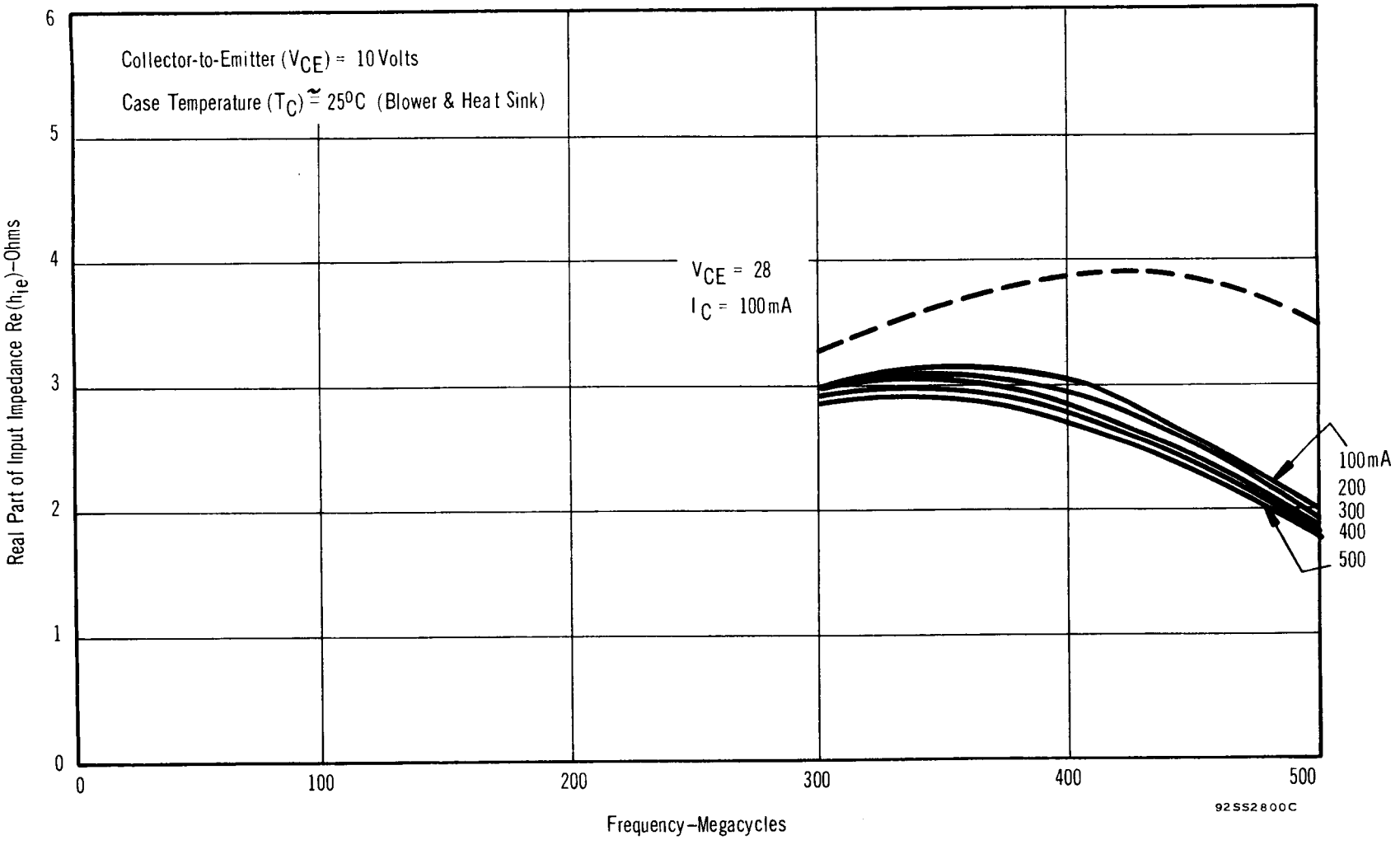

FIGURE 28 SERIES INPUT RESISTANCE AS A FUNCTION OF FREQUENCY

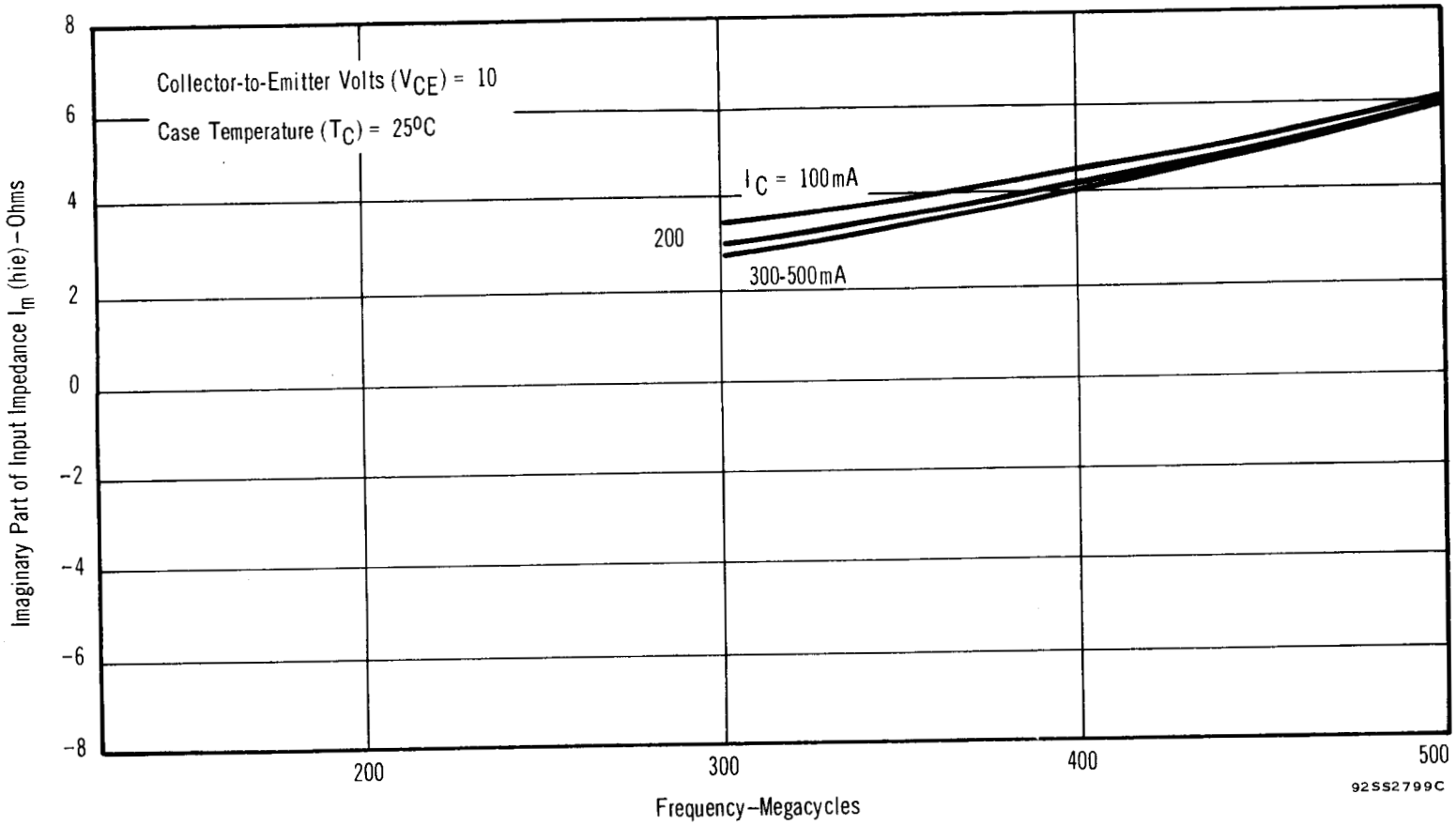

FIGURE 29 SERIES INPUT REACTANCE AS A FUNCTION OF FREQUENCY

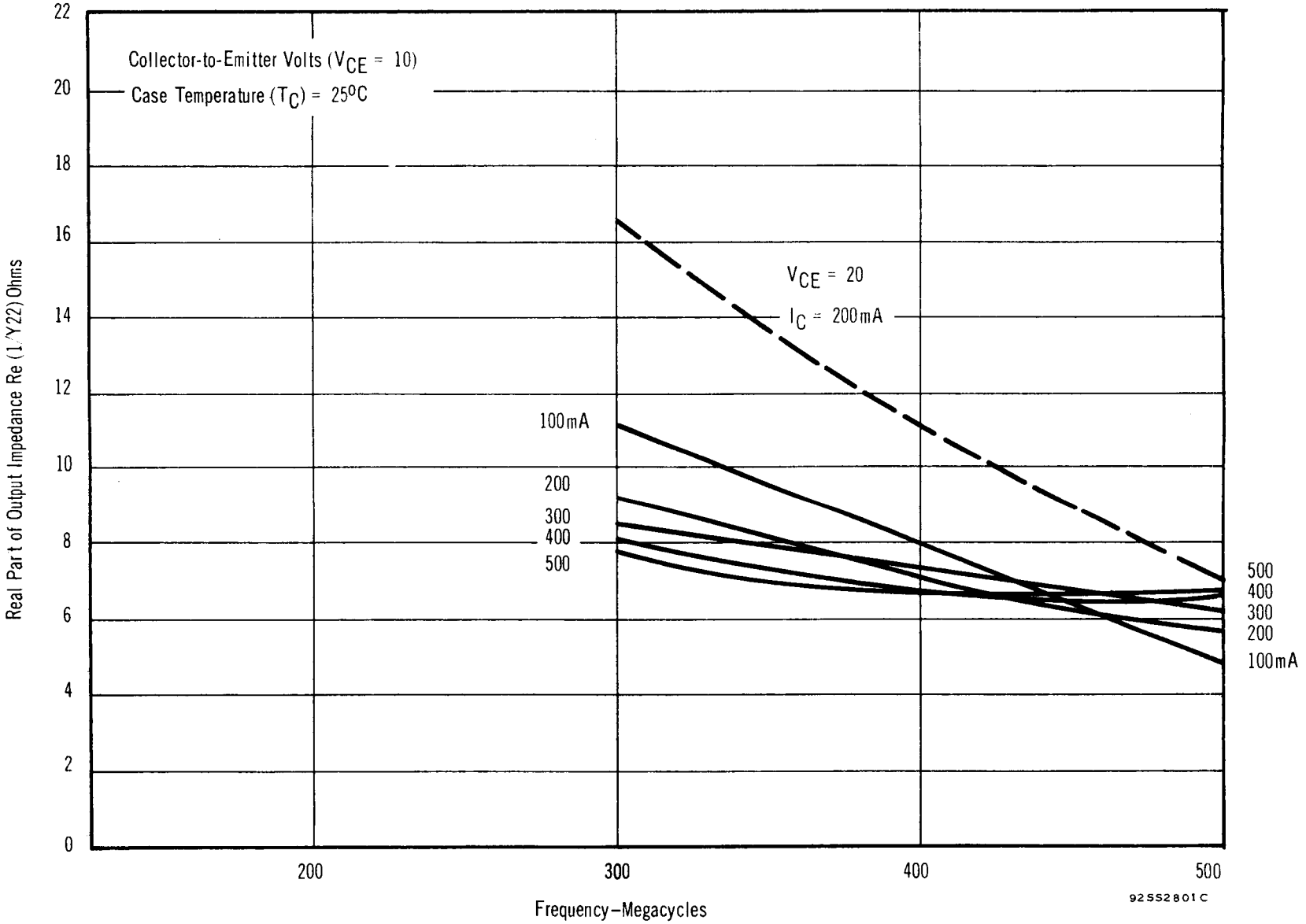

FIGURE 30 OUTPUT RESISTANCE AS A FUNCTION OF FREQUENCY

j. Measurement of Thermal Resistance

Measurements were made by monitoring the change in V_{BE} with increasing device temperature resulting from power dissipation. The measurement was made on a Tektronix (type 541) oscilloscope equipped with a Type Z plug-in unit for sensitive voltage measurement. A diagram of the test circuit is shown in Figure 31. Measurements were made at a collector current of approximately 1.0 ampere and a temperature differential of approximately 15°C. The conditions were arrived at in a manner such that the measurement was not influenced by local thermal effects due to second breakdown. This was accomplished by keeping the collector voltage in the 5 to 6 volt range, which is generally free of this condition. Measurements on nine TA2675 units of the final design, ranged from 2.2 to 3.45°C/W with an average of 2.6°C/W.

k. Environmental Testing

TA2675 final samples were subjected to the hermetic seal, temperature cycling, and shock tests indicated in the device specifications. The devices were not subjected to the specified lead fatigue and soldering tests because the TO-60 package has passed identical tests in previous applications. No leakers were detected in the hermetic seal test and no degradation was observed in the junction characteristics of the devices in the temperature cycling and shock tests. However, some power output degradation occurred, as indicated in Table V. The degradation occurred during the final phase of the power output tests rather than during the envoronmental tests. The units (No. 14 and No. 22) that suffered the most degradation exhibited very leaky emitters after the final power output test. This degradation was caused by mistuning during the final output power tests rather than environmental defects.

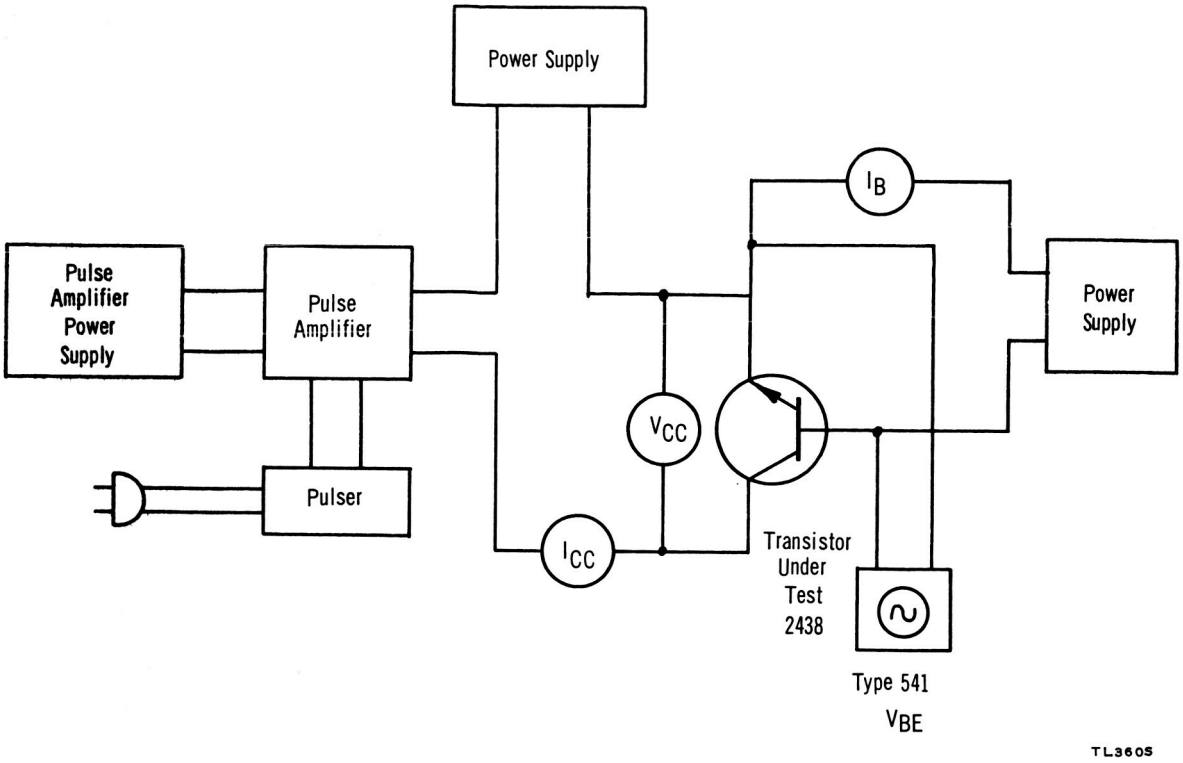

a. Test Circuit

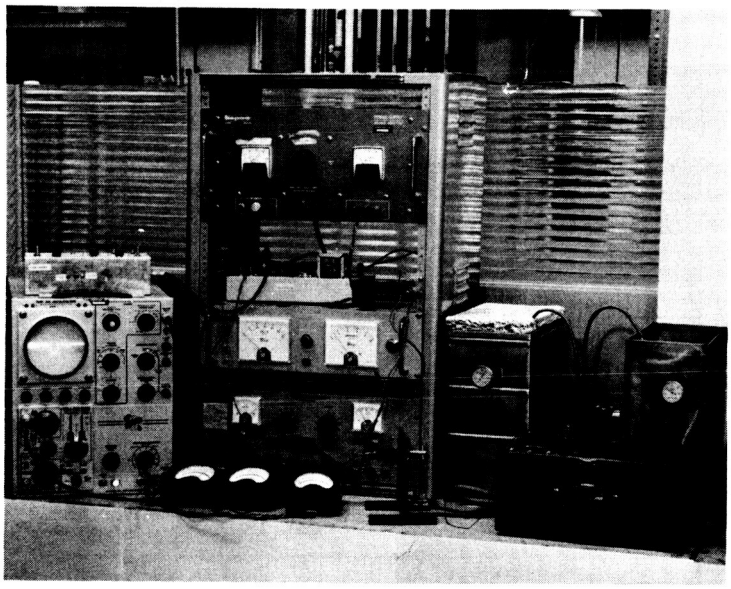

b. Test Set

FIGURE 31 THERMAL RESISTANCE TEST CIRCUIT AND TEST SET

TABLE V

DATA OBTAINED FOR TEN FINAL TA2705 SAMPLE
UNITS SUBJECTED TO POWER OUTPUT AND
ENVIRONMENTAL TESTS

	Initial Readings					Post Shock 1500g for 0.2m sec			Post Temperature Cycling -65 to 200°C 5 Cycles				
Lot No. E-55-1 Unit #	BV_{EBO} @100μA	BV_{CBO} @100μA	I_{CEO} @28V (nA)	P^*_{out} W	I^*_C mA	BV_{EBO} @100μA	BV_{CBO} @100μA	I_{CEO} @ 28V (nA)	BV_{EBO} @100μA	BV_{CBO} @100μA	I_{CEO} @ 28V (nA)	P^*_{out} W	I^*_C A
3	3.5	58	1.2	17.7	1.000	3.5	58	1.5	3.5	58	1.6	16.7	.975
5	3.4	60	1.0	16.9	.960	3.4	60	1.3	3.4	60	2.0	16.7	.900
8	3.3	55	.24	17.5	.84	3.3	55	.30	3.3	55	.31	17.1	.950
14	3.1	56	2.8	15.6	.880	3.1	56	2.9	3.1	56	3.2	14.1	.800
17	3.5	58	.24	16.2	.950	3.5	58	.30	3.5	58	.28	16.2	.955
19	3.6	57	.40	17.7	1.250	3.6	57	.48	3.6	58	.46	16.7	.850
22	3.7	58	.98	17.8	1.000	3.7	58	2.0	3.7	58	7.8	17.8	.950
23	3.4	55	.56	18.2	.950	3.4	55	1.3	3.4	55	1.6	15.1	.850
25	3.5	59	.22	17.7	1.000	3.5	59	.28	3.5	59	.28	16.1	.890
32	3.5	60	.32	16.2	.850	3.5	60	.40	3.5	60	.41	16.9	0.850

* at: f = 430 Mc
V_{CE} = 28 V
P_{in} = 5 W

E. Circuit Evaluation of TA2675

The circuit evaluation effort was confined to Class C operation of the TA2675 as a continuous signal RF power amplifier. Lumped constant element circuits were used.

1. Lumped Constant Circuit Design Approach

To obtain 20 watts of RF power output at 430 megacycles, the required value of collector load resistance must be established. For Class C operation, the load resistor can be determined as follows

$$R_e = \frac{V_{CE}^2}{2P_o}$$

$$\frac{28^2}{(2)(20)} = \frac{784}{40} = 19 \text{ ohms}$$

The above value of collector load resistance assumed that the transistor has zero saturation voltage and will be lower in value depending upon saturation voltage of the device.

If the transistor is only capable of having a collector efficiency of 50 percent, then the available dc input power to the transistor must be:

$$\text{Pdc (supply)} = \frac{P_o}{N_c} \qquad (28)$$

$$\frac{20}{0.5} = 40 \text{ watts.}$$

The TA2675 must be capable of passing 1.43 amperes of dc collector current when a 28 volt collector supply is used.

2. 430 Megacycle Circuit Performance

The TA2675 was evaluated primarily at 430 megacycles to determine whether the device could provide the required RF power performance. Figure 32 shows the lumped constant element circuit used to evaluate the TA2675

The circuit is contained in a rectangular chassis 1½ x 1½ x 6 inches. The input circuit consists of the network formed by C_1, C_2, C_3, and L_1. The inductor (L_1) is represented by a piece of 1/4-inch diameter copper tubing which is one-inch long. The output tank circuit consists of the network formed by C_4, C_5, C_6, L_2, and L_3. The inductor (L_2) is a copper strap 1/8 inch wide and approximately 5/8 inch long. The inductor (L_3) is represented by a piece of 1/4 inch diameter copper tubing which is 1/4-inches long.

The TA2675 product which was evaluated represented groups of transistors in which the device parameters were adjusted to optimize peak current handling capability at 430 megacycles. Figure 33 shows a plot of power output versus power input for low, average, and high limit units of the TA2675 product distribution measured. The low limit value was established at a minimum power gain of three times, or 4.5 dB. With 5 watts of driving power, the low limit unit will deliver 15 watts at 430 megacycles. Although this low limit on power gain may appear to be somewhat arbitrary, it does represent the minimum power gain usually accepted for most commercial VHF power transistors. It was found that with 5 watts of driving power, the TA2675 product is capable of delivering 15 to 18 watts of power output at 430 megacycles. The data obtained in the lumped constant element circuit was compared to the data obtained in the stub tuner circuit. It was found that for an input power of 5 watts, the lumped constant circuit power output was approximately one watt lower than those obtained on the stub tuner test circuit. This may be attributed in part to the power loss in the lumped-constant tuned networks. Figure 34 shows a plot of the collector circuit efficiency versus RF input driving power for the TA2675.

The lower limit units have a collector circuit efficiency of approximately 55 percent at 5 watts of driving power. The high limit units had an average collector circuit efficiency of approximately 60 percent for 5 watts of input driving power.

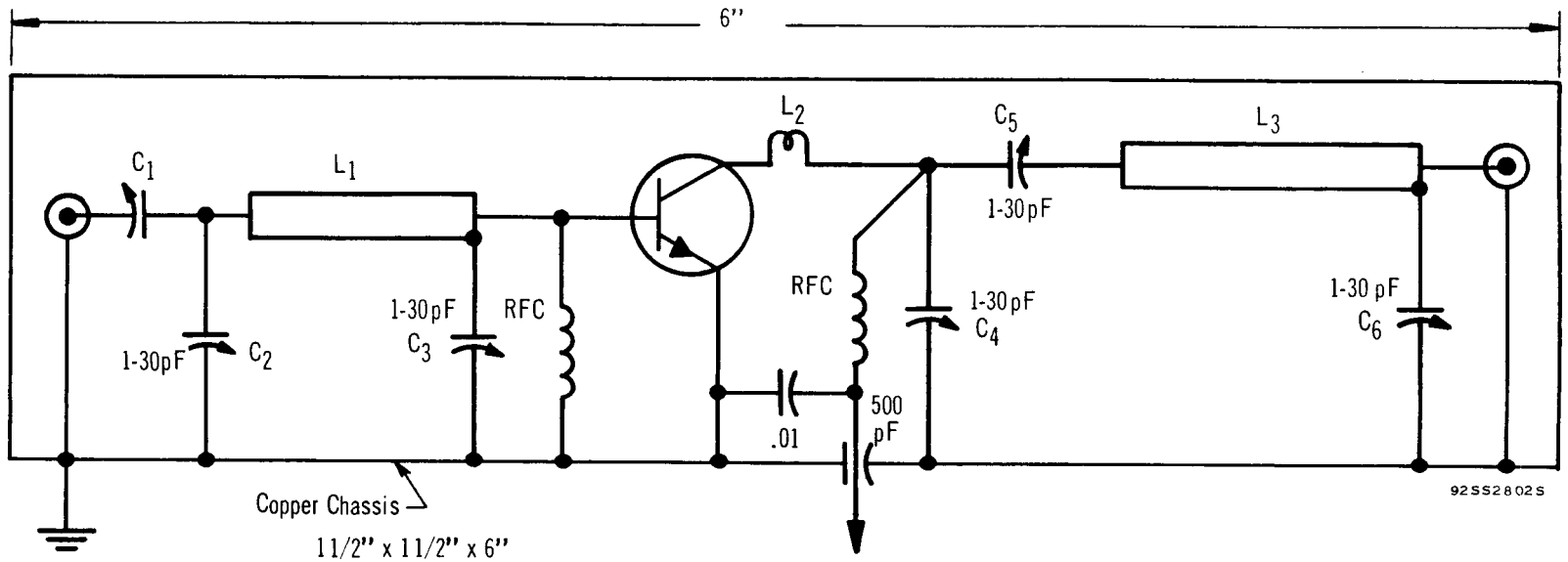

L_1 = 1/4" Dia. Cu Tubing; ℓ = 1"

L_2 = 1/8" Cu Strap; ℓ = 5/8"

L_3 = 1/4" Dia. Cu Tubing; = 2 1/4"

FIGURE 32 TA2675 430 MEGACYCLE TEST CIRCUIT

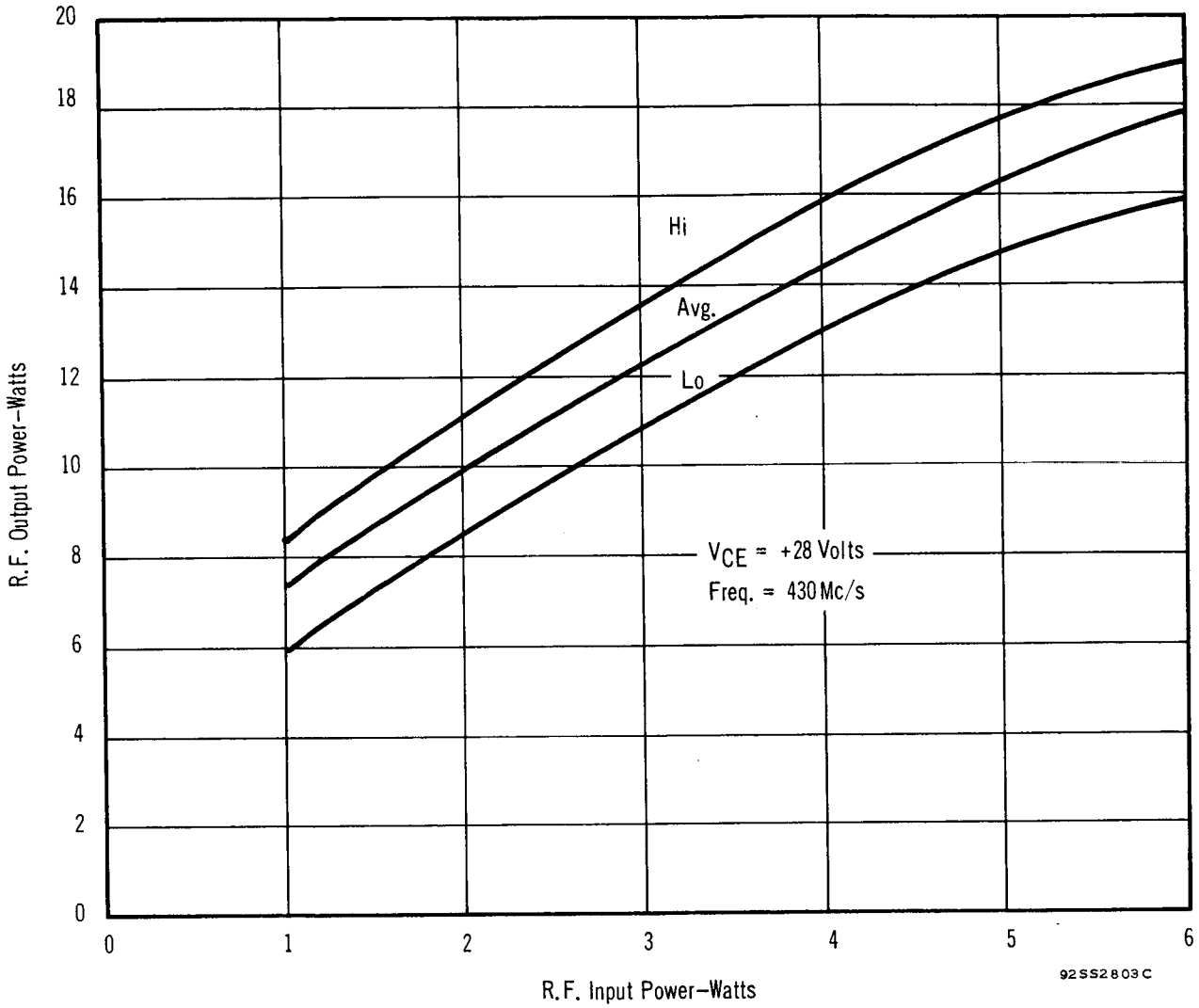

FIGURE 33 POWER OUTPUT AS A FUNCTION OF POWER INPUT (TA2675)

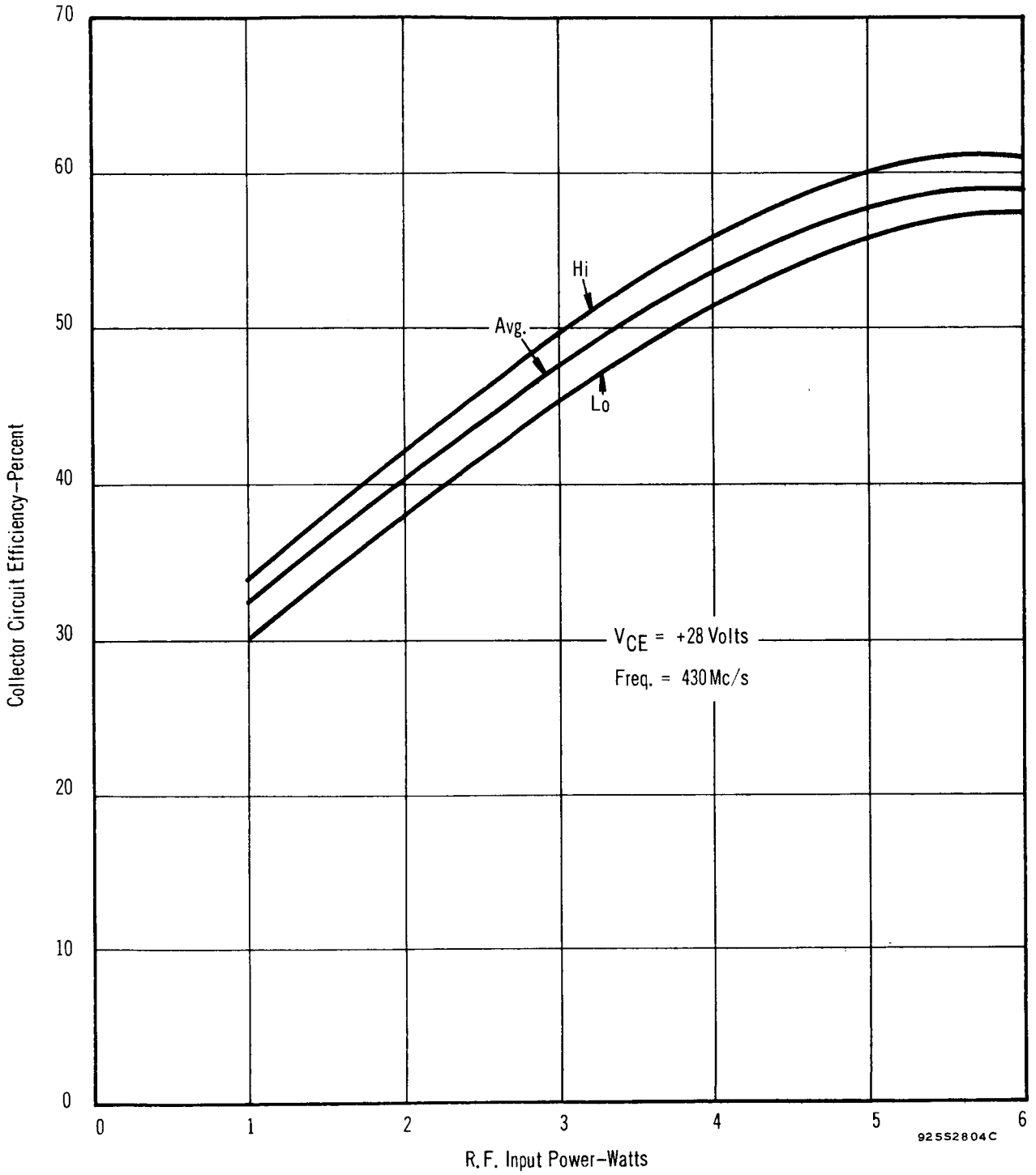

FIGURE 34 COLLECTOR EFFICIENCY AS A FUNCTION OF POWER INPUT (TA2675)

3. 300 Megacycle Circuit Performance

The TA2675 product was evaluated at 300 megacycles to check lower frequency performance. The test circuit used was basically the same as the one shown in Figure 32. A plot of power output versus input power is shown in Figure 35. With 5 watts of input driving power, the TA2675 was found capable of delivering 23.5 to 26 watts of RF output power. Figure 36 shows a plot of collector circuit efficiency versus input power. The TA2675 product's collector efficiency ranged from 57.5 to 64 percent and 300 megacycles for an input drive of 5 watts.

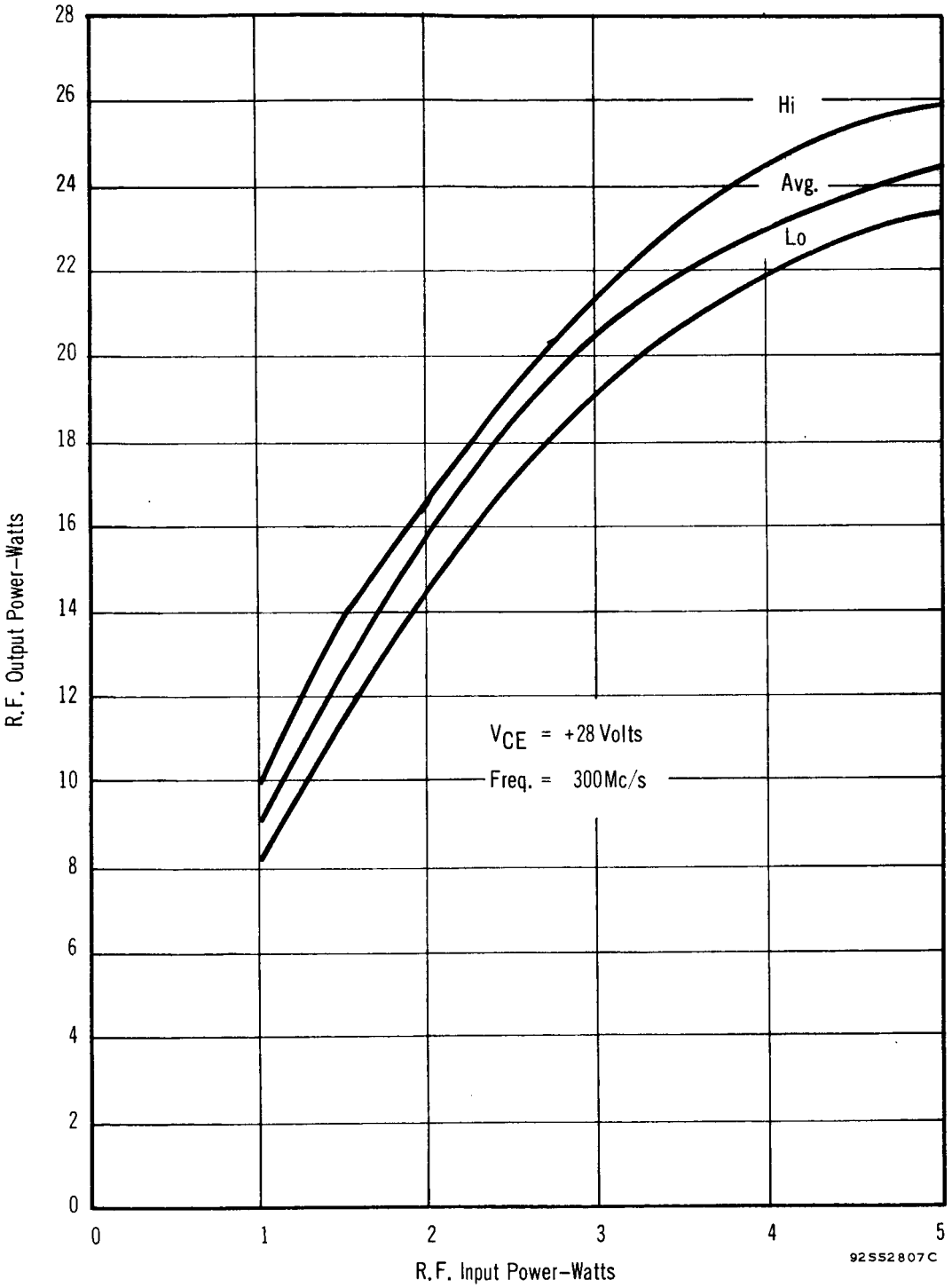

FIGURE 35 POWER OUTPUT AS A FUNCTION OF POWER INPUT (TA2675)

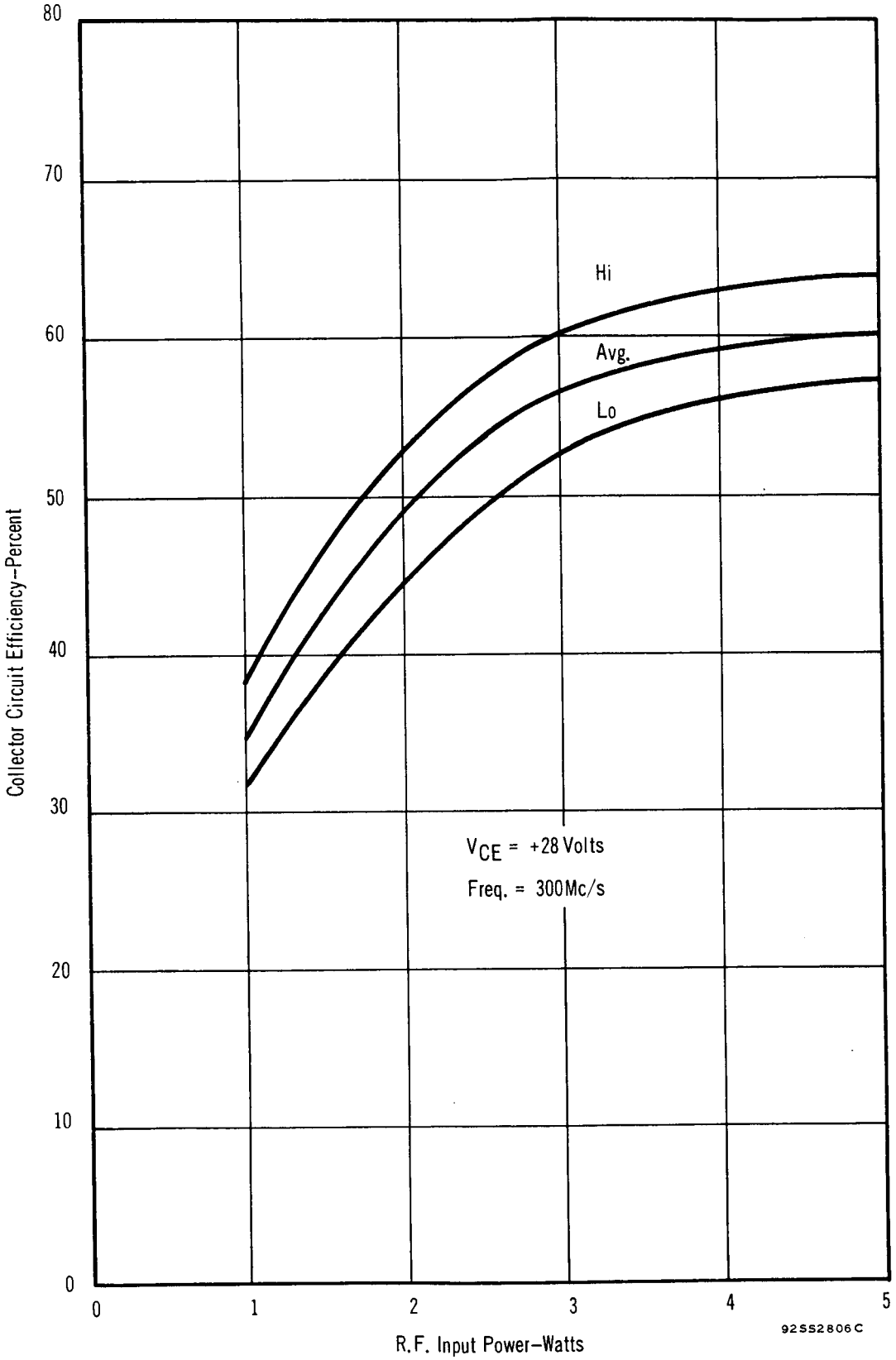

FIGURE 36 COLLECTOR EFFICIENCY AS A FUNCTION OF POWER INPUT (TA2675)

III. NEW TECHNOLOGY

A. General Processing

The 20 watt, 430 megacycle transistor was processed using epitaxial silicon wafers. The substrate is antimony doped to a resistivity of approximately 0.010 ohm-cm^2 and has an epitaxial phosphorus doped 1.6 to 2.1 ohm-cm surface layer. The overall wafer thickness is 6.0 to 8.0 mils. The wafer surface must be polished free of all defects, bumps, holes, and grown so that exact pattern reproduction and photo-mask alignment can be achieved.

The diffusion and impurity profiles are specifically designed for high-frequency, high-power output. The junction depths are shown in Figure 1. The base diffusion is about 0.055 mil. However, under the emitter the diffusion base depth has been pushed out to 0.085 mil. A low sheet resistance P+ layer which goes to a depth of about 0.095 mil is needed to reduce base spreading resistance. The emitter diffusion depth is about 0.065 mil which leaves a base width of 0.018 mil.

The photoengraving masks and processing required for the successful fabrication of this transistor indicate a marked improvement in the state-of-the-art since the beginning of this program. The final pattern design was about 75 mils long. When printing such a large image on the master masks, the aberrations of the lens caused distortion at the ends of the pattern. To correct for this distortion, strict control over photo-resist exposure and development was needed. Slight variations in exposure light intensity, from day to day, caused variations in exposure which overshadows exposure time. This was corrected by frequent light intensity checks and adjustments. Developing procedures were initiated to control swelling and shrinking of photo resist which drastically limit the reproducibility of line width. With these process improvements, it was possible to align 0.1 mil emitter lines inside 0.4 mil base regions with enough precision and accuracy to prevent emitter P+ overlap.

B. Base-Width Measurement

Base-width control is one of the most important parameters in the successful fabrication of overlay transistors. Variation across a wafer or between wafers is inadequately determined with a single measurement per wafer. A nondestructive measurement is essential to establish the necessary control over base and emitter diffusion and ultimately the base width.

A key, shown in Figure 37, was designed into the photoengraving masks. A four-point probe is used with the key to measure the sheet resistance of the base-width under the emitter. A schematic of the equipment used to make this measurement is shown in Figure 38. The base width is then determined from the curve shown in Figure 39. The curve is established by calculating the sheet resistance of sublayers and transposing to current versus thickness. Because of the base push-out under the emitter on this device, the sublayer sheet resistance calculations were made using the base depth immediately under the emitter. A Gaussian impurity distribution is assumed. Since base push-out varies with emitter depth, the accuracy of the measurement is within 0.0015 mil at the designed base-width and the error will increase to $\pm$ 0.003 mil with base-widths 40 percent from the norm.

Using this non-destructive measurement, variations in base-width of 0.005 mil were observed from top to bottom on a single wafer. This explained the wide variation in beta and f_T that had been experienced at that time. Improved control on base and emitter diffusions resulted in a reduction in the variation of W across a wafer, and even within a run of 10 wafers, to less than 0.002 mil.

Data accumulated on the unit cell indicates a significant improvement was made in control of f_T once non-destructive base-width measurements became routine. Before non-destructive basewidths measurements were used, f_T varied by $\pm$ 40 percent. After non-destructive basewidth measurements became routine, f_T varied by only $\pm$ 10 percent. The reason for tightening the range was that the measurements provided a much more representative reading of base-width for the wafer.

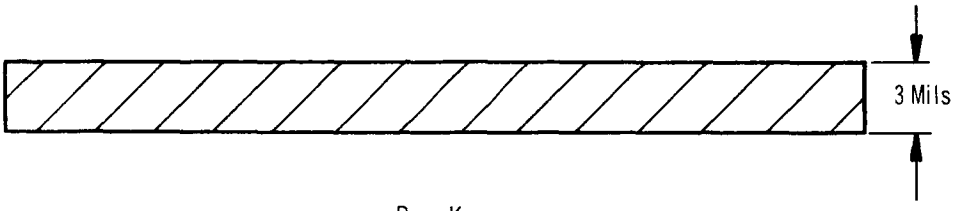

Base Key

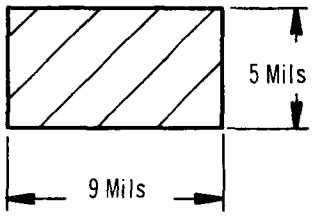

Emitter Key

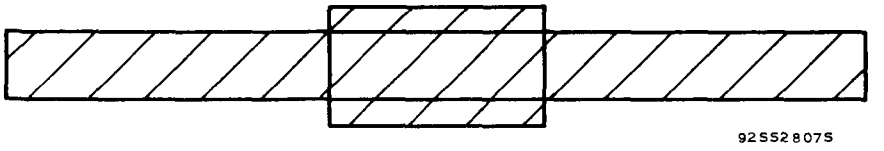

Emitter Key Superimposed Over Base Key As On Finished Transistor

FIGURE 37 ELECTRICAL BASE WIDTH MEASUREMENT KEY

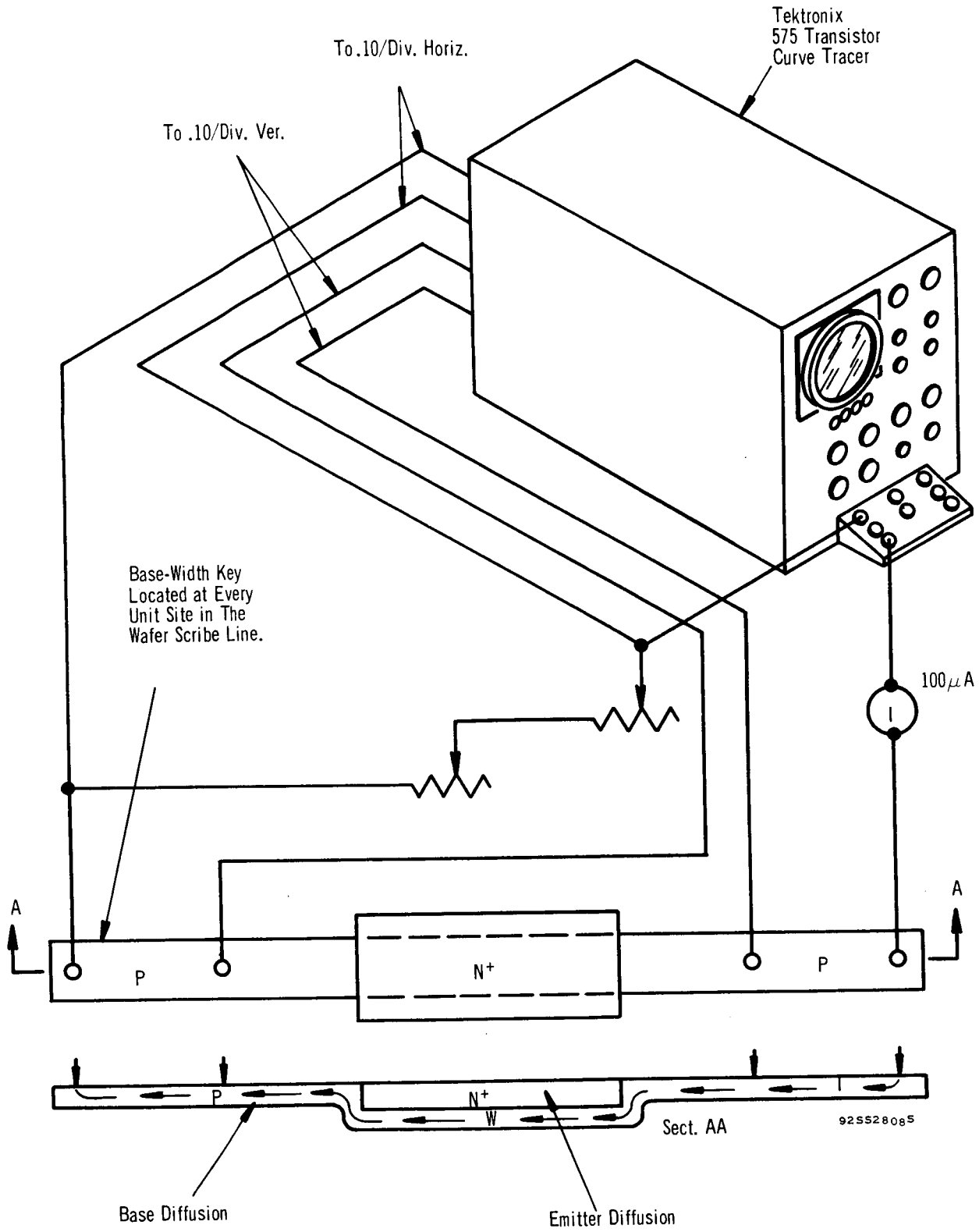

FIGURE 38 CIRCUIT FOR MEASURING BASE SHEET RESISTANCE UNDER THE EMITTER

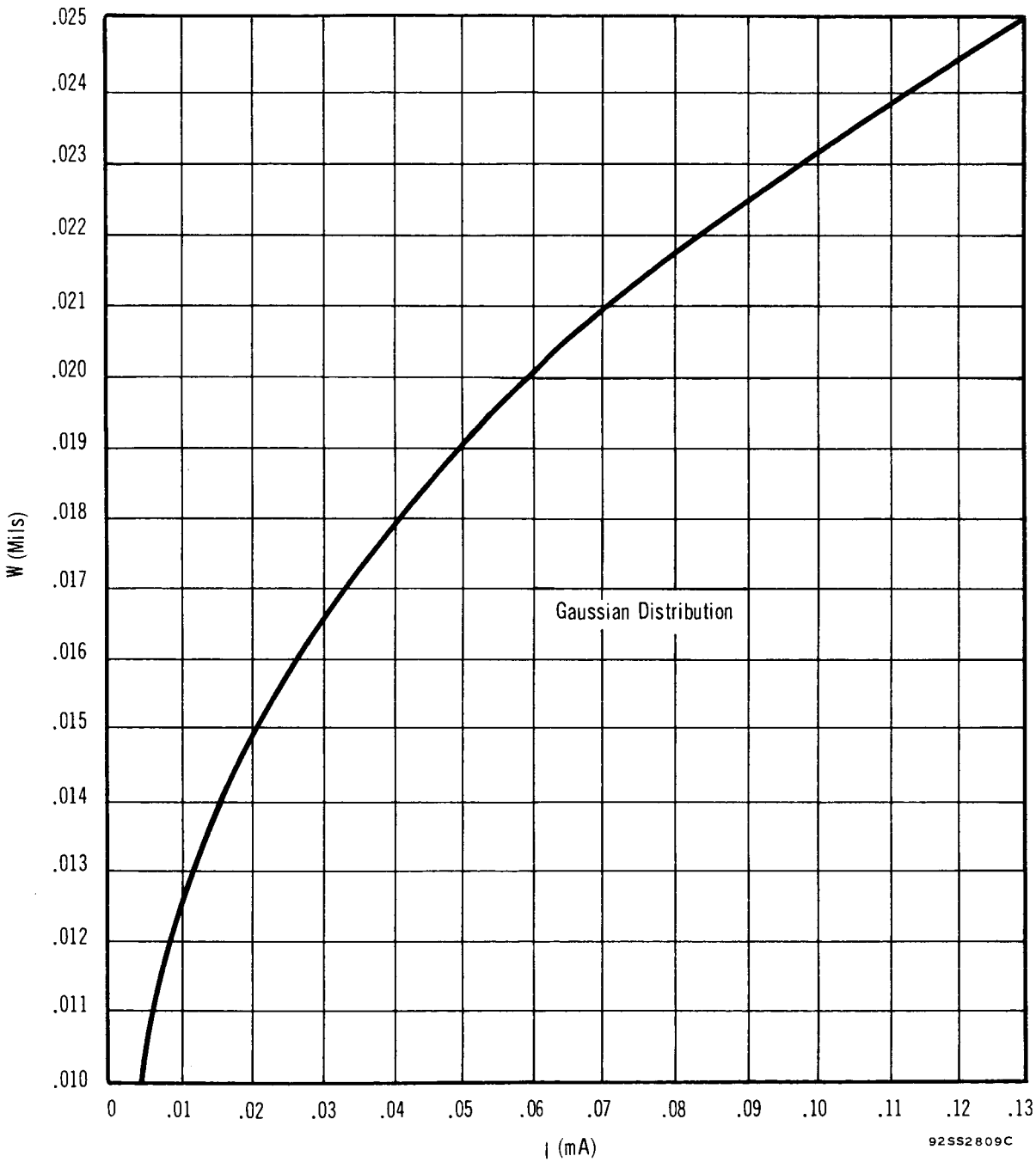

FIGURE 39 BASE WIDTH AS A FUNCTION OF MEASUREMENT CURRENT

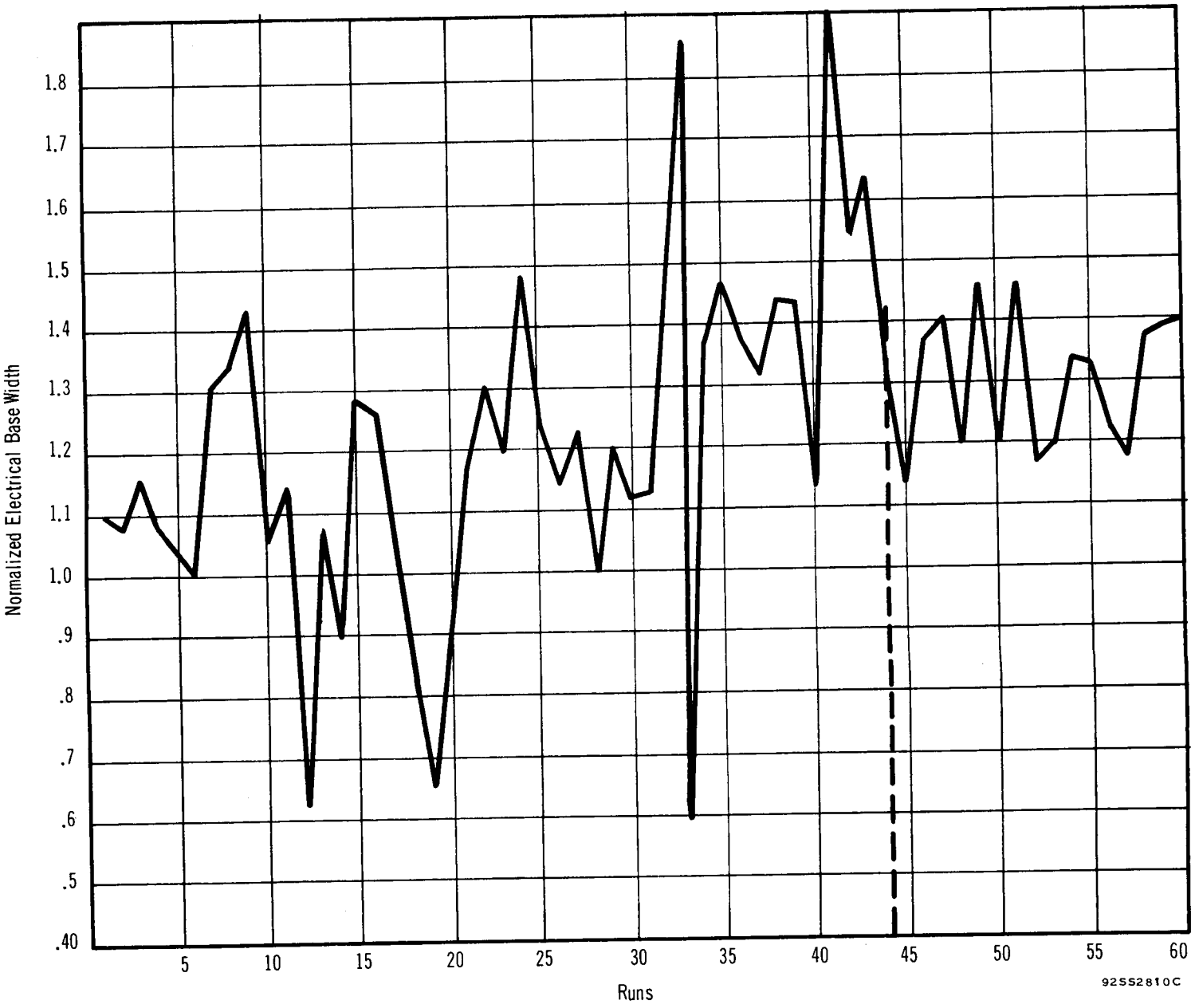

FIGURE 40 NORMALIZED ELECTRICAL BASE WIDTH VERSUS RUN NUMBER

C. Deposited Oxide

The fabrication of this transistor required thick oxide layers as thick dielectrics under the emitter and base bonding pads. This reduces stray capacitance to a minimum. The oxide is also used as a processing device to reduce the effects of pinhole etching in the vicinity of the collector-base periphery and to improve diode yields.

After P+ oxidation, a thick SiO_2 layer is grown over the entire wafer. The base areas are etched through the entire oxide so that, after base diffusion, the base-collector junction has been formed well under the thick oxide by lateral diffusion. The thermally grown oxide in the base areas is about one-third the thickness of the deposited oxide. The emitter areas are etched into the thin oxide and any pinholes, which may be etched at the same time near the collector-base periphery, will penetrate one-third the oxide depth. The remaining two-thirds will protect the junction from degradation even though an additional 2000Å of oxide is converted to glass.

D. Lateral Diffusion

It would be very difficult to align and open a line having adequate contact width within the 0.10 x 1.4 mils emitter line on this transistor to contact the emitter. It was necessary, therefore, to depend entirely on the diffusion perpendicular to the emitter depth to extend far enough under the surrounding oxide, to protect the emitter-base junction from surface effects and shorting by the contact metal.

The base impurity distribution, with the high concentration at the surface, and the depletion of phosphorus reduces the lateral diffusion of the emitter to about 40 percent of the emitter diffusion depth, or 0.025 mil. During the emitter diffusion approximately 0.010 mil of oxide is converted to phosphorus glass and removed. But because of the oxide etch factor, the oxide at the edges of the emitter is cut back 0.015 to .020 mil. Consequently, the lateral diffusion is reduced 0.005 to 0.010 mil. Obviously, extreme care is needed not to violate any of the forgoing aspects of lateral diffusion by large fluctuations in emitter diffusion control.

The necessary control for this diffusion was established by the development of an improved phosphorus deposition process. Control on the phorphorus glass grown during the diffusion was established by adjusting the gaseous dopant vapor pressure in the furnace using a by-pass gas mixing system. The glass thickness was further controlled by adjusting the doping time. The emitter diffusion depth is controlled separatly by adjustment of drive-in time. Fiallly, phosphorus glass removal was very carefully monitored and the optimum etching time was determined. It was necessary at this time to be careful to remove only phosphorus glass and not additional SiO_2. Subsequent cleaning steps require tight control to prevent degradation of the oxide at the emitter edge.

IV. REFERENCES

1. E. M. Conwell and Weisskopf, "Theory of Impurity Scattering in Semiconductors", Phy. Rev., Vol. 77, pp. 388-390, 1950.
2. E. J. Ryder, "Mobility of Holes and Electrons in High Electric Fields", Phy. Rev., Vol. 90, pp. 766-769, June, 1953.
3. C. T. Kirk, Jr., "A Theory of Transistor Cutoff Frequency (f_T) Falloff at High Current Densities", IRE Transactions on Electron Devices, Vol. ED-9, No. 2, March, 1962.
4. H. F. Cooke and R. R. Webster, "Packages For Small Signal VHF and UHF Transistors", EDN, Vol 9, No. 11, Oct. 1964.

V. CONCLUSIONS AND RECOMMENDATIONS

An improved overlay structure has been developed which results in higher emitter periphery to emitter area and emitter periphery to base area ratios, than previously available. The new structure and technology developed made possible the use of emitters as narrow as 0.1 mil. These advancements resulted in units which delivered up to 21.3 watts with 6.3 dB power gain and 72 percent efficiency as a 430 megacycle class C amplifier, operating from a 28 volt supply. The median device, from the 305 final samples delivered, had a power out of 17.7 watts with 5.5 dB gain and 60 percent efficiency. At 20 watts output, the median device required 5.6 watts input power with a 5.5 dB gain and had an efficiency of 62 percent. These results compare with a goal of 20 watts output, 6 dB power gain, and 50 percent efficiency. Thus, some increase in efficiency was obtained at the expense of power gain.

The package design indicates that significant improvements in power gain can be obtained by further improvements in packaging. If emitter lead inductance were decreased, significant improvements in power gain and a higher frequency range of operations would result.

APPENDIX

DATA ON 305 TA2675 FINAL SAMPLES

The power output values obtained from measurements made on the 305 TA2675 sample units delivered to NASA are listed in Table VI . The output measurements were made on the tuned line circuit illustrated in Figure 14. Distributions of power outputs and collector efficiencies of these samples are illustrated in Figures 41 through 44.

TABLE VI

DATA ON 305 TA2675 SAMPLES DELIVERED TO NASA

Unit #	BV_{EBO} I_E=100μA	BV_{CBO} I_C=100μA	LV_{CEX} I_C=10mA V_{EB}=1.4V	$BV_{CEO(SUS)}$ I_C=10mA	I_{CEO} V_{CE}=28V (mA)	h_{FE} V_{CE}=4V I_C=1A	h_{FE} V_{CE}=4V I_C=2A	$V_{CE(SAT)}$ I_C=750mA I_B=150mA	C_{ob} V_{CB}=30V pF	P_{out} P_{in}=5W V_{CE}=28V f=430Mc I_C=mA	η (%)	P_{in} P_{out}=20W V_{CE}=28V f=430Mc I_C=mA	η (%)
E9-2													
33	4.1	20	80	43	.20	91.	40.	.20	16.6	16.8/960	63.4		
34	3.6	14	80	44	.21	83.4	28.6	.20	16.3	15.2/960	57.3		
35	3.8	12	77	50	.35	43.5	22.3	.23	16.7	15.7/880	63.6		
36	4.0	12	78	45	.375	78.0	34.8	.21	16.7	15.7/860	65.2		
37	4.2	42	74	43	.055	57.8	30.8	.22	16.7	15.7/880	63.6		
38	3.9	12	78	44	2.5	66.7	21.3	.225	16.6	15.3/950	58.6		
39	3.6	51	78	47	.092	71.4	33.4	.21	16.7	15.8/910	61.8		
40	3.8	31	80	43	.114	76.9	25.	.21	16.3	15.3/950	58.6		
41	4.3	17	77	41	.25	76.9	28.6	.215	16.7	15.9/930	60.9	P_{out} P_{in}=5W V_{CE}=35V f=430mc	
43	4.2	67	81	45	.35	79.3	33.4	.185	17.4	16.5/750	56.0	19.4/910	50.4
44	3.7	49	78	47	.08	55.6	33.4	.19	17.8	16.1/920	54.8	19.3/910	50.2
46	4.2	63	76	43	.31	66.7	33.4	.175	17.7	16.2/930	53.8	19.5/950	53.0
47	3.2	64	79	45	.114	69.0	30.8	.195	17.5	16.2/920	53.2	19.8/950	51.0
48	4.1	72	85	42	.13	91.0	40.0	18.9	17.1	16.6/930	55.2	19.8/980	55.5
49	4.1	70	81	42	.126	76.9	30.8	18.5	17.5	16.4/950	57.7	19.2/920	50.6

TABLE VI (Cont.)

DATA ON 305 TA2675 SAMPLES DELIVERED TO NASA

Unit #	BV_{EBO} I_E=100μA	BV_{CBO} I_C=100μA	LV_{CEX} I_C=10mA V_{EB}=1.4V	$BV_{CEO(SUS)}$ I_C=10mA	I_{CEO} V_{CE}=28V (mA)	h_{FE} V_{CE}=4V I_C=1A	h_{FE} V_{CE}=4V I_C=2A	$V_{CE(SAT)}$ I_C=750mA I_B=150mA	C_{ob} V_{CB}=30V pF	P_{out} P_{in}=5W V_{CE}=28V f=430Mc I_C=mA	η (%)	P_{in} P_{out}=20W V_{CE}=28V f=430Mc I_C=mA	η (%)
E10-3													
4	3.3	30	80	31	.255	51.3	50.0	.165	20.4	15.8/980	55.3	7.0/1210	59.1
6	3.8	66	82	31	.0027	58.9	53.4	.165	20.3	15.5/1050	52.6	7.2/1240	57.5
7	4.0	34	76	28	.24	90.9	80.0	.155	20.8	17.0/1080	56.2	6.2/1220	58.6
9	2.3	68	81	35	.0063	50.0	47.1	.165	20.5	15.5/960	53.2	7.1/1150	62.2
10	.8	36	72	42	.084	50.0	50.0	.160	21.6	16.0/1040	55.0	7.1/1300	55.0
12	3.2	56	80	31	.022	55.6	50.0	.175	20.5	15.7/1050	53.3	6.9/1210	59.0
13	4.1	71	82	26	.007	52.7	89.0	.160	20.1	17.1/1000	60.6	6.1/1150	62.2
17	3.2	21	60	30	.70	58.8	57.2	.170	19.1	16.0/980	56.0	6.8/1150	62.2
19	3.8	6	79	30	.86	52.7	50.0	.155	23.2	15.5/970	53.6	7.1/1180	60.6
24	3.4	63	81	31	.003	52.6	47.2	.165	20.4	15.6/950	52.8	7.0/1190	60.0
26	4.2	63	81	28	.003	83.4	69.6	.165	20.3	16.4/940	55.1	6.6/1130	63.2
E10-4													
21	3.7	10	60	34	2.8	62.5	53.1	.195		16.5/1130	52.0		
24	4.1	30	80	31	.9	71.5	67.7	.215	18.9	17.1/1030	59.4	6.2/1140	62.6
25	4.0	21	80	32	1.26	58.1	50.0	.210	18.5	17.1/1020	59.9	6.2/1160	61.6
26	3.2	6	81	30	1.18	76.9	67.7	.190	19.2	16.5/1020	57.8	6.4/1140	62.6

TABLE VI (Cont.)

DATA ON 305 TA2675 SAMPLES DELIVERED TO NASA

Unit #	BV_{EBO} I_E=100μA	BV_{CBO} I_C=100μA	LV_{CEX} I_C=10mA V_{EB}=1.4V	$BV_{CEO(SUS)}$ I_C=10mA	I_{CEO} V_{CE}=28V (mA)	h_{FE} V_{CE}=4V I_C=1A	h_{FE} V_{CE}=4V I_C=2A	$V_{CE(SAT)}$ I_C=750mA I_B=150mA	C_{ob} V_{CB}=30V pF	P_{out} P_{in}=5W V_{CE}=28V f=430Mc I_C=mA	η (%)	P_{in} P_{out}=20W V_{CE}=28V f=430Mc I_C=mA	η (%)
E10-4													
27	4.0	60	84	30	.125	71.5	61.6	.210	18.4	17.1/1060	57.6	6.1/1140	62.6
28	4.1	19	83	34	.52	77.0	67.7	.190	18.9	15.7/1020	55.0	7.2/1200	59.6
29	3.4	11	82	31	.83	62.5	58.1	.215	18.6	16.6/1020	58.1	6.5/1120	63.7
32	4.0	14	74	29	2.1	105	89.0	.185		17.8/980	65.0	6.0/1120	63.7
33	3.3	10	80	32	2.1	58.8	50.0	.200		15.2/970	56.1	6.9/1120	63.7
34	4.0	73	82	29	.0035	90.8	80	.185		17.6/1080	58.2	6.0/1180	60.6
35	3.8	67	82	29	.14	83.3	72.8	.200	18.6	16.8/1050	57.0	6.5/1110	64.3
36	4.0	78	83	30	8μa	77.0	66.8	.200	19.0	17.0/980	61.9	6.3/1170	61.0
37	3.8	64	82	30	.05	71.5	61.6	.200		17.6/1040	60.4	6.2/1140	62.6
38	3.7	25	73	27	.5	90.9	80.0	.175		17.5/1040	60.1	6.1/1110	64.3
39	3.4	75	82	30	.02	66.6	59.7	.190		15.4/960	57.4	7.1/1070	66.7
41	4.0	46	82	32	.46	62.5	50.0	.215		17.3/1050	58.7	6.3/1150	62.1
42	3.7	9	84	32	1.2	77	66.7	.190		17.6/1060	59.4	6.1/1170	61.0
43	3.6	45	81	28	.35	100	84.2	.185		17.0/1060	57.3	6.3/1170	61.0
44	4.0	16	80	27	3.0	110.1	89.0	.180		17.2/1130	54.4	6.0/1150	62.1
46	2.7	75	84	31	.03	71.5	61.5	.200		16.8/1050	57.1	6.5/1150	62.1
47	3.7	7	80	29	1.6	95.4	80.0	.180		17.3/1120	55.2	6.1/1190	62.6

TABLE VI (Cont.)

DATA ON 305 TA2675 SAMPLES DELIVERED TO NASA

Unit #	BV_{EBO} I_E=100μA	BV_{CBO} I_C=100μA	LV_{CEX} I_C=10mA V_{EB}=1.4V	$BV_{CEO(SUS)}$ I_C=10mA	I_{CEO} V_{CE}=28V (mA)	h_{FE} V_{CE}=4V I_C=1A	h_{FE} V_{CE}=4V I_C=2A	$V_{CE(SAT)}$ I_C=750mA I_B=150mA	C_{ob} V_{CB}=30V pF	P_{out} P_{in}=5W V_{CE}=28V f=430Mc I_C=mA	η (%)	P_{in} P_{out}=20W V_{CE}=28V f=430Mc I_C=mA	η (%)
E10-4													
48	3.5	41	81	27	25.	105	89.0	.170		16.8/1100	54.5	6.5/1200	59.6
49	4.0	9	83	35	1.2	62.5	53.4	.200		15.9/1050	54.0	7.0/1200	59.5
E13-1													
11	3.6	4.8	72	44	2.9	52.7	30.8	.32	17.2	15.5/900	59.1		
12	4.0	5	71	29	10.6	105.5	33.4	.26	18.1	15.7/1000	56.0		
13	3.8	26	70	40	.45	160	58.1	.19	17.2	16.8/1050	52.3		
14	3.3	60	78	42	.003	71.5	28.6	.30	16.7	15.2/910	60.4		
15	4.0	4.7	66	32	3.9	174	57.2	.21	18.2	15.4/950	58.0		
17	3.7	60	80	35	.067	143	57.1	.21	17.1	17.0/1030	59.0		
18	3.9	4.5	77	40	.86	110.2	44.5	.24	16.9	16.2/1000	57.8		
19	4.0	20	77	47	.5	60.7	33.4	.21	16.9	15.3/890	61.4		
20	3.8	70	80	43	.003	100.	40.0	.22	16.6	15.7/900	60.0		
21	4.1	68	79	44	.003	87	40.0	.29	16.9	16.4/920	63.6		
22	4.0	19	74	35	.65	105	50.0	.21	17.3	16.6/900	63.4		
23	3.6	45	75	42	.003	77	33.4	.22	16.7	15.2/860	63.0		
26	4.0	48	75	33	.003	110.2	50.0	.20	17.0	16.1/920	62.5		

TABLE VI (Cont.)

DATA ON 305 TA2675 SAMPLES DELIVERED TO NASA

Unit #	BV_{EBO} I_E=100μA	BV_{CBO} I_C=100μA	LV_{CEX} I_C=10mA V_{EB}=1.4V	$BV_{CEO(SUS)}$ I_C=10mA	I_{CEO} V_{CE}=28V (mA)	h_{FE} V_{CE}=4V I_C=1A	h_{FE} V_{CE}=4V I_C=2A	$V_{CE(SAT)}$ I_C=750mA I_B=150mA	C_{ob} V_{CB}=30V pF	P_{out} P_{in}=5W V_{CE}=28V f=430Mc I_C=mA	η (%)	P_{in} P_{out}=20W V_{CE}=28V f=430Mc I_C=mA	η (%)
E13-1													
27	4.1	69	81	40	.003	110.2	40.0	.20	16.9	16.6/980	60.4		
28	4.0	66	75	33	.004	125	57.2	.235	17.1	16.6/980	60.4		
29	4.1	67	77	37	.003	100	44.5	.24	17.0	15.5/900	61.5		
30	3.8	55	77	44	.003	71.5	28.8	.25	16.8	15.5/860	63.6		
31	3.8	63	80	38	.018	133	50.0	.19	16.7	16.2/1040	55.7		
32	3.4	65	80	41	.092	118	33.3	.20	16.7	15.9/1020	55.8		
34	3.9	30	78	31	6.5	91	36.4	.185	16.8	15.9/950	59.8		
35	3.7	5.2	71	40	1.44	71.5	50.0	.21	17.6	15.9/980	57.9		
37	3.8	67	79	38	.003	143.5	57.2	.19	16.8	16.8/930	64.5		
39	4.2	62	75	35	.003	111	57.2	.24	17.3	16.8/1030	58.8		
E33-1*													
6	4.0	3.8	72	57	.19	36.4	25.8	.185	18.4	17.3/1130	54.7	7.2/1250	57.2
7	4.0	65.0	71	60	.027	33.4	24.2	.185	18.4	16.8/1130	53.1		
8	4.0	2.6	72	56	1.04	36.4	25.8	.18	18.5	15.9/1180	46.6		
9	3.5	12.5	72	42	.245	43.5	28.6	.19	18.3	16.6/1110	53.5		

* New Pattern

TABLE VI (Cont.)

DATA ON 305 TA2675 SAMPLES DELIVERED TO NASA

Unit #	BV_{EBO} I_E=100μA	BV_{CBO} I_C=100μA	LV_{CEX} I_C=10mA V_{EB}=1.4V	$BV_{CEO(SUS)}$ I_C=10mA	I_{CEO} V_{CE}=28V (mA)	h_{FE} V_{CE}=4V I_C=1A	h_{FE} V_{CE}=4V I_C=2A	$V_{CE(SAT)}$ I_C=750mA I_B=150mA	C_{ob} V_{CB}=30V pF	P_{out} P_{in}=5W V_{CE}=28V f=430Mc I_C=mA	η (%)	P_{in} P_{out}=20W V_{CE}=28V f=430Mc I_C=mA	η (%)
33-1													
10	3.5	66	72	53	.004	44.5	30.8	.195	18.5	15.9/960	60.0		
11	4.0	65	71	58	.028	43.5	28.6	.18	18.4	17.3/1020	60.6	6.8/1200	59.5
13	2.3	63	72	54	.003	50.0	33.3	.175	18.3	17.3/1060	58.2	6.9/1150	62.2
14	4.0	63	71	60	.052	36.4	26.7	.185	18.3	16.8/1000	60.0		
15	3.4	64	72	52	.03	44.5	30.8	.20	18.4	15.4/910	60.4		
16	3.8	2.7	72	55	.61	43.5	30.8	.175	18.3	17.3/1060	58.2	7.1/1200	59.5
17	3.5	60	71	54	.003	46.5	30.8	.175	18.5	15.8/990	57.1		
542-1 *			* New Pattern										
1	3.6	34	68	34	.235	105	72.6	.19	19.0	18.3/1040	62.6	5.6/1150	62.1
2	3.4	4	64	34	1.3	100	57.2	.19	18.6	18.4/1070	60.2	6.5/1170	60.0
3	3.5	37	62	41	.46	87	61.6	.21	19.2	18.4/1120	58.7	5.7/1200	60.0
4	3.5	23	61	30	.66	133	80.0	.225	19.2	18.4/1070	61.5	5.5/1170	61.2
5	3.4	56	67	32	.3	105	66.7	.185	18.9	18.0/1050	61.2	5.9/1160	61.5
6	3.3	52	61	55	.16	83.3	57.2	.185	18.9	17.8/1030	61.6	6.3/1160	61.5
7	3.8	33	49	28	1.5	143	89	.215	19.4	19.4/1160	59.4	5.2/1200	60.0
9	3.2	57	62	46	.085	44.5	33.4	.19	19.3	16.7/1000	59.6	6.8/1130	63.2

TABLE VI (Cont.)

DATA ON 305 TA2675 SAMPLES DELIVERED TO NASA

Unit #	BV_{EBO} I_E=100μA	BV_{CBO} I_C=100μA	LV_{CEX} I_C=10mA V_{EB}=1.4V	$BV_{CEO(SUS)}$ I_C=10mA	I_{CEO} V_{CE}=28V (mA)	h_{FE} V_{CE}=4V I_C=1A	h_{FE} V_{CE}=4V I_C=2A	$V_{CE(SAT)}$ I_C=750mA I_B=150mA	C_{ob} V_{CB}=30V pF	P_{out} P_{in}=5W V_{CE}=28V f=430Mc I_C=mA	η (%)	P_{in} P_{out}=20W V_{CE}=28V f=430Mc I_C=mA	η (%)
E-44													
4-32	3.6	55.	67.	33.	< .01	43.5	40.0	.14	20.9	17.4/1020	60.9	5.9/1150	62.1
4-33	4.0	57.	66.	30.	.012	51.3	45.4	.13	20.	18.0/1060	60.7	5.6/1150	62.1
4-36	4.0	26.	66.	30.	.30	62.4	55.6	.14	19.9	18.8/1090	61.6	5.3/1130	63.3
4-38	3.6	54.	65.	32.	< .01	43.5	39.2	.14	20.9	17.7/1040	60.8	5.9/1160	61.6
4-40	3.6	55.	68.	32.	< .01	44.4	40.	.14	20.7	17.5/1020	60.2	5.8/1170	61.2
4-41	3.5	54.	65.	33.	< .01	47.6	42.6	.14	21.5	17.5/1060	59.0	6.1/1230	58.1
4-45	3.8	55.	65.	31.	< .01	50.0	42.6	.14	20.7	17.5/1060	59.0	6.0/1200	59.6
4-46	3.8	56.	66.	31.	< .01	47.6	44.4	.13	20.5	17.6/1010	62.2	5.8/1130	63.3
4-47	4.0	56.	66.	31.	< .01	47.6	43.5	.14	20.1	17.7/970	61.3	5.7/1080	66.1
4-48	4.0	51.	66.	30.	.07	90.9	76.9	.13	21.	18.5/1230	53.8	5.4/1150	62.1
4-49	3.8	54.	66.	32.	< .01	43.5	37.1	.14	20.5	17.7/1000	63.3	5.8/1120	63.8
4-53	4.1	55.	65.	31.	.044	62.4	57.2	.14	20.2	18.0/1160	55.5	5.7/1170	61.1
4-54	4.1	54.	64.	12.4	3.0	63.3	58.9	.13	28.6	18.5/1160	57.0	5.5/1190	60.1
4-55	4.1	58	66.	31	< .01	62.4	48.8	.13	20.1	17.8/1100	57.8	5.9/1030	69.4
4-57	3.9	56	68	35	< .01	40.0	36.4	.144	20.4	17.0/1000	60.7		
4-60	4.1	52	70	26	< .01	70.5	57.1	.154	20.4	18.0/1030	62.5		
4-63	4.0	58	68	30	< .01	57.3	50.0	.140	20.0	17.8/1060	60.0		

TABLE VI (Cont.)

DATA ON 305 TA2675 SAMPLES DELIVERED TO NASA

Unit #	BV_{EBO} I_E=100μA	BV_{CBO} I_C=100μA	LV_{CEX} I_C=10mA V_{EB}=1.4V	$BV_{CEO(SUS)}$ I_C=10mA	I_{CEO} V_{CE}=28V (mA)	h_{FE} V_{CE}=4V I_C=1A	h_{FE} V_{CE}=4V I_C=2A	$V_{CE(SAT)}$ I_C=750mA I_B=150mA	C_{ob} V_{CB}=30V pF	P_{out} P_{in}=5W V_{CE}=28V f=430Mc I_C=mA	η (%)	P_{in} P_{out}=20W V_{CE}=28V f=430Mc I_C=mA	η (%)
F-44													
5-66	3.3	56.0	75.0	32.0	<.01	103.0	77.0	.14	20.6	17.6/1020	61.6	6.1/1170	61.1
5-67	3.6	50.0	75.0	36.0	<.01	90.0	66.7	.15	20.9	18.2/1060	61.4	5.8/1170	61.1
5-68	4.1	15.0	69.0	31.0	1.3	98.0	71.4	.13	20.0	18.5/1050	62.9	5.5/1130	63.3
5-71	3.8	56.0	70.0	34.0	.028	51.3	38.5	.16	20.5	17.4/1050	59.1	6.2/1230	58.1
5-72	3.6	57.0	80.0	32.0	.07	104.2	77.0	.14	20.8	18.6/1090	60.6	5.6/1180	60.6
5-75	3.4	57.0	75.0	32.0	<.01	105.2	71.4	.15	21.2	18.3/1040	62.9	5.6/1130	63.3
5-76	4.1	32.0	70.0	30.0	.25	92.6	76.9	.13	19.6	18.8/1070	62.7	5.4/1040	68.6
5-77	4.1	58.0	71.0	30.0	.082	101.0	83.4	.13	20.0	17.8/960	66.2	5.8/1080	66.1
5-79	4.3	53.0	70.0	33.0	.03	76.9	64.6	.13	19.5	18.8/1060	63.4	5.4/1060	67.4
5-81	4.1	4.2	68.0	38.0	8.2	76.9	71.4	.13		19.0/1000	67.9	5.3/1050	68.1
5-82	4.1	54.0	69.0	37.0	.015	70.5	60.6	.14	20.0	17.8/950	67.0	5.8/1060	67.4
5-83	4.1	35.0	68.0	30.0	.25	98.0	76.9	.14	20.0	18.8/1000	67.1	5.3/1050	68.1
5-84	4.2	47.0	67.0	33.0	.18	72.4	64.6	.14	20.1	18.3/950	62.1	5.6/1030	69.4
5-85	4.3	58.0	70.0	32.0	<.01	80.0	65.6	.13	19.6	18.0/1080	59.6	5.9/1100	65.0
5-86	4.2	5.0	67.0	33.0	1.3	70.4	60.6	.13	20.0	18.6/980	65.1	5.4/1040	68.7
5-87	4.3	26.0	68.0	33.0	.40	74.1	60.6	.13	19.0	18.6/1010	65.7	5.5/1080	66.1

TABLE VI (Cont.)

DATA ON 305 TA2675 SAMPLES DELIVERED TO NASA

Unit #	BV_{EBO} I_E=100μA	BV_{CBO} I_C=100μA	LV_{CEX} I_C=10mA V_{EB}=1.4V	$BV_{CEO(SUS)}$ I_C=10mA	I_{CEO} V_{CE}=28V (mA)	h_{FE} V_{CE}=4V I_C=1A	h_{FE} V_{CE}=4V I_C=2A	$V_{CE(SAT)}$ I_C=750mA I_B=150mA	C_{ob} V_{CB}=30V pF	P_{out} P_{in}=5W V_{CE}=28V f=430Mc I_C=mA	η (%)	P_{in} P_{out}=20W V_{CE}=28V f=430Mc I_C=mA	η (%)
B-44													
4-68	4.0	50	66	31	< .01	55.0	46.5	.154	20.5	17.5/1150	54.4		
4-70	4.0	52	66	32	.06	47.6	41.6	.144	20.7	18.8/1070	62.7		
4-71	4.0	48	66	37	.07	49.6	42.6	.146	20.6	17.0/1060	57.4		
4-75	3.8	58	69	33	< .01	45.5	40.0	.139	20.1	18.0/970	66.3		
4-78	3.5	60	70	35	< .01	36.4	36.4	.140	21.0	18.0/950	67.7		
4-79	4.0	60	69	26	< .01	83.2	72.7	.138	20.8	18.5/1100	60.0		
4-80	3.6	58	70	33	< .01	43.5	39.8	.150	20.6	18.5/1000	66.1		
5-51	3.8	12.0	69.0	32.0	1.2	98.0	80.	.1[illegible]	20.0	18.8/1080	62.6	5.4/1150	62.1
5-52	3.8	5.4	69.0	33.0	1.0	89.4	64.6	.13	21.2	18.5/1120	59.0	5.6/1200	59.6
5-53	4.0	5.7	68.0	33.0	1.4	74.1	60.6	.12	20.0	19.0/1100	61.7	5.3/1150	62.1
5-55	3.7	4.0	69.0	31.0	4.7	95.3	76.9	.14	24.7	19.0/1110	61.2	5.3/1160	61.6
5-57	3.9	17.6	68.0	31.0	.85	105.2	80.0	.1[illegible]	19.4	19.0/1140	59.6	5.4/1180	60.6
5-58	3.8	50.0	73.0	32.0	.18	106.3	80.0	.14	20.6	18.4/1140	57.6	5.7/1230	58.1
5-59	3.8	27.0	72.0	33.0	.35	92.6	68.9	.13	20.7	18.4/1150	57.1	5.7/1260	56.7
5-62	3.5	59.0	76.0	34.0	.085	90.9	66.7	.13	21.0	17.8/1080	58.9	6.9/1210	59.1
5-63	3.2	32.0	74.0	31.0	.32	108.8	71.5	.14	21.3	18.6/1060	62.3	5.6/1170	61.1

TABLE VI (Cont.)

DATA ON 305 TA2675 SAMPLES DELIVERED TO NASA

Unit #	BV_{EBO} I_E=100μA	BV_{CBO} I_C=100μA	LV_{CEX} I_C=10mA V_{EB}=1.4V	$BV_{CEO(SUS)}$ I_C=10mA	I_{CEO} V_{CE}=28V (mA)	h_{FE} V_{CE}=4V I_C=1A	h_{FE} V_{CE}=4V I_C=2A	$V_{CE(SAT)}$ I_C=750mA I_B=150mA	C_{ob} V_{CB}=30V pF	P_{out} P_{in}=5W V_{CE}=28V f=430Mc I_C=mA	η (%)	P_{in} P_{out}=20W V_{CE}=28V f=430Mc I_C=mA	η (%)
E-44													
5-88	4.3	38.0	69.0	31.0	.16	82.0	66.7	.14	19.6	18.5/980	64.8	5.5/1060	67.4
5-89	4.0	35.0	71.0	30.0	.36	108.8	91.0	.14	20.0	19.5/1060	65.7	5.2/1080	66.1
5-90	4.4	49.0	69.0	32.0	.10	74.1	58.8	.15	19.8	19.5/1080	64.5	5.2/1120	63.8
5-91	3.5	59.0	78.0	31.0	.05	108.8	74.1	.14	20.9	18.1/1110	58.2	5.8/1170	61.1
5-92	3.7	25.0	72.0	31.0	.29	111.1	83.4	.14	20.4	18.0/940	60.4	5.8/1060	67.4
5-93	4.0	30.0	70.0	30.0	.24	111.1	91.0	.13	19.7	19.6/1050	66.6	5.2/1070	66.8
5-94	4.2	56.0	68.0	32.0	.02	66.7	54.1	.15	20.0	18.7/1040	64.1	5.5/1100	65.0
5-95	4.2	27.0	77.0	28.0	.18	64.5	57.1	.14	20.1	18.6/1060	62.6	5.6/1140	62.7
5-115	4.0	56.0	72.0	31.0	.03	92.6	66.6	.15	20.2	17.7/1010	62.6	5.7/1150	62.1
5-116	4.2	59.0	70.0	32.0	<.01	75.7	64.6	.14	19.7	18.6/1010	65.7	5.4/1080	66.1
5-121	4.2	56.0	69.0	33.0	<.01	65.7	57.2	.14	20.1	18.0/1050	61.2	5.7/1140	62.7
5-123	4.0	32.0	76.0	32.0	.30	90.9	74.1	.14	20.0	18.6/1000	66.4	5.4/1080	66.1
5-125	3.6	48.0	73.0	31.0	.088	100.0	69.0	.15	21.0	18/1050	61.2	5.7/1180	60.6
5-126	4.0	59.0	70.0	30.0	<.01	107.5	83.4	.14	20.1	19.5/1040	67.0	5.1/1060	67.4
5-128	4.1	4.6	70.0	28.0	7.0	96.1	76.9	.13	18.6	19.6/1040	67.4	5.2/1060	67.4
5-130	3.5	60.0	77.0	35.0	.13	87.0	60.6	.14	21.4	17.7/1060	59.6	5.8/1190	60.1
5-136	4.0	12.4	70.0	30.0	1.2	104.2	80.0	.13	20.7	19.5/1070	65.1	5.2/1100	65.0
5-137	4.2	52.0	70.0	31.0	.07	73.6	58.9	.14	19.7	18.6/1030	64.5	5.4/1080	66.1

TABLE VI (Cont.)

DATA ON 305 TA2675 SAMPLES DELIVERED TO NASA

Unit #	BV_{EBO} I_E=100μA	BV_{CBO} I_C=100μA	LV_{CEX} I_C=10mA V_{EB}=1.4V	$BV_{CEO(SUS)}$ I_C=10mA	I_{CEO} V_{CE}=28V (mA)	h_{FE} V_{CE}=4V I_C=1A	h_{FE} V_{CE}=4V I_C=2A	$V_{CE(SAT)}$ I_C=750mA I_B=150mA	C_{ob} V_{CB}=30V pF	P_{out} P_{in}=5W V_{CE}=28V f=430Mc I_C=mA	η (%)	P_{in} P_{out}=20W V_{CE}=28V f=430Mc I_C=mA	η (%)
E-44-1 16	3.8	62	81	40	.048	58.8	50.0	.175	19.8	19.0/1030	66.0	5.4/1090	65.6
17	4.0	63	80	38	<.01	66.7	50.0	.175	19.5	18.5/980	67.4	5.7/1080	66.1
18	4.0	55	58	31	<.01	36.4	36.4	.20	26.0	15.0/1150	46.6		
20	4.1	51	74	30	.116	117.6	70.2	.195	19.5	20.0/1160	61.6	5.0/1160	61.6
21	4.0	60	79	32	<.01	117.6	88.8	.175	19.7	20.0/1140	62.7	5.0/1140	62.7
22	3.8	63	80	41	<.01	55.6	47.1	.175	20.1	18.4/1000	65.8	5.7/1090	65.5
23	4.0	64	80	38	<.01	71.4	57.2	.175	19.8	18.9/1030	67.5	5.6/1060	67.4
24	3.9	63	80	38	<.01	66.7	57.2	.170	19.6	17.4/8[illegible]0	72.4	6.1/980	68.8
26	4.0	61	80	36	<.01	77.0	61.6	.180	19.4	19.0/970	70.0	5.6/1040	68.8
27	3.5	66	81	46	<.01	33.4	28.6	.185	20.5	15.5/870	63.6		
30	3.9	66	78	42	<.01	44.4	35.4	.20	20.2	16.5/880	67.1	7.0/1120	63.7
31	4.1	60	73	30	.045	154.0	105.2	.22	20.4	20.0/1100	65.0	5.0/1100	65.0
32	4.2	34	67	29	.25	125.0	80.0	.20	19.9	18.6/1050	65.9	5.5/1160	61.6
33	4.0	64	80	33	.02	90.9	66.7	.20	19.2	19.4/1070	65.0	5.3/1120	63.6
34	4.1	46	56	28	-	154.0	100.0	.20	20.9	19.7/1160	60.6	5.1/1170	61.1

TABLE VI (Cont.)

DATA ON 305 TA2675 SAMPLES DELIVERED TO NASA

Unit #	BV_{EBO} I_E=100μA	BV_{CBO} I_C=100μA	LV_{CEX} I_C=10mA V_{EB}=1.4V	$BV_{CEO(SUS)}$ I_C=10mA	I_{CEO} V_{CE}=28V (mA)	h_{FE} V_{CE}=4V I_C=1A	h_{FE} V_{CE}=4V I_C=2A	$V_{CE(SAT)}$ I_C=750mA I_B=150mA	C_{ob} V_{CB}=30V pF	P_{out} P_{in}=5W V_{CE}=28V f=430Mc I_C=mA	η (%)	P_{in} P_{out}=20W V_{CE}=28V f=430Mc I_C=mA	η (%)
E-44-1 *													
6	4.0	5	70	43	2.25	44.5	36.4	.175	19.5	18.2/1160	61.4	5.8/1160	61.5
7	4.0	4.3	70	32	2.25	125.0	40.0	.185		20.0/1100	66	5.0/1100	65.0
8	3.9	60	68	40	.004	50	36.4	.185	19.4	17.6/1070	58.8	6.3/1220	57.6
9	3.0	60	71	40	.003	50	40	.175	19.1	17.2/1030	59.8	6.3/1200	59.6
10	3.8	62	71	41	.003	62.5	53.3	.20	19.9	18.4/1100	59.7	5.6/1170	61.1
11	4.0	47	72	39	.004	58.8	44.5	.19	19.3	18.3/1100	59.4	5.7/1200	65.0
12	4.0	60	70	30	.01	143.0	100.0	.215	19.5	21.0/1170	73.5	4.7/1130	63.3
13	3.8	60	71	40	.003	62.5	53.4	.185	19.6	18.4/1120	64.4	5.6/1210	59.1
14	4.0	62	73	39	.004	52.6	40.0	.190	19.2	17.8/1160	60.0	6.1/1270	56.4
E-44-4		* New Pattern											
7	4.0	55	68	30	<.01	58.8	50.0	.315	21.0	18.7/1110	61.8	5.5/1060	67.5
8	4.0	57	70	29	.013	100.0	84.3	.16	21.2	19.4/1160	59.8	5.3/1160	61.6
10	3.5	55	70	32	.038	66.7	53.4	.18	21.4	18.4/960	68.7	5.7/1040	68.6
11	4.1	44	69	29	.194	77.0	66.7	.16	20.2	20.0/1100	65.0	5.0/1100	65.0
12	4.1	50	68	29	.5	64.7	64.0	.17	20.2	19.3/1140	60.5	5.2/1140	62.6
13	4.0	54	69	30	.1	55.6	47.1	.18	21.0	18.5/1060	62.3	5.7/1070	61.8

TABLE VI (Cont.)

DATA ON 305 TA2675 SAMPLES DELIVERED TO NASA

Unit #	BV_{EBO} I_E=100μA	BV_{CBO} I_C=100μA	LV_{CEX} I_C=10mA V_{EB}=1.4V	$BV_{CEO(SUS)}$ I_C=10mA	I_{CEO} V_{CE}=28V (mA)	h_{FE} V_{CE}=4V I_C=1A	h_{FE} V_{CE}=4V I_C=2A	$V_{CE(SAT)}$ I_C=750mA I_B=150mA	C_{ob} V_{CB}=30V pF	P_{out} P_{in}=5W V_{CE}=28V f=430Mc I_C=mA	η (%)	P_{in} P_{out}=20W V_{CE}=28V f=430Mc I_C=mA	η (%)
E-44-4													
14	4.0	55	70	30	.07	50.0	42.1	.18	20.1	18.6/950	69.9	5.5/1020	70.0
15	3.2	50	70	30	.29	46.5	40.0	.18	22.0	17.0/950	64.0	6.3/1100	65.0
16	3.2	60	71	31	<.01	44.5	41.0	.18	21.7	17.0/940	64.7	6.3/1100	65.0
18	4.0	57	69	30	<.01	52.6	42.1	.19	20.3	16.5/1050	56.1	6.5/1050	68.0
19	4.0	60	73	30	<.01	66.7	57.1	.165	20.3	19.5/1160	60.0	5.3/1000	71.5
20	3.8	54	69	33	<.01	45.4	42.1	.20	20.8	17.5/950	65.8	5.7/1080	66.1
21	4.0	59	70	31	<.01	50.0	42.1	.19	20.8	16.5/960	62.6	6.4/1110	64.5
22	3.1	25	70	36	.81	42.1	36.4	.20	21.7	16.0/960	59.6	6.7/1180	60.6
23	4.0	54	72	33	.023	52.6	44.4	.18	20.8	18.2/1050	62.0	5.7/1150	62.3
24	4.1	58	70	31	<.01	55.6	44.4	.20	20.1	18.3/1060	61.6	5.7/1150	62.1
26	3.9	59	70	32	<.01	48.7	42.6	.19	21.0	18.4/1030	63.8	5.6/1110	64.4
27	3.1	60	73	38	.23	36.4	33.4	.185	21.7	17.0/1010	60.1	6.3/1180	60.5
E-44-5													
6	4.0	60	79	31	<.01	117.6	89.0	.175	20.3	20.5/1070	68.8	4.7/1040	68.8
8	4.1	53	76	30	.09	117.6	89.0	.175	20.3	19.8/1060	66.7	5.1/1070	66.8
9	4.1	61	74	31	<.01	95.2	80.0	.175	20.0	19.5/1020	68.1	5.1/1040	68.6
11	4.0	40	73	33	.30	87.0	72.8	.175	20.5	19.5/1050	66.4	5.2/1080	66.2

TABLE VI (Cont.)

DATA ON 305 TA2675 SAMPLES DELIVERED TO NASA

Unit #	BV_{EBO} I_E=100μA	BV_{CBO} I_C=100μA	LV_{CEX} I_C=10mA V_{EB}=1.4V	$BV_{CEO(SUS)}$ I_C=10mA	I_{CEO} V_{CE}=28V (mA)	h_{FE} V_{CE}=4V I_C=1A	h_{FE} V_{CE}=4V I_C=2A	$V_{CE(SAT)}$ I_C=750mA I_B=150mA	C_{ob} V_{CB}=30V pF	P_{out} P_{in}=5W V_{CE}=28V f=430Mc I_C=mA	η (%)	P_{in} P_{out}=20W V_{CE}=28V f=430Mc I_C=mA	η (%)
3-4-5													
12	4.4	61	73	35	<.01	55.6	42.1	.20	20.4	17.5/970	64.4	5.8/1150	62.2
13	4.4	55	72	32	<.01	77.0	61.5	.175	19.9	18.0/1060	60.7	5.8/1050	68.0
15	4.0	58	74	31	.026	111.2	80.0	.175	20.1	19.3/1020	67.5	5.2/1050	68.0
17	3.3	41	80	38	.30	95.2	61.5	.22	21.5	18.0/1050	61.3	6.1/1180	60.6
18	4.4	57	71	33	.04	71.4	61.5	.18	20.2	19.4/1000	67.8	5.2/1030	69.3
19	4.3	40	72	31	.40	90.8	72.7	.16	19.5	20.3/1050	69.1	4.9/1030	69.3
20	4.3	60	73	32	<.01	77.0	66.7	.17	19.9	19.6/1010	69.3	5.1/1020	70.0
24	4.0	61	80	31	<.01	117.7	88.8	.21	20.5	19.0/1060	64.0	5.3/1150	62.1
26	4.5	56	74	32	<.01	80.0	66.7	.19	19.7	19.0/1040	65.3	5.3/1070	66.8
27	4.4	27	74	32	.55	87	72.7	.19	19.4	19.0/1040	65.3	5.3/1180	66.2
28	3.8	34	87	37	.30	111.2	80.0	.185	20.7	18.8/1080	62.2	5.4/1150	62.2
29	4.0	34	75	30	.275	100.0	84.2	.19	19.7	19.0/1010	67.1	5.3/1070	66.8
30	4.0	36	77	33	.164	100.0	80.0	.215	20.5	17.6/1070	59.0	6.5/1260	56.7
32	4.0	58	73	34	.05	77.0	66.7	.20	20.2	18.2/1030	64.8	5.7/1140	62.6
4-4-5													
R-R	3.7	15.0	72.0	31.0	1.22	105.2	80.0	.23		17.6/1080	58.2		

TABLE VI (Cont.)

DATA ON 305 TA2675 SAMPLES DELIVERED TO NASA

Unit #	BV_{EBO} I_E=100μA	BV_{CBO} I_C=100μA	LV_{CEX} I_C=10mA V_{EB}=1.4V	$BV_{CEO(SUS)}$ I_C=10mA	I_{CEO} V_{CE}=28V (mA)	h_{FE} V_{CE}=4V I_C=1A	h_{FE} V_{CE}=4V I_C=2A	$V_{CE(SAT)}$ I_C=750mA I_B=150mA	C_{ob} V_{CB}=30V pF	P_{out} P_{in}=5W V_{CE}=28V f=430Mc I_C=mA	η (%)	P_{in} P_{out}=20W V_{CE}=28V f=430Mc I_C=mA	η (%)
55-2													
2-R	3.5	62.0	77.0	43.0	.01	66.7	50.0	.21		16.3/1000	58.3		
3-R	3.0	68.0	77.0	41.0	.3	55.5	42.2	.225		14.5/910	56.9		
4-R	3.8	58.0	71.0	41.0	.01	62.5	50.0	.215		16.1/980	58.8		
6-R	3.3	49.0	72.0	48.0	.1	52.7	44.5	.195		15.7/940	59.7		
E-55													
2-7	3.7	56.0	71.0	37.0	< .01	92.6	94.1	.14	18.2	18.0/1010	63.6	5.6/1090	65.6
2-8	3.7	58.0	70.0	38.0	< .01	83.4	66.6	.13	18.4	17.9/980	65.3	5.7/1090	65.6
2-11	3.7	54.0	66.0	37.0	< .01	96.1	69.0	.12	19.1	17.8/1060	60.0	6.1/1200	59.6
2-8	3.4	60	75	43	< .01	76.9	53.4	.140	18.1	17.5/1000	62.5		
2-10	3.4	58	70	43	< .01	63.4	52.6	.130	18.4	16.5/920	63.9		
2-12	3.5	33	74	38	.33	71.5	52.6	.150	18.2	17.5/950	65.9		
2-15	3.6	55	75	38	< .01	80.0	45.5	.200	18.0	16.7/820	72.8		
2-16	3.8	58	70	36	.016	105.1	77.0	.124	18.0	19.0/1010	67.3		
2-14	3.4	55.0	72.0	40.0	< .01	82.0	58.9	.14	18.3	17.7/1030	61.4	6.0/1150	62.1
2-15	3.6	54.0	65.0	37.0	< .01	96.1	66.6	.12	19.2	18.0/1070	60.1	5.9/1180	60.6
2-18	3.8	55.0	68.0	35.0	< .01	125.0	91.0	.12	18.8	17.8/1070	59.4	5.8/1170	61.1

TABLE VI (Cont.)

DATA ON 305 TA2675 SAMPLES DELIVERED TO NASA

Unit #	BV_{EBO} I_E=100μA	BV_{CBO} I_C=100μA	LV_{CEX} I_C=10mA V_{EB}=1.4V	$BV_{CEO(SUS)}$ I_C=10mA	I_{CEO} V_{CE}=28V (mA)	h_{FE} V_{CE}=4V I_C=1A	h_{FE} V_{CE}=4V I_C=2A	$V_{CE(SAT)}$ I_C=750mA I_B=150mA	C_{ob} V_{CB}=30V pF	P_{out} P_{in}=5W V_{CE}=28V f=430Mc I_C=mA	η (%)	P_{in} P_{out}=20W V_{CE}=28V f=430Mc I_C=mA	η (%)
E-55													
2-19	3.8	56.0	68.0	36.0	< .01	96.1	76.9	.13	18.5	17.8/1000	63.6	5.8/1100	65.0
2-22	3.8	4.2	68.0	37.0	2.3	104.0	80.0	.13	17.5	18.5/1010	65.4	5.5/1090	65.6
2-25	3.6	40.0	68.0	34.0	.46	108.7	80.0	.13	19.0	18.1/1070	64.7	5.6/1150	62.1
2-28	3.8	4.6	70.0	36.0	2.8	105.2	78.5	.13	20.0	18.5/1030	64.1	5.5/1100	65.0
8-4	3.8	59.0	68.0	35.0	< .01	125.0	90.9	.14	19.7	18.5/1040	63.6	5.5/1110	64.4
9-2	2.9	12.8	62.0	40.0	1.4	35.7	30.8	.13	20.6	19.5/1080	64.4	5.2/1100	65.0
9-3	4.0	45.0	60.0	30.0	.18	138.9	122.0	.12	20.2	19.5/1040	66.9	5.2/1100	65.0
2-17	3.6	54	67	38	< .01	83.4	58.8	.112	19.1	18.5/1030	64.1		
2-18	3.5	60	72	42	< .01	71.0	57.1	.130	18.4	18.5/1000	66.1		
2-20	4.0	55	69	39	< .01	111.1	80.0	.122	18.5	18.0/980	67.0		
2-21	3.9	60	71	39	< .01	77.0	60.6	.130	18.3	19.5/1060	65.7		
2-23	3.5	8.8	70	36	1.90	113.3	77.0	.134	18.7	19.0/1080	62.9		
2-24	3.6	59	72	36	< .01	104.1	80.0	.154	17.9	18.5/950	69.6		
2-25	3.8	4.0	66	36	3.20	112.5	66.6	.130	18.3	17.8/950	67.0		
2-28	3.5	55	68	38	.028	117.7	66.6	.132	18.6	18.0/1000	64.4		
2-29	3.1	27	71	45	.92	46.6	40.0	.140	18.6	17.0/950	63.9		
2-30	3.2	24	70	44	.36	47.6	40.8	.142	18.6	17.0/930	65.3		

TABLE VI (Cont.)

DATA ON 305 TA2675 SAMPLES DELIVERED TO NASA

Unit #	BV_{EBO} I_E=100μA	BV_{CBO} I_C=100μA	LV_{CEX} I_C=10mA V_{EB}=1.4V	$BV_{CEO(SUS)}$ I_C=10mA	I_{CEO} V_{CE}=28V (mA)	h_{FE} V_{CE}=4V I_C=1A	h_{FE} V_{CE}=4V I_C=2A	$V_{CE(SAT)}$ I_C=750mA I_B=150mA	C_{ob} V_{CB}=30V pF	P_{out} P_{in}=5W V_{CE}=28V f=430Mc I_C=mA	η (%)	P_{in} P_{out}=20W V_{CE}=28V f=430Mc I_C=mA	η (%)
E-55													
2-32	3.7	65	71	41	.56	71.5	58.8	.134	18.5	17.0/870	69.9		
2-33	4.0	62	68	36	<.01	101.0	79.3	.128	18.3	19.0/980	69.4		
2-35	3.7	64	70	36	.08	112.2	79.8	.130	18.6	19.0/1000	67.9		
2-37	3.5	65	72	42	.027	66.7	57.0	.140	18.4	17.0/880	69.1		
2-38	3.8	62	68	38	.017	91.0	66.5	.128	18.9	18.5/980	67.4		
2-40	3.2	65	72	45	.35	45.9	58.8	.146	18.8	15.5/880	63.6		
2-41	3.9	62	68	37	<.01	96.3	72.8	.136	18.3	19.3/1040	66.4		
2-42	3.6	63	68	39	<.01	82.0	60.6	.138	18.7	18.2/1000	65.0		
2-45	3.8	64	70	37	<.01	91.0	69.0	.150	18.0	17.5/920	68.0		
8-6	3.2	13	74	40	.65	108.8	66.6	.150	19.8	18.6/1040	63.9		
8-8	3.8	53	73	35	.055	112.2	87.0	.140	19.8	18.8/1070	62.8		
8-11	3.8	60	72	36	<.01	119.0	80.0	.150	19.7	18.0/1090	59.1		
8-13	3.7	37	72	37	.12	111.1	69.0	.150	19.2	17.9/1040	61.5		
8-14	3.9	60	72	36	.028	106.4	74.1	.160	19.2	19.3/1120	61.6		
8-16	3.8	54	72	35	.150	112.2	87.0	.150	19.6	16.7/1050	56.9		
8-18	3.5	3.7	72	35	6.0	106.4	71.5	.160	18.9	18.6/1050	63.3		

TABLE VI (Cont.)

DATA ON 305 TA2675 SAMPLES DELIVERED TO NASA

Unit #	BV_{EBO} I_E=100μA	BV_{CBO} I_C=100μA	LV_{CEX} I_C=10mA V_{EB}=1.4V	$BV_{CEO(SUS)}$ I_C=10mA	I_{CEO} V_{CE}=28V (mA)	h_{FE} V_{CE}=4V I_C=1A	h_{FE} V_{CE}=4V I_C=2A	$V_{CE(SAT)}$ I_C=750mA I_B=150mA	C_{ob} V_{CB}=30V pF	P_{out} P_{in}=5W V_{CE}=28V f=430Mc I_C=mA	η (%)	P_{in} P_{out}=20W V_{CE}=28V f=430Mc I_C=mA	η (%)
E-55													
8-20	3.5	55	74	36	.18	117.8	69.0	.150	20.04	17.0/990	61.4		
8-21	3.5	57	71	60	<.01	58.9	46.6	.180	19.4	17.7/1000	63.2		
8-24	3.5	58	75	42	<.01	89.3	57.1	.170	19.4	16.8/980	61.3		
8-25	3.8	56	72	36	<.01	108.8	74.1	.150	19.4	18.5/1060	62.5		
2-11	3.6	35	71	35	.42	100.0	74.1	.140	18.4	18.6/1030	64.5		
2-7	3.9	60	71	36	<.01	100.0	77.0	.140	18.0	17.8/910	69.8		
9-7	3.7	48	63	40	.135	54.1	47.1	.160	22.3	16.2/960	60.3		
9-10	3.4	4	62	39	1.56	58.9	53.3	.150	22.4	16.7/980	60.9		
9-11	3.6	34	64	36	1.2	68.9	61.6	.185	21.2	17.6/980	64.1		
9-12	3.9	4	60	33	2.0	143.0	121.2	.155		18.6/1100	60.4		
9-13	4.1	51	63	31	.11	117.6	100.0	.14m	20.8	18.8/1090	61.6		
9-17	3.4	50	63	36	.63	66.7	57.2	.15	22.0	17.0/1040	58.5		
9-18	3.6	6.5	62	37	1.6	74.2	66.7	.17	21.6	18.5/1060	62.2		
9-22	3.9	30	64	31	.365	133.2	117.5	.15	20.3	19.0/1030	65.9		
9-23	4.1	4	61	30	3.35	131.5	117.5	.15		19.8/1080	65.5		
9-25	4.2	37	62	30	.5	143.0	125.0	.15	20.4	20.0/1060	67.4		
9-26	3.4	19	62	36	3.35	74.1	66.7	.165	20.9	17.6/1060	59.4		

TABLE VI (Cont.)

DATA ON 305 TA2675 SAMPLES DELIVERED TO NASA

Unit #	BV_{EBO} I_E=100μA	BV_{CBO} I_C=100μA	LV_{CEX} I_C=10mA V_{EB}=1.4V	$BV_{CEO(SUS)}$ I_C=10mA	I_{CEO} V_{CE}=28V (mA)	h_{FE} V_{CE}=4V I_C=1A	h_{FE} V_{CE}=4V I_C=2A	$V_{CE(SAT)}$ I_C=750mA I_B=150mA	C_{ob} V_{CB}=30V pF	P_{out} P_{in}=5W V_{CE}=28V f=430Mc I_C=mA	η (%)	P_{in} P_{out}=20W V_{CE}=28V f=430Mc I_C=mA	η (%)
9-27	3.8	40	62	35	.21	125.0	111.1	.15	20.3	19.5/1080	64.5		
9-29	3.6	8	60	30	7.6	117.7	100.0	.165	21.5	17.5/980	63.9		
9-40	3.6	4.8	60	33	3.5	91.0	80.0	.15	20.0	18.5/1020	64.8		
9-42	3.9	54.0	64	31	.02	133.3	112.3	.12	20.6	17.6/1050	59.9		
9-45	3.8	48.0	62	33	.22	105.1	95.4	.12	20.7	17.0/1020	59.6		
9-46	3.2	8.1	61	36	5.3	58.0	50.0	.14	20.0	18.1/1130	57.2		
9-48	3.5	10.8	62	31	5.5	114.0	93.1	.13	21.7	18.8/1070	62.8		
9-49	3.4	37.0	62	36	1.4	100.0	80.0	.14	20.4	17.5/950	65.8		
9-50	4.0	43.0	60	30	.82	125.0	111.0	.12	20.8	20.2/1020	70.6		
9-51	4.0	47.0	63	29	.50	147.8	127.0	.12	20.7	21.7/1060	73.1		
9-52	4.1	25.0	61	30	.70	125.0	111.0	.12	19.4	19.1/980	69.8		
9-53	3.1	32.0	62	37	.25	53.3	46.5	.13	22.7	17.6/1050	59.9		
9-55	4.0	54.0	62	31	.12	125.0	118.7	.12	20.7	19.6/1080	64.9		
9-56	4.1	51.0	61	31	<.01	119.0	105.0	.11	21.2	20.3/1060	68.5		
9-57	4.0	52.0	62	32	.064	102.2	91.9	.11	20.8	19.6/1060	66.0		
9-60	3.5	51.0	61	35	.65	95.3	85.3	.13	20.8	18.4/1070	61.5		
9-62	3.1	15.0	63	38	2.0	62.5	50.0	.15	21.2	18.6/1080	61.5		
9-63	4.0	53.0	62.0	31	.07	117.8	100.0	.12	20.7	19.3/1040	66.4		

TABLE VI (Cont.)

DATA ON 305 TA2675 SAMPLES DELIVERED TO NASA

Unit #	BV_{EBO} I_E=100μA	BV_{CBO} I_C=100μA	LV_{CEX} I_C=10mA V_{EB}=1.4V	$BV_{CEO(SUS)}$ I_C=10mA	I_{CEO} V_{CE}=28V (mA)	h_{FE} V_{CE}=4V I_C=1A	h_{FE} V_{CE}=4V I_C=2A	$V_{CE(SAT)}$ I_C=750mA I_B=150mA	C_{ob} V_{CB}=30V pF	P_{out} P_{in}=5W V_{CE}=28V f=430Mc I_C=mA	η (%)	P_{in} P_{out}=20W V_{CE}=28V f=430Mc I_C=mA	η (%)
E-55													
9-64	3.6	53.0	62	33	.10	112.0	100.0	.12	20.5	19.9/1080	65.9		
9-65	4.0	4.1	61	33	6.0	98.2	87.0	.13	20.7	18.9/1010	66.9		
9-70	3.1	3.2	60	38	5.6	54.4	46.5	.15	21.5	17.6/1050	59.9		
9-76	3.8	26.0	61	34	.52	91.0	80.0	.12	21.0	18.1/1050	61.6		

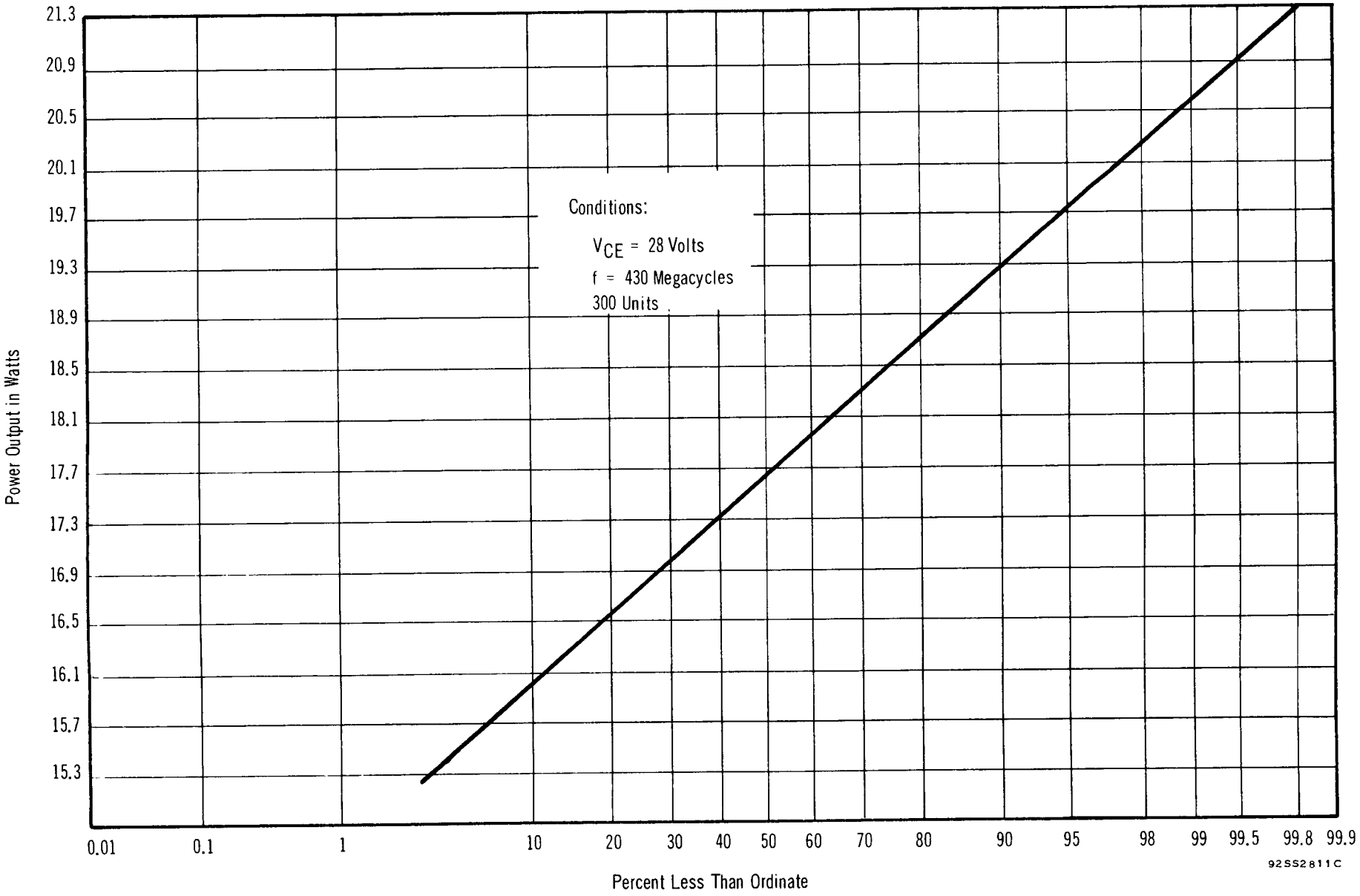

FIGURE 41 DISTRIBUTION OF POWER OUTPUT FOR A 5-WATT DRIVE

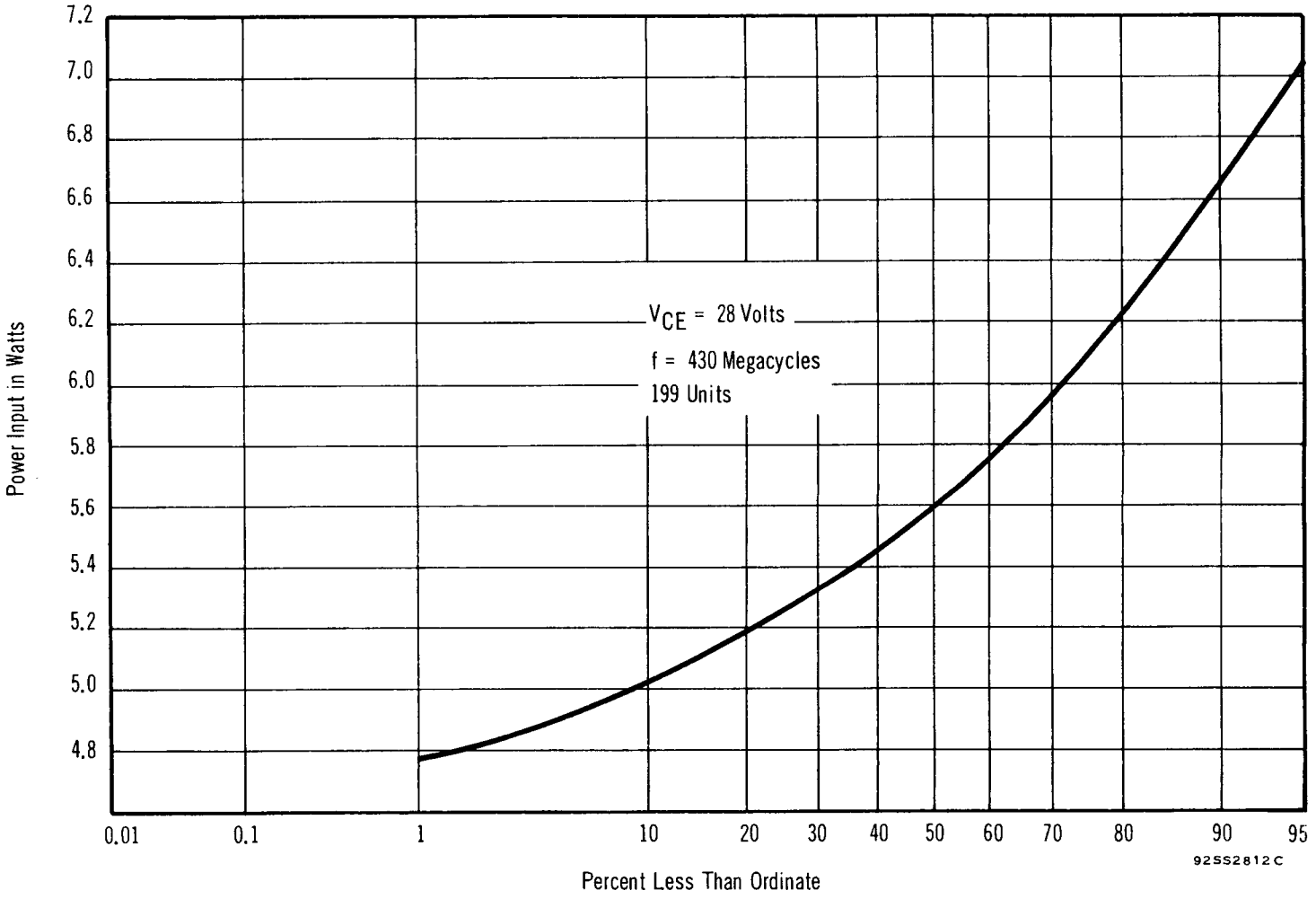

FIGURE 42 DISTRIBUTION OF POWER INPUT FOR A 20-WATT POWER OUTPUT

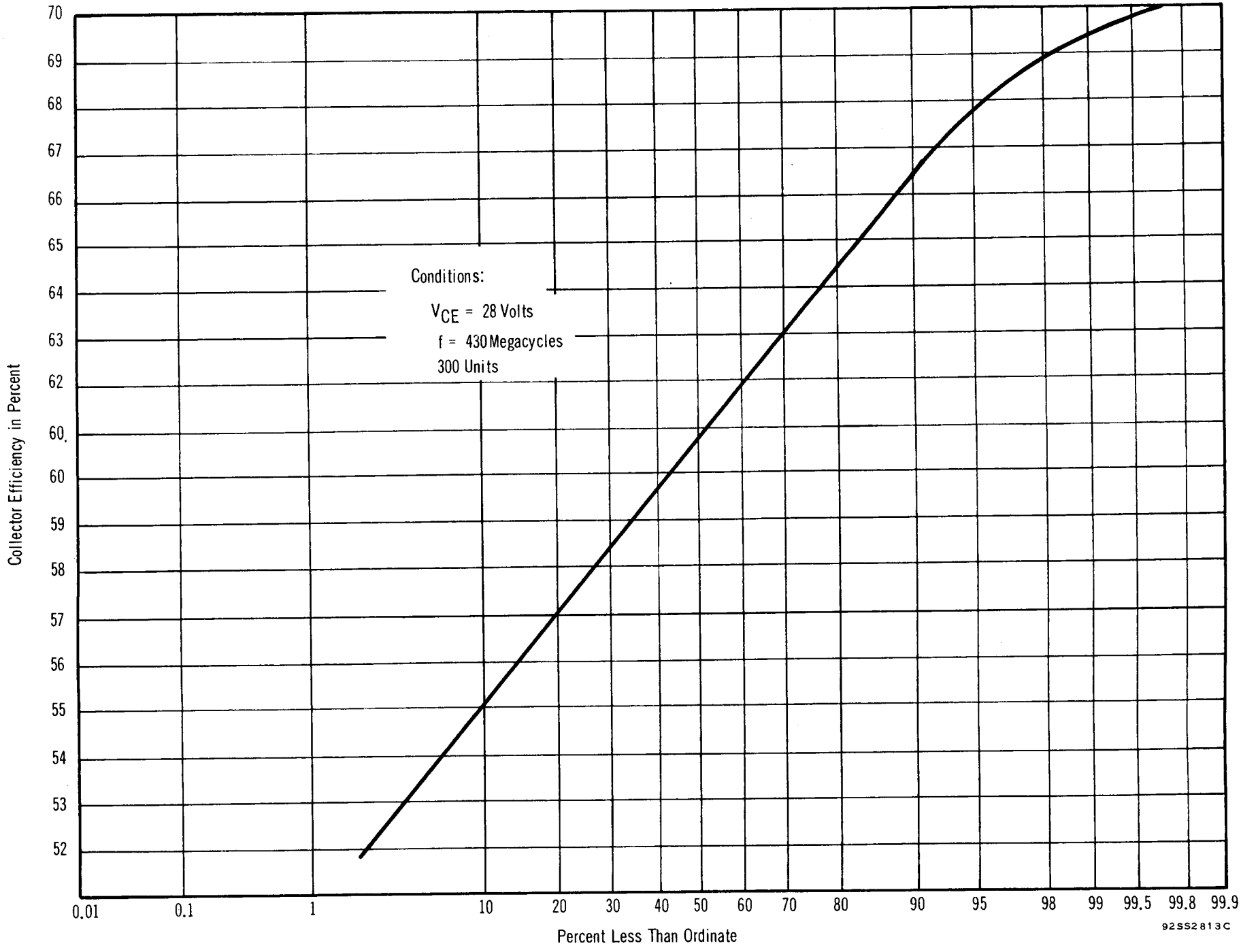

FIGURE 43 DISTRIBUTION OF COLLECTOR EFFICIENCY FOR A 5-WATT DRIVE

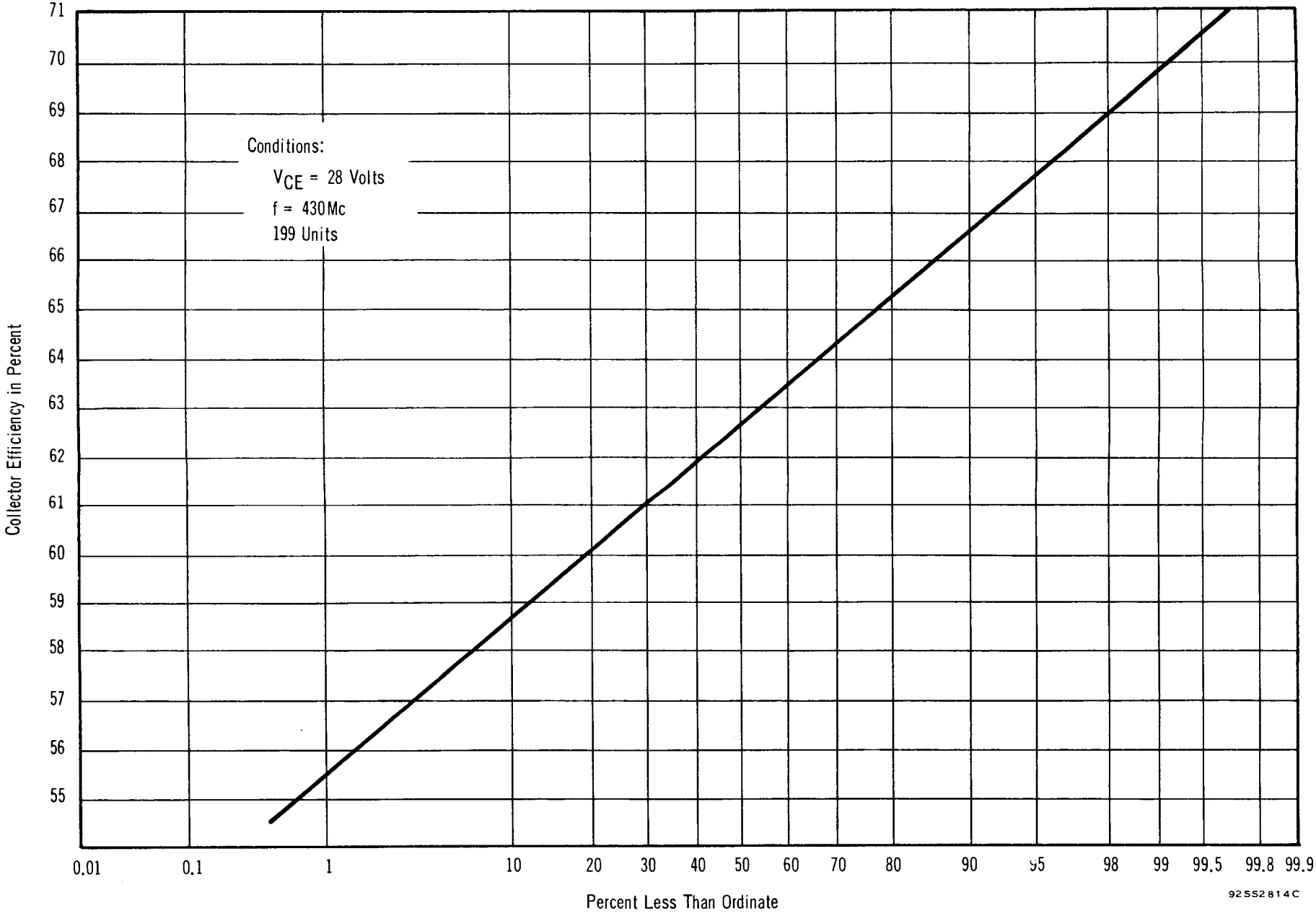

FIGURE 44 DISTRIBUTION OF COLLECTOR EFFICIENCY FOR A 20-WATT POWER OUTPUT